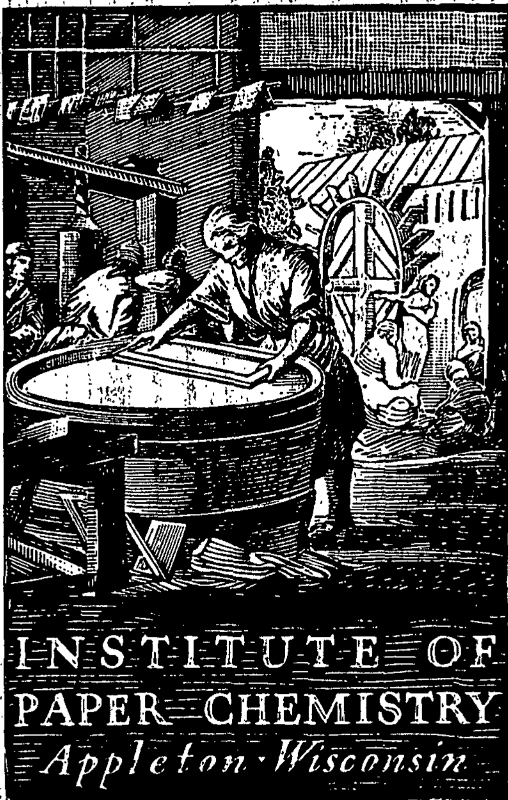

RELATIONSHIP BETWEEN CORE PERFORMANCE AND THE PROPERTIES OF THE CORE STOCK (PHASE I)

Project 2906

Report One

A Progress Report

to

FIBRE TUBE AND CORE RESEARCH GROUP

March 24, 1971

THE INSTITUTE OF PAPER CHEMISTRY

Appleton, Wisconsin

RELATIONSHIP BETWEEN CORE PERFORMANCE AND THE PROPERTIES OF THE CORE STOCK (PHASE I)

Project 2906

Report One

A Progress Report

to

FIBRE TUBE AND CORE RESEARCH GROUP

March 24, 1971

TABLE OF CONTENTS

THE INSTITUTE OF PAPER CHEMISTRY

Appleton, Wisconsin

RELATIONSHIP BETWEEN CORE PERFORMANCE AND THE PROPERTIES OF THE CORE STOCK (PHASE I)

SUMMARY

The objective of this study was to investigate the relationship between tube and core performance and the properties of the core stocks. For this purpose, twenty-one samples of core stock were obtained from the participating companies and made up into three-inch diameter cores. The wall thickness was nominally 0.270 inch. The cores were constructed using either eight core stock plies in the case of 0.030-inch core stocks or ten plies in the case of 0.025-inch core stocks. Standard inner and outer liners were used for all runs except for two special runs.

The experimental cores were evaluated for axial crush, side crush, beam strength, and torque strength. Properties of the core stock which were evaluated included weight, caliper, modified ring compression strength, tensile strength, stretch, modulus and stiffness, Taber stiffness, plybond, tearing strength, porosity, and water drop.

A statistical analysis was carried out to determine which properties of the core stock were best related to each core performance test. It is emphasized that the statistical relationships are specific to the particular core size and construction employed herein.

Each core test was also analyzed from a theoretical mechanics viewpoint to obtain equations relating core performance to core geometry and core stock properties. These equations are more general in scope than the statistical relationships, but their accuracy must be verified for cores of varying diameter and wall thickness. This will be done using the data from Phase II of the study which is in progress.

The following conclusions may be drawn from the results of this study:

A. Statistical Relationships Between Core Performance Tests

1. The axial crush, beam strength, and torque strength tests were all highly intercorrelated. This implies that these three performance tests are primarily dependent on the same property or properties of the core stock.
2. Side crush strength was also highly correlated to the other core tests though to a somewhat lesser degree. This implies that while the side crush strength is probably dependent on the same property(s) of the core stock as the other core strength tests, it also may depend, in part, on other properties of the core stocks which do not affect the other core performance tests to a measurable degree.

B. Statistical Relationship Between Core Performance Tests and Core Stock Properties

Side Crush

1. Side crush strength was most highly correlated with the modified ring compression strength oriented at either 30 or 60° to the machine direction (P_{m30}, P_{m60}) of the core stock. The 30° orientation corresponds to the complement of the angle of wind and its importance may be explained by the fact that the bending and compression stresses generated in the side crush test are oriented at 30° to the M.D. for the cores of this study.
2. Allowing for the different number of plies used for the 0.025- and 0.030-inch core stock runs, the average error of prediction was 7.5%, when side crush strength was predicted from P_{m30}. Thus, it appears that side crush is highly dependent on the edgewise compression characteristics of the core stock.

3. Multifactor analysis indicated that side crush strength may depend in a secondary way on the tensile stiffness (30° to M.D.) and/or the ratio of bending to shear modulus ($\underline{E}/\underline{G}$) in addition to $\underline{P}_{m30}$. The error of prediction was reduced to 4.7% using all three factors.

Axial Crush

4. Axial crush strength was most highly correlated with modified ring compression strength in the C.D. and 60° to M.D. orientations — correlation coefficients of 0.98 and 0.96, respectively. For these cores, the 60° orientation corresponds to the angle of wind which is the stressed direction in the axial crush test. Thus, the high correlation between axial crush and 60° modified ring compression would be expected on physical grounds. While the C.D. modified ring compression orientation gave a slightly higher correlation coefficient, the difference was small and may result from test variability and/or the high intercorrelations between ring compression orientations.

5. Allowing for the different number of plies used for the cores made from 0.025 and 0.030-inch core stocks the average errors of prediction were 4.4 and 3.3%, when axial crush was predicted from the 60° and C.D. directions, respectively. Thus, axial crush strength is highly dependent on the modified ring compression strength of the core stock.

Beam Strength

6. The 36- and 72-inch span beam strengths were most highly correlated with modified ring compression strength in the C.D. and 60° to M.D. (angle of wind) orientations. The correlation coefficients were 0.99 and 0.97, respectively, for the above two orientations with either span. In the beam test the bending stresses generated are in the direction corresponding

to the angle of wind — i.e., the 60° modified ring compression orientation. Thus, the high correlation for the 60° direction is physically reasonable. The slightly higher correlation for the C.D. direction may result from chance fluctuations in the data.

7. Allowing for the different number of plies used for the cores made from 0.025- and 0.030-inch core stocks the average prediction errors were as follows when beam strength was predicted from C.D. or 60° modified ring compression

	36-in. Span	72-in. Span
60° modified ring compression	3.8	4.2
C.D. modified ring compression	2.9	3.0

Thus, beam strength is highly dependent on the modified ring compression strength of the core stock.

Torque Strength

8. Torque strength was most highly correlated with modified ring compression strength in the C.D. and 60° directions. Each property exhibited a correlation coefficient of 0.95. This suggests that torque test failure occurs when the "normal" compression stresses induced in the core walls during test exceed the compression strength of the material under combined load.

9. Allowing for the different number of plies used for the cores made from 0.025- and 0.030-inch core stocks, the average prediction error was 4.5% using C.D. modified ring, and 4.4% using 60° modified ring. Thus, it appears that torque strength is highly dependent on the edgewise compression characteristics of the core stock.

C. Engineering Analyses of Core Performance

Side Crush

1. Assuming that core failure is caused by bending stresses developed at the point of loading the following equation was developed:

$$P_s = \frac{1.335\ P_{m\Theta}}{\{0.9549\ [(D_i/t) + 1][t-2h_l-h_c]\}\ h_c/t^2} \qquad \text{(I)}$$

where

P_s = side crush, lb./in.

$P_{m\Theta}$ = modified ring compression strength oriented at the complement of the wind angle, Θ, lb./in.

D_i = inside core diameter, in.

t = core wall thickness, in.

h_c = core stock thickness, in.

h_l = liner thickness, in.

2. The above equation indicates that side crush should increase as $P_{m\Theta}$ or t increase. Side crush strength will decrease as D_i increases. This is in accord with expectations based on the literature. Verification of the effects of the various geometrical factors is in progress. Further modification of the equation may be necessary when the data from Phase II are available.

3. The average prediction error using Equation (I) was 8.7%.

Axial Crush

4. Assuming that failure occurs when the compression strength of the material is exceeded, the maximum axial crush strength is given by the following equation

$$P_a = \frac{\pi(D_o^2 - D_i^2)\, P_{m\alpha}}{4h_c} \qquad \text{(II)}$$

where

$\underline{P_a}$ = axial crush, lb.

$\underline{D_o}$ = outside diameter, in.

$\underline{D_i}$ = inside diameter, in.

$\underline{P_{m\alpha}}$ = modified ring compression strength at the angle of wind, lb./in.

$\underline{h_c}$ = core stock thickness, in.

5. Equation (II) indicates that axial crush is directly proportional to the area of the core cross section and the modified ring compression strength at the angle of wind.

6. The average prediction error of Equation (II) was 5.35%.

<u>Beam Strength</u>

7. Assuming that the maximum load is limited by the edgewise compression strength of the core stock in the direction of the bore of the core the following equations were developed for the 36- and 72-inch span beams.

<u>36-inch span</u>

$$P_b = \frac{1.188\ \pi(D_o^4 - D_i^4)\, P_{m\alpha}}{8\, L\, D_o\, h_c} + 53.50 \qquad \text{(III)}$$

<u>72-inch span</u>

$$P_b = \frac{1.212\ \pi(D_o^4 - D_i^4)\, P_{m\alpha}}{8\, L\, D_o\, h_c} + 16.85 \qquad \text{(IV)}$$

where

$\underline{P_b}$ = beam strength, lb.

$\underline{D_o}$ = outside diameter, in.

$\underline{D_i}$ = inside diameter, in.

$P_{m\alpha}$ = modified ring compression strength at the angle α from the M.D. (α corresponds to the wind angle), lb./in.

L = beam length

h_c = core stock thickness, in.

8. The average prediction accuracies of Equations (III) and (IV) were 3.6 and 3.7%, respectively.

Torque Strength

9. Several alternative expressions were formulated to relate torque strength to the shear or compression strength of the core stock as well as the core geometry. Two of the equations developed are shown below:

$$T = 0.925\ (\pi/16)[(D_o^4 - D_i^4)/D_o]\tau_{ac} + 501.1 \qquad \text{(Va)}$$

$$(1/\tau_{ac})^2 = (h_c/P_{mx})^2[1+P_{mx}/P_{my}] + (h_c/P_{my})^2 \qquad \text{(Vb)}$$

$$T = 0.726\ (\pi/16)[(D_o^4 - D_i^4)/D_o](P_{my}/\sin 2\alpha) + 463.6 \qquad \text{(VI)}$$

where

T = maximum torque strength, lb. in.

D_o = outside diameter, in.

D_i = inside diameter, in.

τ_{ac} = shear strength in axial-circumferential (a-c) plane, p.s.i.

h_c = core stock thickness, in.

P_{mx} = M.D. tensile strength, lb./in.

P_{my} = C.D. modified ring compression strength, lb./in.

α = angle of wind, deg.

10. The average predictive accuracies of Equations (V) and (VI) were 5.3 and 5.1%.

11. As discussed in the text, Equation (VI) may only hold satisfactorily for angles of wind near the angle (58°) used in fabricating the cores of this study. On the other hand, it appears that Equation (V) may yield results which are independent of the angle of wind due to the assumptions made in deriving the formulas. Further information relative to the effect of angle of wind and other factors on torque strength is needed to determine the range of application of the equations.

INTRODUCTION

This investigation is directed to the study of (a) spiral wound tube and core performance under various stress environments encountered in use, and (b) the development of relationships between spiral wound tube and core performance and the properties of the base stocks and dimensions.

Information developed in these studies should be helpful in (a) identifying properties of the core stock that are important to end-use performance and, hence, to board manufacture, (b) design of the tube or core in respect to selection of core stocks and dimensions for various end uses, and (c) prediction of the performance of the tube or core in a variety of end-use environments based on a knowledge of the properties of the base stock and dimensions.

The study has been divided into two phases as follows:

Phase I Effect of Materials

Phase II Effect of Tube or Core Dimensions

In the first phase, twenty-one samples of core stock were obtained from the participating companies and made up into three-inch inside diameter cores for the purpose of determining the effect of material on core performance. The results obtained in this phase are summarized herein.

The second phase of the study involving tube or core dimensions is currently in progress. Cores have been fabricated having inside diameters of 3, 6, and 10 inches and wall thicknesses of 0.150, 0.270, 0.480, and 0.660 inch. The evaluation of these cores and the materials from which they were fabricated is in progress. Results obtained will be summarized in a future report.

Generally, tubes are used to protect an enclosure, whereas cores are used to give support to something wrapped around them. However, they are basically the same in a structural sense. Therefore, in this report both terms are used interchangeably.

In fabricating the cores for this study the same nominal inner and outer liners were used with each core stock sample. Inasmuch as the liners were essentially a constant factor, their contribution to core performance has been neglected in formulating relationships between core tests, core geometry, and core stock properties. Their inclusion would have complicated the derivation and verification of relationships between core tests and core stock properties and, in general, the significance of factors associated with the liners could not be experimentally verified using the data from this study.

In addition to a statistical analysis of the relationships between core performance and core stock properties, a major portion of the analysis was directed toward deriving equations utilizing the principles of mechanics. The latter equations relate core performance to core stock properties and core geometry and thus may be of more general application. It is emphasized, however, that verification of the geometrical factors in the equations cannot be performed until the results from Phase II are available. It is to be expected that some modification of the equations may be necessary and desirable after evaluation of the Phase II cores.

BACKGROUND CONSIDERATIONS

A search of the literature pertaining to fiber cores and tubes reveals that the literature is almost exclusively directed to patents covering equipment design and processing or the composition of the cylinder wall. Only a limited number of references were found which were directly concerned with the structural performance of tubes and cores and its relationship to the properties of the core stock.

However, cylindrical structures fabricated from materials other than paper are used in innumerable applications and have been studied extensively. Despite the different use of fiber tubes and cores, they involve the same basic types of force application as do other cylinder structures such as axial thrust, torque, bending, and side compression loads. Thus, there is a large body of theoretical and experimental knowledge which is applicable to wound fiber tubes and cores. In this regard, however, the fibrous nature of the core stock and its anisotropic mechanical properties require consideration.

With the foregoing in mind, the literature pertaining to a number of common core performance tests is discussed in the following sections together with a brief review of the structural aspects of the test. Additional information may be found in later sections of this report which discuss the engineering analyses of the data generated in this study.

AXIAL COMPRESSION

A circular cylinder subjected to axial compression load may fail in any of several modes depending on the height, radius, and wall thickness of the cylinder. The principal failure modes are as follows:

1. Buckling Modes
   - A. Euler column (buckling) mode
   - B. Local buckling mode
     1. short cylinder range
     2. transition range
     3. long cylinder range

2. Short Column Crush Mode

Buckling Modes

A discussion of cylinder buckling is given in Reference (1). For the case of varying height and constant radius and thickness the several buckling modes are illustrated in Fig. 1. Theory indicates that an important parameter is H^2/rt, where H equals height, r equals radius, and t equals wall thickness. Practical experience with metals, along with theory indicates that when this parameter is greater than about 100, the cylinder buckles into the classical long cylinder mode with diamond-shaped buckles over the cylinder wall. For cylinders with H^2/rt less than unity, buckling appears as a simple bowing of the cylinder walls. This is termed the short cylinder range. A transition range is identified ($1 < H^2/rt < 100$) which is a combination of the adjacent modes.

All of the above three modes are termed local buckling because the buckled surface exhibits deviations from the original cylindrical shape. For very long cylinders, on the other hand ($H^2/rt >> 100$), classical Euler buckling may occur as illustrated in Fig. 1.

The equations relating buckling load (P_{cr}) to cylinder geometry and material properties (for isotropic materials) may be written as follows for each buckling mode illustrated in Fig. 1.

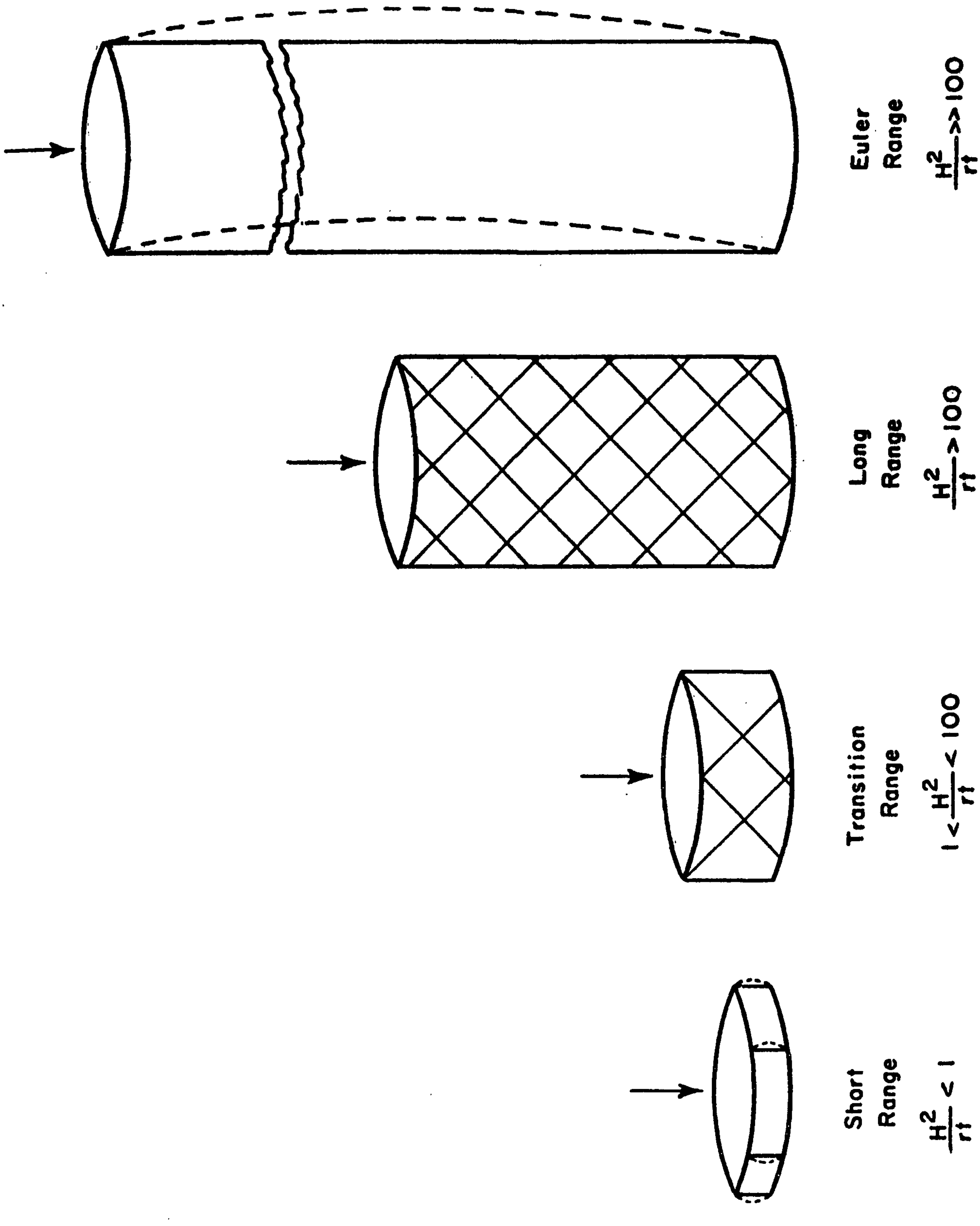

Figure 1. Modes of Buckling for Circular Cylinders Under Axial Compression

Short range

$$P_{cr} = k_1 \, Et^3/H^2 \qquad (1)$$

Transition range

$$P_{cr} = k_2 \, Et^3/H^2 \qquad (2)$$

Long cylinder

$$P_{cr} = k_3 \, Et^2/r \qquad (3)$$

Euler column

$$P_{cr} = k_4 \, EtR^2/H^2 \qquad (4)$$

where

$\underline{P_{cr}}$ = buckling load per unit length of cylinder perimeter, lb./in.

$\underline{E}$ = modulus of elasticity, p.s.i.

$\underline{t}$ = cylinder wall thickness, in.

$\underline{R}$ = cylinder radius, in.

$\underline{H}$ = cylinder height, in.

$\underline{k}_1$, $\underline{k}_2$, $\underline{k}_3$, $\underline{k}_4$ = buckling coefficients which are functions of Poisson's ratio, end fixity, and cylinder geometry

The above equations indicate that essentially the buckling strength of cylinders varies inversely as the square of the height, with the exception of the long cylinder range where the buckling strength is independent of height and depends instead on the radius of the cylinder.

It should be emphasized that the above summary is appropriate to the buckling of cylinders made from isotropic materials. In general, cylinder buckling theory for these materials is not as accurate as say, flat plate buckling or column buckling theory. Further, as far as is known, the applicability of these theories to paperboard has not been studied. There is little doubt that the theories should be modified to account for the anisotropy of paperboard. Work along these lines has been done for plywood (2).

Short Column Crush Mode

The above discussion has been concerned with the various possible buckling modes. The short column crush mode of failure prevails for short sturdy cylinders and results when the edgewise compression strength of the cylinder is exceeded before buckling. Thus, as the height of a cylinder of constant radius, thickness, and material is progressively decreased, the load at which buckling occurs progressively increases. Eventually a height is reached where the load at which buckling instability could occur is equal to the edgewise compression strength of the material. With further decrease in height, the cylinder crushes before it buckles and the maximum load sustained by the cylinder holds constant at the edgewise compression strength of the material. This is illustrated by the horizontal line AB in Fig. 2 for the case of the crossover point lying in the Euler column range. Theoretically, the crossover point could occur in any of the buckling ranges. This is because the edgewise compression strength is a failure property of the material while cylinder buckling depends on the prefailure property, modulus of elasticity, and these two properties are, in principle, independent. However, it is believed that the wall thickness and radius of most common cores is such that axial compression failure occurs due to exceeding the edgewise compression strength of the core wall (short column crush mode). It seems likely that the local buckling failure modes may only occur for very thin-walled tubes having a relatively large radius and Euler buckling may only occur for tubes of small radius and very long lengths. For this reason, the line AB in Fig. 2 is drawn to place the crossover point A in the Euler range.

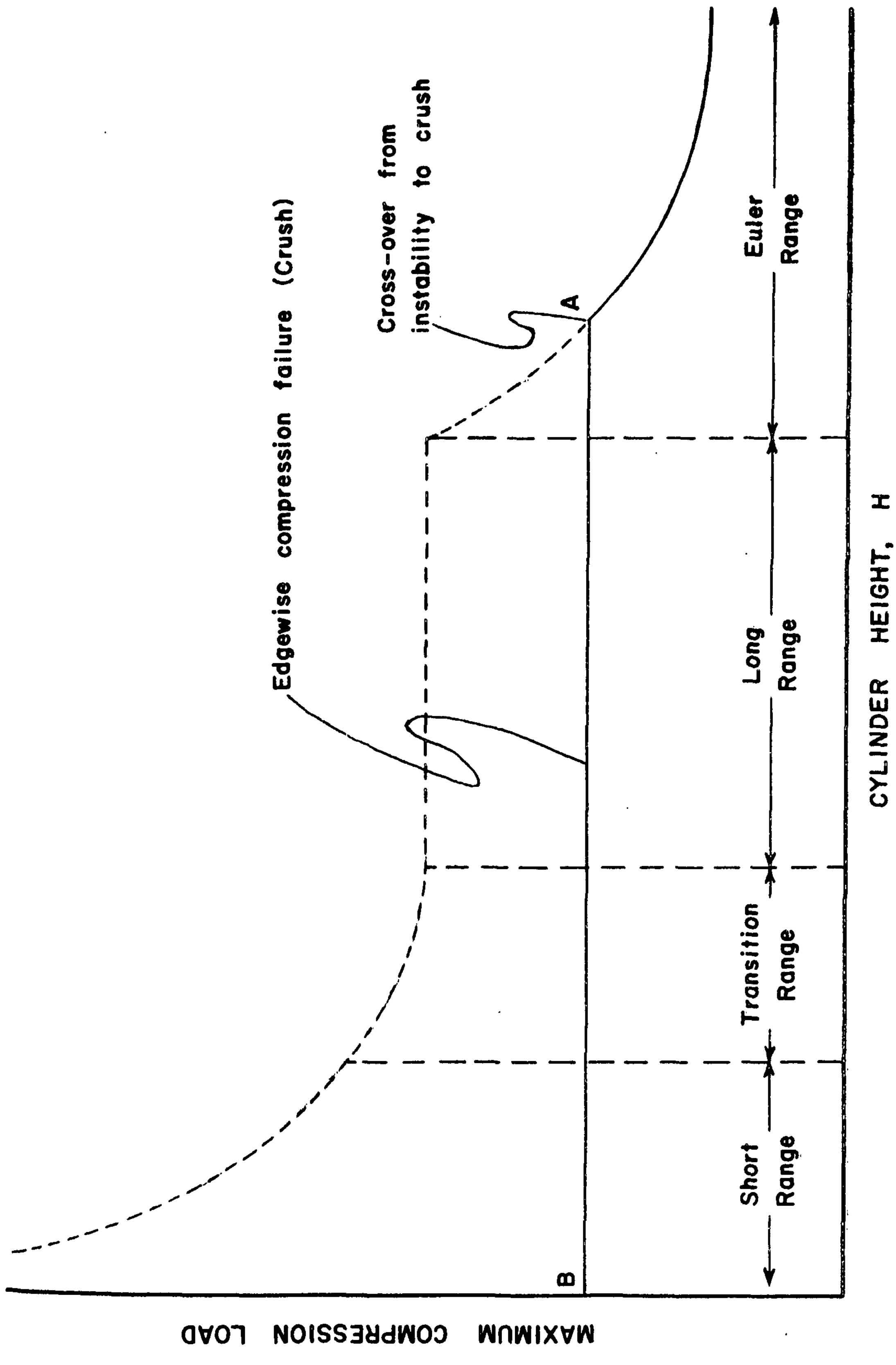

Figure 2. Hypothetical Relationship of Edgewise Compression Strength to Cylinder Buckling

For the short column crush mode the maximum axial crush load (P_a) may be expressed as follows

$$P_a = A\ P_m/h \qquad (5)$$

where

P_a = maximum axial crush load, lb.

A = cross-sectional area of tube, sq. in.

P_m = edgewise compression strength of core stock in direction of load, lb./in.

h = thickness of core ply, in.

Thus, the axial crush load should depend on the edgewise compression strength and thickness of the core stock and the cross-sectional area of the tube.

A search of the literature pertaining to fiber tubes and cores revealed only one paper by Tenzer (3) which discussed in any detail axial compression behavior of tubes and cores. His results are reviewed in the following paragraphs.

Tenzer evaluated the effect of (a) direction of wind, (b) tube diameter, (c) tube length, and (d) number of plies in axial compression. With regard to direction of wind, he found, using 60-mm. diameter, 3-ply tubes, as would be expected, that the axial compression strength is higher when the machine direction of the web is parallel to the tube axis (parallel wound) than when the machine direction of the web is perpendicular (vertically wound) to the tube axis. The axial strengths of spiral wound tubes were lower than the strengths of the convolute wound tubes in two comparisons; in one comparison the axial strength of the spiral wound tubes was intermediate between the parallel and vertically wound convolute tubes. Thus, Tenzer concluded that "spirally wound tubes have the lowest axial compression strength, at least lower than that of parallel wound tubes."

Assuming that no buckling takes place it appears that the axial strength of tubes should be directly proportional to the compression strength of the core stock in the direction of loading. Inasmuch as the machine direction edgewise compression strength is higher than the cross direction strength it would be expected that parallel wound convolute tubes should exhibit higher strengths than vertically wound convolute tubes as was found by Tenzer. By the same reasoning it would be anticipated that the axial compression strength of spiral wound tubes would be intermediate between the parallel and vertically wound convolute tubes because the edgewise compression strength of the core stock at intermediate orientations to the machine direction is lower than the machine direction strength but higher than the cross direction strength. This assumes that the gaps between the spiral wound plies do not excessively weaken the construction.

For constant wall thickness Tenzer also showed that the axial strength of tubes increased linearly with tube diameters in the range from about 40 to 100 mm. For a tubular cross section the cross-sectional area is as follows

$$A = \pi t\ (D_i + t) \qquad (6)$$

where

$\underline{A}$ = area

$\underline{t}$ = wall thickness

$\underline{D_i}$ = inner diameter

Thus, for constant wall thickness the cross-sectional area increases linearly with the diameter and, hence, the axial compression strength also increases linearly with diameter assuming no buckling occurs.

With regard to the effect of tube length, Tenzer's results indicated that the axial strength of 3-ply 60-mm. diameter tubes was independent of length in a range from 50 to 200 mm. This result would be expected if buckling does not occur.

When the number of plies and, hence, the wall thickness of the tubes were varied at constant inner diameter Tenzer found that the axial compression strength increased substantially as the number of plies was increased as would be expected. He further stated that the axial compression strength was linearly related to the average tube diameter — i.e., (D_i+t) in Equation (6). This appears questionable because it neglects the effect of the other thickness term in Equation (6).

Based on the above results, Tenzer concluded that the axial compression strength of tubes should be related to material properties and tube dimensions by the following equation which is essentially similar to Equation (5):

$$P_a = \sigma_d \pi d_m t \qquad (7)$$

where

P_a = axial compression strength

σ_d = material strength in the direction of load (ring compression strength)

d_m = mean diameter

t = wall thickness

He concluded that the ring compression strength of the core stock in the appropriate orientation was the material property (σ_d) best related to axial compression strength. A high correlation was obtained between axial compression strength and ring compression strength. However, Tenzer did not develop any quantitative relationship between σ_d and ring compression so as to permit use of Equation (7) for prediction of the axial compression strength of tubes — either convolute or spiral wound.

BEAM STIFFNESS AND STRENGTH

For a homogeneous isotropic uniform beam the following approximate expression relates the curvature of the beam to the bending moment and beam properties within the proportional limit (4):

$$d^2y/dx^2 = -M/EI \tag{8}$$

where

y = deflection of beam at the point with coordinate x, in.

M = bending moment, in.lb.

E = modulus of elasticity in bending, p.s.i.

I = moment of inertia, in.^{4}

The solution of Equation (8) for a particular beam taking account of beam supports yields an equation for the deflected shape of the beam. In the case of tubes and cores, NFCTA Method T114 specifies that the beam shall be supported at the ends and loaded at the midspan — i.e., a three-point beam test. For this case the maximum deflection occurs at midspan as shown in the following equation

$$y = PL^3/48EI \tag{9}$$

where

y = deflection at midspan, in.

P = applied load, lb.

L = span, in.

E = modulus of elasticity, p.s.i.

I = moment of inertia, in.^{4}

Equation (9) shows that, in addition to its dependence on load P and length L, the midspan deflection is inversely proportional to the modulus of elasticity in bending, *E*, and the cross-sectional moment of inertia, *I*. Taken together the product *EI* is identified as the flexural stiffness of the beam. The greater the flexural stiffness, the less the curvature of the beam for any given load.

The three-point beam test suffers from one disadvantage, namely, the deflection of the specimen is the result of two effects, shear and bending — the proportion of these being a function of beam dimensions and material properties. Thus, a portion of the deflection is due to bending and a portion is due to shear deformation. As a result, the apparent stiffness, *EI*, calculated from Equation (9) underestimates the true flexural stiffness.

Roark (4) gives the following expression for estimating the shear deflection of a center-loaded three-point uniform beam

$$y_s = F(PL)/4GA \qquad (10)$$

where

y_s = deflection due to shear, in.

F = form factor = 2.0 for thin walled tube

P = load, lb.

L = span, in.

G = shear modulus, p.s.i.

A = cross-sectional area, sq. in.

Using Equation (10), it may be shown that the ratio of the true stiffness to the apparent stiffness will be as follows for the case of a three-point uniform tubular beam made from isotropic material

$$EI/(EI)_a = 1 + [3F(E/G)(R_o^2 + R_i^2)/L^2)] \qquad (11)$$

where

$\underline{EI}$ = true flexural stiffness, lb.-in.^{2}

$(\underline{EI})_{\underline{a}}$ = apparent flexural stiffness, lb.-in.^{2}

$\underline{P}$ = load, lb.

$\underline{L}$ = span, in.

$\underline{E}$ = modulus of elasticity, p.s.i.

$\underline{G}$ = shear modulus, p.s.i.

$\underline{R}_o$ = outside radius, in.

$\underline{R}_i$ = inside radius, in.

$\underline{F}$ = form factor = 2.0 for thin-walled tube

Equation (11) indicates that the ratio of the true to apparent flexural stiffness for tubes and cores increases as (1) the ratio of $\underline{E}/\underline{G}$ and (2) $(\underline{R}_o{}^2+\underline{R}_i{}^2)/\underline{L}^2$ increases. Thus, shear effects tend to become more important for materials of low shear modulus and, for a given material, shear effects become more important at small spans. Roark (4) comments that deflections due to shear are often much more important for wood beams than metal beams because of the relatively low shear modulus of wood relative to its modulus of elasticity.

One way of circumventing the disadvantages associated with three-point beam tests is to use an alternate type of test set-up, namely, a four-point beam as shown in Fig. 3 (5-7). For this type of test only flexural stresses act over the central span. Therefore, measurement of load and the deflection at the middle of the central span enable calculation of the true flexural stiffness. Application of this technique to the evaluation of the flexural stiffness of corrugated board is discussed in Reference (8).

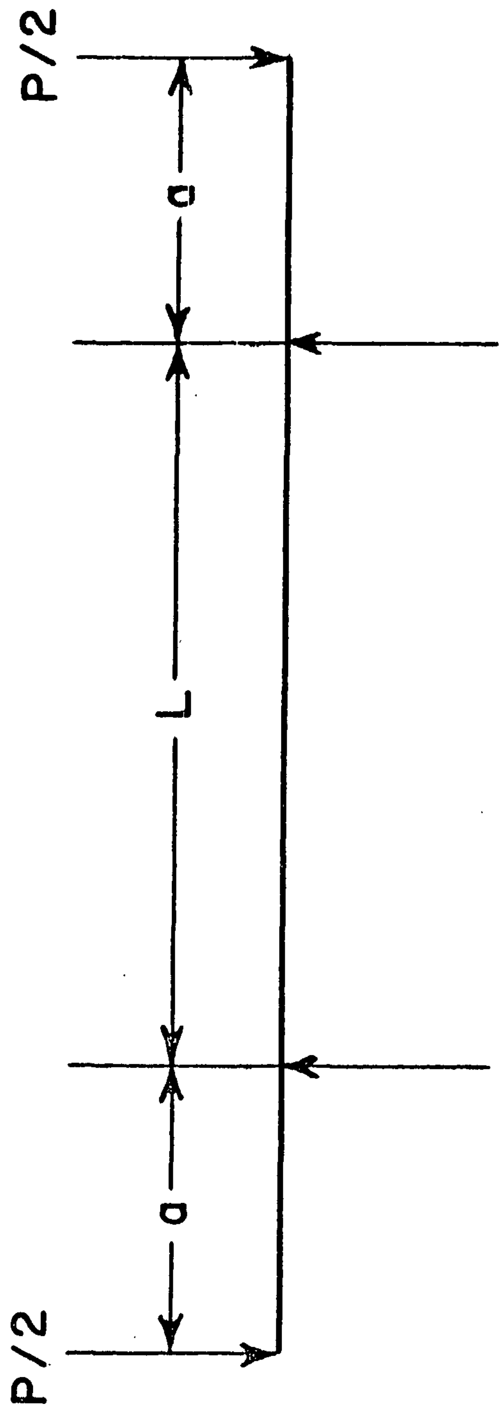

Figure 3. Four-Point Beam

With regard to beam failure, Roark (4) indicates that the maximum strength of a beam made from nonductile material may be calculated as follows

$$M_m = S'(I/c) \tag{12}$$

where

M_m = maximum bending moment, lb.-in.

S' = modulus of rupture, p.s.i.

I = moment of inertia, in.^{4}

c = distance from neutral axis to extreme fiber layer, in.

For the case of a three-point tubular beam the solution of Equation (12) is as follows

$$P_b = S'\pi(R_o{}^4 - R_i{}^4)/R_o\ L \tag{13}$$

where

P_b = maximum beam load, lb.

S' = modulus of rupture, p.s.i.

R_o = outside diameter, in.

R_i = inside diameter, in.

L = beam span, in.

Thus, the maximum beam load is dependent on the geometry of the tube, the beam span, and the modulus of rupture. The modulus of rupture is a property of the material and other factors such as the shape of the cross section, the span-depth ratio, etc.

A rupture factor is usually defined as the ratio of the modulus of rupture to the ultimate uniaxial strength of the material. In the case of brittle metals the latter is usually taken as the ultimate tensile strength. However, for wood, the rupture factor is based on the ultimate compression strength (4).

Practically, rupture factors must be experimentally determined by tests on beams of varying material, cross-section and span-depth ratios in order to determine how the rupture factor is affected by these variables. When this has been done, an estimate of maximum beam load for design purposes may be made as follows:

1. Determine the appropriate uniaxial strength of the beam material.
2. Multiply (1) above by the rupture factor to obtain the modulus of rupture.
3. Correct the modulus of rupture for span-depth and cross-section effects if necessary.
4. Substitute (3) above in Equation (13) to calculate the expected maximum beam load.

It is evident from the above that prediction of maximum beam strength from the properties of the material is more empirical and difficult in theory than prediction of beam stiffness. In either case, however, the anisotropic nature of paperboard must be taken into account in the application of the foregoing equations.

In view of the foregoing it would be anticipated that convolutely wound tubes and cores made with the machine direction of the core stock parallel to the length of the tube would exhibit a substantially higher stiffness and strength than convolute tubes made with the machine direction perpendicular to the length of the tube. Spiral wound tubes would be expected to give stiffnesses and strengths intermediate between the two convolute cases, depending on the winding angle employed. In this connection, Biggs and Dunlap (9) showed that, as the winding angle (measured from bore) increased from about 17 to 37°, a marked decrease in beam strength occurred. This was accompanied by an increase in side crush strength as the winding angle increased. They concluded that the beam strength to crush ratio appeared to be at a maximum for winding angles between 17 and 22°. Dryssen (10) has also discussed the bending strength and other properties of tubes with respect to the automatic roll changing devices employed on modern printing presses.

SIDE CRUSH

For a thin ring loaded by two radial forces 180° apart (see Fig. 4), the resulting bending moment within the elastic limit at any cross section of the ring is as follows (4):

$$M = PR(0.3183 - (\sin \Theta)/2) \qquad (14)$$

where

M = bending moment, lb.-in.

P = applied load, lb.

R = radius, in.

Θ = angle from plane of load application

Inspection of Equation (14) indicates that the maximum positive bending moment is obtained when $\Theta = 0°$ (plane CD in Fig. 4) and the maximum negative bending moment is obtained when $\Theta = 90°$ (plane AB in Fig. 4). The magnitudes of the bending moments at 0° and 90° are as follows:

(a) 0° $\qquad M = 0.3183\ PR \qquad (15)$

(b) 90° $\qquad M = -0.1817\ PR \qquad (16)$

Thus, the magnitude of the bending moment is greatest along the radial plane coinciding with the points of load application. Consequently, the bending stresses induced in the ring are highest along this plane and failure, due to bending stresses, would be expected in the regions near the points of load application.

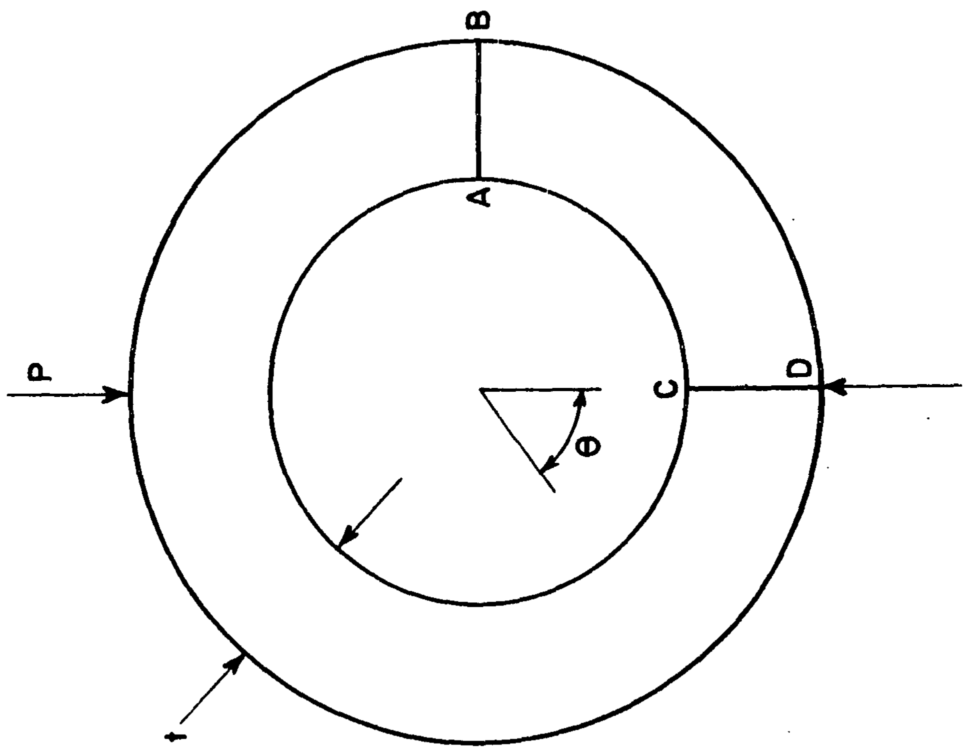

Figure 4. Core Loading Diagram

Direct compression and shear stresses are also induced in the ring as shown by the following expressions (4):

$$T = P\,(\sin\Theta)/2 \qquad (17)$$

$$V = P\,(\cos\Theta)/2 \qquad (18)$$

where

T = circumferential compression force, lb.

V = radial shear force, lb.

P = applied load

Θ = angle from plane of load application

Thus, shear forces are a maximum along the radial plane coinciding with the points of load application (plane CD) and decrease to zero when $\Theta = 90°$ (plane AB). The circumferential compression force is zero when $\Theta = 0°$ and a maximum when $\Theta = 90°$.

Reference (4) indicates that the above formulas are based on the following assumptions:

1. Ring is of uniform cross sections.
2. Stresses are below the elastic limit.
3. The radius is large relative to the thickness.
4. Deflections are due to bending — i.e., direct compression and shear stresses are negligible.

Assumption (2) leads to error because failure of fiber cores in side crush involves stresses beyond the elastic limit. Methods for analyzing bending stresses in the plastic range exist (11-13), but are laborious to apply and are beyond the scope of the present study.

With regard to Assumption (3), the diameter-to-thickness ratio of the cores for this study (Phase I) is in the neighborhood of 11 to 12 which calls for "thick" tube theory; however, a study of Reference (4) indicates that the error incurred by applying "thin" tube may be modest. This may be more of a factor for certain of the thick-walled constructions of Phase II.

The effects of Assumption (4) are difficult to evaluate because there is little available information relative to the shear properties of paperboard. Observation of the cores tested in this study indicated that ply delamination occurred as the load on the specimen approached the initial peak. The delamination occurred near the points of load application. As the core deflection increased, the ply delamination became more severe and appeared to progress around the core to as far as 45° or more on either side of the points of load application. Compression failure wrinkles along the lines of load application on the top and bottom outside surfaces were observed when the specimens were unloaded. These observations relative to mode of failure indicate that (1) peak load is associated with failure of the core material near the points of load application, and (2) shear effects may require consideration.

With the foregoing in mind the bending stress at the plane CD may be evaluated. If it is then assumed that failure occurs when the compression strength of the outside ply of core stock is exceeded, the following equation is obtained relating the maximum side crush load to the core geometry and edgewise compression strength of the core stock. (Note: Derivation of the equation is discussed in Appendix I.)

$$P_s = \frac{P_{m\Theta}}{0.9549\ (\frac{D_i}{t} + 1)\ (t - 2h_1 - h_c)(h_c/t^2)} \qquad (19)$$

where

$\underline{P_s}$ = side crush load, lb./in.

$\underline{P_{m\Theta}}$ = edgewise compression strength of core stock in direction Θ degrees from M.D., where Θ is the complement of the angle of wind. (Same for all plies), lb./in.

$\underline{D_i}$ = inside diameter of tube, in.

$\underline{t}$ = wall thickness of tube, in.

$\underline{h_c}$ = thickness of tube stock, in.

$\underline{h_1}$ = thickness of outer liner, in.

The above equation indicates that $\underline{P_s}$ should be directly related to the edgewise compression strength of the core stock in the appropriate direction and nonlinearly related to the tube diameter and wall thickness. While no empirical adjusting constants are shown in the equation, such may be necessary. Roark (4), for example, comments that circular rings generally exhibit a higher rupture factor than a portion of such a ring "tested as a statically determinate curved beam."

In the field of fiber tubes and cores Tenzer (3) evaluated the effect of a number of variables on side crush strength of tubes. His procedure differed somewhat, however, from the procedure specified in NFCTA T-108. In particular, the tubes rested on a flat lower platen and load was applied to the top through a narrow steel bar rather than the two flat platens specified in T-108. He indicated that his procedure resulted in clearly defined maximum loads within the range of deflections studied. In contrast he indicated that when the tubes were compressed between flat platens, the load increased steadily with increasing deflection within the range of deflections studied. In this connection it should be noted that the load-deflection curves for the tubes of this study (3-inch diameter, 0.270-inch wall thickness) did exhibit an initial peak at relatively small deflections and this was defined as the maximum tube load. After the initial peak load was attained the load first decreased and then increased again to a higher peak at a relatively great tube deflection. However, it was believed that the higher loads attained at the relatively great tube deflection levels were not of practical importance because the core is so distorted as to be unusable. In any event the difficulties with parallel platen loading which Tenzer encountered were not evident for the tube construction used in this study; however, it appears possible that this type of behavior could be obtained for certain tube constructions.

Keeping the above in mind, Tenzer found that vertically wound convolute tubes exhibited higher side crush strengths than parallel wound convolute tubes. This results from the fact that the side crush strength of vertically wound tubes depends on the machine-direction properties of the core stock, whereas cross-direction properties are involved for the parallel winding orientation.

Tenzer's results indicated that side crush strength decreased in a nonlinear fashion as the tube diameter increased. Side crush strength increased nonlinearly with increasing number of plies.

Based on the above, Tenzer proposed the following equation for side crush strength:

$$P_s = 2\sigma_b\, t^2 L/3\, d_m \qquad (20)$$

where

$\underline{P_s}$ = side crush strength, lb.

$\underline{\sigma_b}$ = material strength in the direction of load (ring compression strength), p.s.i.

$\underline{t}$ = wall thickness, in.

$\underline{L}$ = tube length, in.

$\underline{d_m}$ = mean tube diameter, in.

He concluded that the ring compression strength of the core stock in the appropriate orientation was the material property (σ_b) best related to side crush strength. However, Tenzer did not develop any quantitative relationship between σ_b and ring compression so as to permit use of Equation (20) for prediction of the side crush strength of tubes.

Dryssen (10) describes the Tampella tester for evaluating the torsion and compression tests on tubes. The latter test appears to be quite different from the side crush procedures specified in T-108 or in Tenzer's work, because the tube is compressed between two narrow arms which are oriented at right angles to the tube axis.

Eulenstein (14) compared the strength (apparently in side crush) of tubes made with silicate of soda and polyvinyl alcohol as adhesives and concluded that stiffer tubes were obtained using silicate of soda.

TORQUE STRENGTH

When a circular tube made from isotropic material is loaded by means of equal and opposite twisting couples applied to its ends, the maximum shear stress in the elastic range developed in the tube walls is as follows (4):

$$S_s = 2T\, R_o/\pi\, (R_o^4 - R_i^4) \tag{21}$$

where

S_s = maximum shear stress, p.s.i.

T = torque, in.lb.

R_o = outer radius, in.

R_i = inner radius, in.

For a given size tube, Equation (21) reveals that the torque is directly related to the maximum shear stress developed in the tube wall.

Failure in torsion tests apparently may occur in a number of ways depending on the type of material. For example, Roark (4) indicates that "bars of ductile material usually break in shear, the surface of the fracture being normal to the axis and practically flat." He also states that brittle materials often break in tension exhibiting a helicoidal surface. In the case of the tubes evaluated for this study the failure lines followed the spiral pattern associated with the angle of wind. It is not clear whether the wrinkling in the line of failure should be attributed to shear or compression failure, however, it seems likely that failure occurs when the compression strength of the core stock is exceeded.

If the torque value at failure is substituted in Equation (21), the resulting shear stress value is termed the modulus of rupture in torsion. Roark (4) indicates that the modulus of rupture value in torsion may vary from about 80 to 100+% of the ultimate tensile strength in the case of solid bars of steel and from 100+ to 190% for solid bars of cast iron.

In the case of fiber tubes and cores Dryssen (10) describes the Tampella tester for evaluating torsion strength. The tester appears similar in principle to that used in NFCTA T-116.

OTHER CORE TESTS

Jones (15) patented a test apparatus for evaluating the compressibility of tubes or cores of the type used for winding rolls of plastic film. In the apparatus, a metal strap is passed in a loop about a compressible sleeve, and so arranged that tension forces can be applied to the ends of the strap. The internal diameter of the sleeve is approximately equal to the outside diameter of the core. The force required to reduce the diameter a specified amount is measured.

In 1952 Wagenhals (16) patented a device intended to test the strength of the joint between the cap and tube of a capped tube. Air was passed through a nozzle positioned within the tube and directed against the capped end.

Tenzer (3) describes an edge tear test which essentially involves forcing a core having a taper of 1:6 into the end of a tube. He indicated that the strength is much affected by frictional forces and concluded that it did not appear to be suitable as a routine test.

CORE STOCK PROPERTIES

In general, from the literature it appears that the properties of the core stock which are deemed to be of importance fall mainly in two classes, namely, (1) properties affecting the strength of the tube or core, and (2) properties affecting the winding operation. Among the properties mentioned by Bigger (17) and Brosman (18) were the following: weight, thickness, tensile, burst, stiffness, porosity, size, stretch, and dimensional stability. In his studies, Tenzer (3) evaluated a number of properties of the core stock including tensile strength, stretch, bursting strength, tear strength, edge tear strength, folding endurance, and ring stiffness. As mentioned previously, he found that the axial and side crush strengths of cores were best related to ring compression strength.

In terms of its mechanical behavior, paperboard is often classed as an orthotropic material (19-22). Jones (23) recently investigated the relationship between the in-plane elastic moduli of paper and concluded that the orthotropic model described the elastic behavior of paper for stresses parallel to the sheet plane. An orthotropic material is characterized by the presence of three mutually perpendicular planes of elastic symmetry and its reaction to stress can be expressed in terms of properties measured along three mutually perpendicular axes lying in the respective planes. In the case of paperboard, these axes correspond to (1) the machine direction (x), (2) the cross direction (y), and (3) the thickness direction (z). Detailed mathematical treatments of such materials may be found in References (24) and (25).

For spiral wound tubes the above considerations are important because, in general, the stresses applied to the tubes in the various tube performance tests are applied at an angle to the orthotropic axis of the material and this must be taken into account. For an orthotropic material where stress is applied parallel to the plane of the sheet the following equations relate the elastic moduli:

$$1/E_\Theta = \cos^4 \Theta/E_x + \sin^4 \Theta/E_y + \sin^2 \Theta \cos^2 \Theta[(1/G_{xy}) - (2\nu_{xy}/E_x)] \quad (22)$$

$$1/G_\Theta = 4[(\sin^2 \Theta \cos^2 \Theta/E_x) + (\sin^2 \Theta \cos^2 \Theta/E_y) + (2\nu_{xy} \sin^2 \Theta \cos^2 \Theta/E_x)] + (\cos^2 \Theta - \sin^2 \Theta)^2/G_{xy} \quad (23)$$

where

E_Θ = modulus of elasticity at an angle Θ measured from the machine direction, p.s.i.

E_x = modulus of elasticity in machine direction (x), p.s.i.

E_y = modulus of elasticity in cross direction (y), p.s.i.

G_{xy} = shear modulus corresponding to xy direction, p.s.i.

G_Θ = shear modulus at angle Θ, p.s.i.

ν_{xy} = Poisson's ratio for stress in machine direction (x) and contraction in cross direction (y)

Θ = angle measured from "x" direction (M.D.), deg.

Thus, equations of the above type may be used to estimate the elastic moduli corresponding to the actual directions of stress for the spiral wound core and tube tests. Modified forms of the above equations have been proposed by Horio and Onogi (26) and Campbell (27).

MATERIALS

In order to study the effect of core material properties on core performance, twenty-one different core materials were submitted by the nine cooperators. As may be noted below, five of the cooperators submitted three samples of core stock each. The three samples were to correspond to their low strength, normal strength, and high strength core stocks.

	Company	No. of Samples
1.	Alton Box Board Company	3
2.	J. C. Baxter Company	3
3.	Container Corporation of America	1
4.	Fibreboard Corporation	2
5.	Hoerner Waldorf Corporation	1
6.	International Paper Company	2
7.	Sonoco Products Company	3
8.	Star Paper Tube, Inc.	3
9.	John Strange Paper Company	3

Seventeen of the samples had nominal calipers of 0.030 in. and four of the samples had nominal calipers of 0.025 in.

FABRICATION

The sample rolls were slit into ribbon reels at the Appleton Manufacturing Company, Division of John Strange Paper Company, Menasha, Wisconsin. Each roll was slit into ten ribbon reels with the following widths (front-to-back on slitter): 5-3/16, 5-5/32, 5-1/8, 5-1/16, 5, 5, 5, 5, 5, and 5 inches. At the time of slitting, full roll width samples were obtained at start and end of winding by Institute personnel.

The core fabrication was carried out at the Appleton Manufacturing Company, Menasha, Wisconsin.

All cores were wound on a 3.015-inch mandrel. The cores were made using eight plies of 0.030-inch stock, or ten plies of 0.025-inch stock. Standard inner and outer liners (0.014 inch) were used for all runs except for two special runs made without liners — Runs 2-2 and 11-2. In the latter case, one additional 0.030-inch ply was used in place of the two liner plies.

The inside and outside angles of wind were approximately 58 and 63°, respectively, with respect to the bore.

All cores were fabricated using PVA adhesive, although it was necessary to vary the solids content for certain of the runs as shown below:

Run	Solids Content, %
1-10, 12-16	11.2
11, 17	17.4
18	12.4
19, 20	12.5

Moisture content samples were obtained at the end of each run from three of the ribbon reels.

Approximately sixty to seventy 80-inch cores were obtained for each run.

CONDITIONING

The cores were preconditioned at 25% R.H. and 73°F. for at least ten days and then conditioned at 73°F. and 50 ± 2% R.H. for at least ten days prior to test. Several core specimens were weighed in each atmosphere at periodic intervals to check the adequacy of the above conditioning times.

The core stock and liner samples were preconditioned at least twenty-four hours at 25% R.H. and 73°F. and conditioned for at least forty-eight hours at 73°F., 50 ± 2% prior to test.

TEST PROCEDURES

CORE TESTS

The tests carried out on the cores are listed in Table I. In general, NFCTA* test procedures were employed where possible. However, for the axial crush tests it was necessary to reduce the test rate from 0.5 in./min. to 0.2 in./min. to avoid exceeding the rate of load response of the test machine used.

To prepare the axial crush specimens the following procedure was employed:

1. The specimens were saw-cut to a length slightly in excess of the 4-inch length specified in CT-107.
2. An aluminum plug having a diameter of 3.000 inches was then inserted in the specimen.
3. The specimen and plug were then placed in a V block jig and the loading edges were sanded so as to obtain smooth, flat and parallel edges. A 12-inch diameter vertical disk sander was used. The aluminum plug was removed prior to testing.

CORE STOCK AND LINER TESTS

The tests carried out on the core stocks and liner are tabulated in Table II.

*National Fibre Can and Tube Association.

TABLE I

TESTS ON CORES

Test	No. of Tests	Method
1. Side-to-side crush[b]	16	NFCTA T-108
2. Axial (end-to-end) crush[c]	16	NFCTA CT-107
3. End supported beam strength[d]		
(a) 36-inch span	8	NFCTA T-114
(b) 72-inch span	8	NFCTA T-114
4. Wall thickness	32	NFCTA CT-101, Method B
5. Inside diameter	8	NFCTA CT-102, Method A
6. Outside diameter	--[a]	NFCTA CT-103, Method C
7. Moisture content (at time of test)	3	NFCTA CT-111
8. Weight (4-inch long specimen at time of test)	16	
9. Torque strength[e]	5	NFCTA T-116

[a]Calculated from inside diameter and wall thickness.

[b]Test rate was 2 inches per minute.

[c]Test rate was 0.2 inch per minute.

[d]Test rate was 2 inches per minute.

[e]Tests were carried out by one of the participating companies.
The specimen ends were not notched.

TABLE II

TESTS ON CORE STOCK AND LINERS

		Number of Determinations[a]	
		Core Stock	Liner Stock
1.	Weight	1000 sq. in.	1000 sq. in.
2.	Caliper	18	10
3.	Apparent density	--	--
4.	Bursting strength	18	10
5.	Tensile, stretch, and modulus,		
	M.D.	18	10
	C.D.	18	10
	30° to M.D.	18	10
	60° to M.D.	18	10
6.	Modified ring compression,		
	M.D.	18	10
	C.D.	18	10
	30° to M.D.	18	10
	60° to M.D.	18	10
7.	Taber stiffness,		
	M.D.	18	10
	C.D.	18	10
8.	Elmendorf tearing strength,		
	M.D.	18	10
	C.D.	18	10
9.	TAPPI plybond	12	6
10.	Gurley porosity	12	6
11.	Water drop	12	6

[a]Half the tests were made on the sample corresponding to the start of each run, and half on the sample corresponding to the end of each run.

DISCUSSION OF RESULTS

CORE PERFORMANCE RESULTS

The core test results are summarized in Table III for the twenty-one runs.

Typical load-deflection curves for the axial and side crush tests are shown in Fig. 5. Figure 6 shows typical load-deflection curves for the 36- and 72-inch span beams. In the case of the side crush tests, the maximum loads summarized in this report correspond to the load at the first peak shown in Fig. 5 because the cores were so severely deformed by the time the second peak load was attained. In the case of the 36-inch beams, loads were read at the first peak on the load-deflection curves and at maximum load. For the 72-inch beams, the maximum load attained was read from the curves.

The maximum and minimum values observed during tests of cores from all 21 runs of axial crush, side crush, beam strength and apparent stiffness $(EI)_a$, and torque strength are as follows:

	Maximum	Minimum
Axial crush, lb.	4277 (Run 6)	2454 (Run 20)
Side crush, lb./in.	79.8 (Run 2)	38.8 (Run 21)
Beam strength, max., lb.,		
36-in. span	485 (Run 6)	274 (Run 20)
72-in. span	241 (Run 6)	133 (Run 20)
Beam stiffness, lb.in.^{2}		
36-in. span	937 (Run 6)	580 (Run 1)
72-in. span	1130 (Run 6)	713 (Run 1)
True stiffness	1214 (Run 6)	772 (Run 1)
Torque strength, lb.in.	5334 (Run 6)	2982 (Run 1)

TABLE III

CORE TEST RESULTS

Run	Inside Diameter, in.	Outside Diameter, in.	Wall Thickness, in.	Weight, lb.	Moisture Content, % (o.d.)	Side Crush Load lb./in.	Side Crush Defl., in.	Axial Crush, lb.	Beam Strength, lb. 36-in. Span First Peak	Beam Strength, lb. 36-in. Span Max. Load	Beam Strength, lb. 72-in. Span Max. Load	Beam Stiffness, (EI), $lb.in.^2 \times 10^3$ 36-in.	Beam Stiffness 72-in.	Beam Stiffness True Stiffness[a]	Torque Strength, in.-lb.
1	3.0122	3.5242	0.256	0.244	7.4	48.5	0.235	2483	271	296	146	580	713	772	2982
2	3.0140	3.5560	0.271	0.287	7.6	79.8	0.254	4135	424	458	227	833	1025	1111	5094
3	3.0139	3.5399	0.263	0.265	7.6	66.2	0.228	3360	340	392	188	738	882	943	4152
4	3.0158	3.5658	0.275	0.265	7.9	52.9	0.233	3392	370	407	196	796	995	1086	4260
5	3.0168	3.5448	0.264	0.231	8.1	45.8	0.251	2527	267	312	149	627	770	833	3222
6	3.0144	3.5324	0.259	0.271	8.1	74.0	0.236	4277	438	485	241	937	1130	1214	5334
7	3.0066	3.5166	0.255	0.256	7.5	43.0	0.281	2756	304	349	169	763	984	1089	3594
8	3.0138	3.5378	0.262	0.268	7.7	71.0	0.235	4046	419	448	222	900	1100	1189	5064
9	3.0071	3.5291	0.261	0.281	7.9	58.8	0.281	3468	360	414	206	869	1099	1206	4254
10	3.0081	3.5061	0.249	0.255	7.9	48.4	0.211	3136	330	367	182	772	962	1048	3606
11	3.0120	3.4820	0.235	0.210	8.1	45.3	0.290	2867	324	346	164	766	927	996	3618
12	3.0124	3.5824	0.285	0.281	7.4	50.4	0.201	2590	261	311	150	616	756	819	2886
13	3.0138	3.5578	0.272	0.274	7.3	48.5	0.221	2533	259	316	146	612	742	798	3456
14	3.0127	3.5487	0.268	0.282	7.8	64.7	0.145	3630	368	424	202	790	966	1043	4764
15	3.0132	3.5412	0.264	0.258	7.8	47.7	0.244	2814	315	353	166	694	896	992	3822
16	3.0124	3.5684	0.278	0.271	8.0	56.8	0.301	3298	350	385	187	764	1004	1121	4302
17	3.0132	3.4852	0.236	0.249	8.2	58.3	0.254	3344	379	410	191	763	957	1046	4440
18	3.0143	3.5403	0.263	0.269	7.7	57.8	0.205	3054	325	357	172	704	875	953	4092
19	3.0123	3.5503	0.269	0.291	7.7	69.6	0.233	3816	410	466	227	861	1091	1197	5046
20	3.0126	3.5426	0.265	0.244	7.9	41.7	0.230	2454	245	274	133	607	744	805	3180
21	3.0067	3.5227	0.258	0.249	7.5	38.8	0.211	2522	285	299	144	604	817	926	3258
Av.	3.0123	3.5369	0.262	0.262	7.8	55.6	0.237	3167	335	375	181	746	925	1009	4020

[a] Corrected for shear based on results for 36 and 72-in. span tests using a modification of Eq. (11).

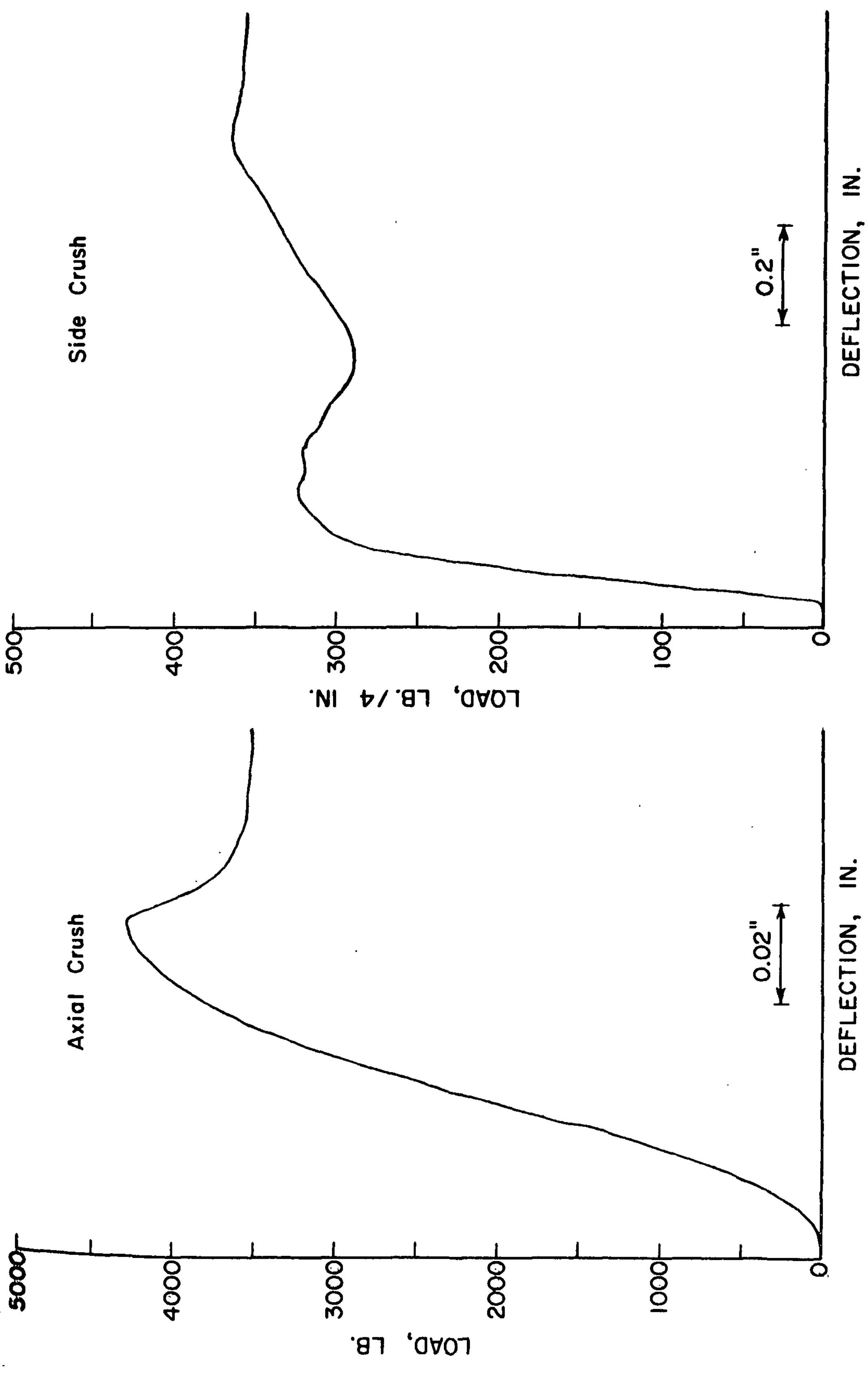

Figure 5. Typical Axial and Side Crush Load-Deflection Curves

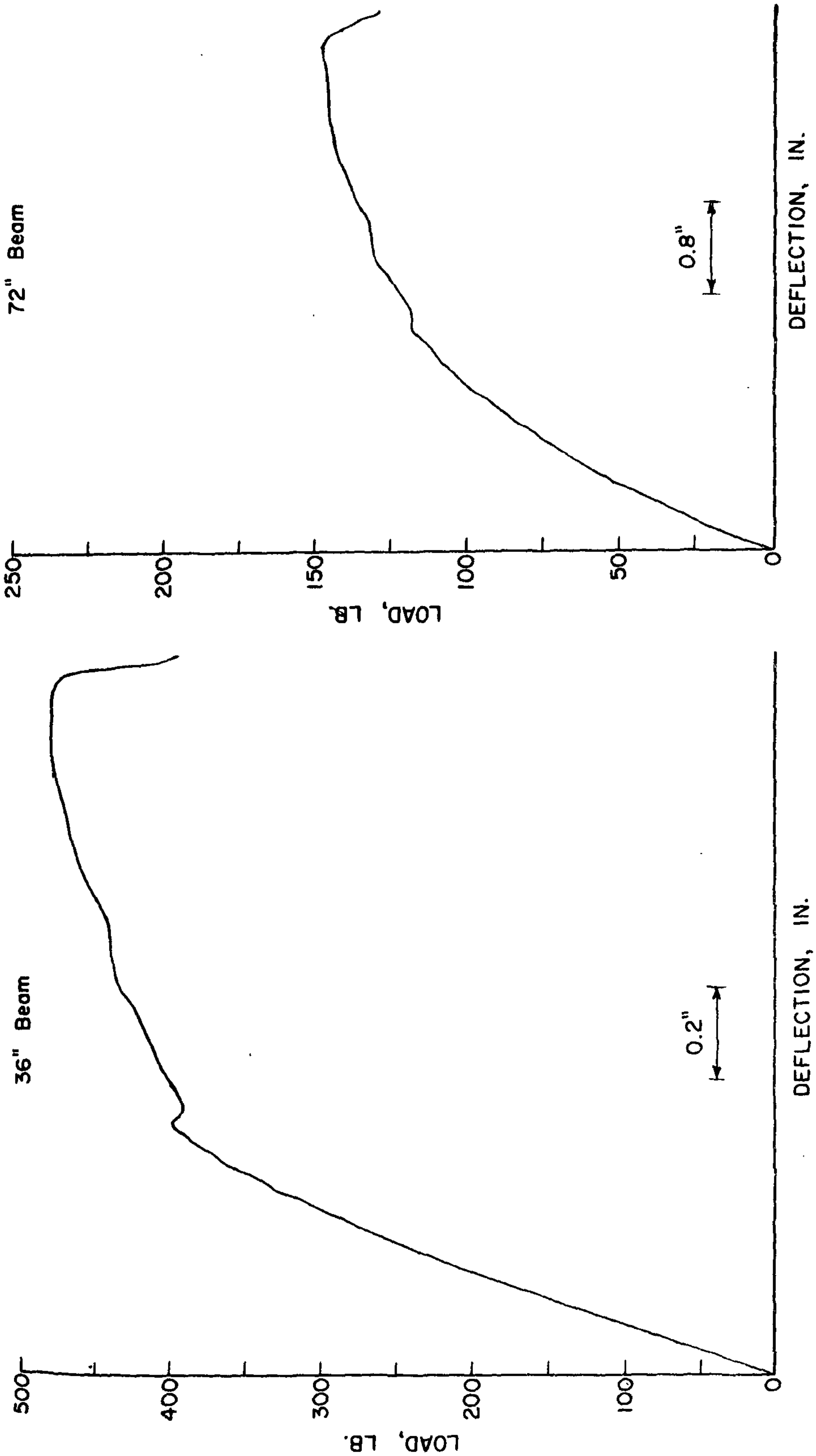

Figure 6. Typical Load-Deflection Curves for 36- and 72-Inch Span Beams

Thus, the core performances varied over a wide range depending on the core stock used. As a matter of interest, it may be noted that the maximum loads for the 72-inch beams averaged about 48% of the maximum loads for the 36-inch beams. This is very close to the expected result (50%) based on theory [see Equations (12) and (13)]. The small discrepancy may represent sampling and test variability or alternatively may indicate the existence of a small span/diameter effect on maximum beam load.

The beam stiffness (EI) values in Table III refer to the stiffness within the proportional limit. In general, the greater the stiffness the lower the deflection at a given load. The differences in apparent stiffness between the 36- and 72-in. spans may be attributed to shear. Therefore, for tubes of this size and construction, it appears that the shear modulus of the tube walls is of such a magnitude as to noticeably affect the beam deflection of the tube.

The correlations between core performance tests are summarized in Table IV. The coefficients in Table IV indicate that all of the core tests involving failure are highly related (coefficients are significant beyond the 0.01 level). Thus, for a core of given size, wall thickness, etc., an increase in a given core performance test will generally result in increases in the other core performance tests. This suggests that the various core performance tests are dependent on essentially the same property or properties of the core stock.

The general conclusions may be qualified somewhat in the case of side crush. Inspection of the coefficients indicates that somewhat lower correlations are obtained between side crush and the other performance tests involving failure. This indicates that side crush performance to some extent may involve properties of the core stock which are not involved in the axial, beam, or torque tests.

TABLE IV

CORRELATION BETWEEN CORE PERFORMANCE TESTS

	Correlation Coefficient[a]								
			36-in. Beam		72-in.		Beam Stiffness		
Test	Axial Crush	Side Crush	First Peak	Max. Load	Beam, Max.	Torque	36-in.	72-in.	True
	N = 21 -- All Samples								
Axial crush	1.000	0.927	0.976	0.979	0.986	0.968	0.880	0.849	0.822
Side crush		1.000	0.865	0.892	0.896	0.896	0.749	0.675	0.730
36-in. beam, first peak			1.000	0.980	0.978	0.964	0.931	0.911	0.888
36-in. beam, maximum load				1.000	0.993	0.968	0.938	0.908	0.880
72-in. beam, maximum load					1.000	0.956	0.947	0.918	0.890
Torque						1.000	0.892	0.865	0.839
Beam stiffness, 36-in.							1.000	0.978	0.953
Beam stiffness, 72 in.								1.000	0.995

[a] 0.05 and 0.01 levels of significance are 0.423 and 0.537, respectively.

The beam stiffness values were also fairly well correlated with the axial crush, beam strength, and torque tests even though the beam stiffness depends on prefailure properties (bending and shear moduli), whereas the other tests depend on the failure strength of the material. The beam stiffness values exhibited lower but statistically significant correlations with side crush.

As mentioned previously, cores were fabricated with and without inner and outer liners for two of the runs. When made without liners, an additional ply of core stock was inserted in place of the liners. A comparison of the effect of liners on core performance may be found in Table V. In general, the cores made without liners exhibited slightly lower side, axial, beam, and torque strength. The apparent beam stiffness values tended to be slightly higher for the cores made without liners as compared to the cores with liners.

CORE STOCK AND LINER TEST RESULTS

The test results on the core stock samples are tabulated in Table VI. Average properties for the liners used are listed in Table VII. A summary of the liner properties by run is shown in Appendix I.

STATISTICAL RELATIONSHIPS BETWEEN CORE PERFORMANCE AND CORE STOCK TESTS

It may be recalled that nominal 0.030-inch core stocks were supplied for all but four runs and cores made with 0.030-inch stocks were constructed having eight plies of core stock plus inner and outer liner. For the four runs involving 0.025-inch core stocks (Runs 4, 5, 6, and 19), the cores were constructed having [illegible] plies of core stock plus inner and outer liner. Because the different number [illegible] plies involved would be an interfering factor in the analyses, it was decided [illegible] investigate the relationships between the various core stock properties and

TABLE V

COMPARISON OF RESULTS FOR CORES MADE WITH AND WITHOUT LINERS

Test Property	Run 2			Run 11		
	With Liner	Without Liner	Diff., %[a]	With Liner	Without Liner	Diff., %[a]
Side crush, lb./in.	79.8	77.2	- 3.3	45.3	43.6	- 3.8
Axial crush, lb.	4135	4009	- 3.0	2867	2666	- 7.0
Beam strength, lb.,						
36-in.	458	450	- 1.7	346	333	- 3.8
72-in.	227	214	- 5.7	164	157	- 4.3
Apparent beam stiffness, $lb.in.^2$,						
36-in.	833	853	+ 2.4	766	760	- 0.8
72-in.	1025	1064	+ 3.8	927	962	+ 3.8
Torque strength, lb.in.	5094	4986	- 2.1	3618	3300	- 8.8
Inside diameter, in.	3.0140	3.0177	+ 0.1	3.0120	3.0167	+ 0.2
Outside diameter, in.	3.5560	3.5617	+ 0.2	3.4820	3.4847	+ 0.1
Wall thickness, in.	0.271	0.272	+ 0.4	0.235	0.234	- 0.4
Moisture content, %	7.6	7.6	0.0	8.1	8.2	+ 1.2

[a] Based on results "with liners" as reference.

TABLE VI

CORE STOCK PROPERTIES

Run No.	Moisture, % o.d. (Time of Fabr.)	Weight, lb./M ft.^{2}	Caliper, pt.	Density, lb./pt.	Bursting Strength, p.s.i.g.	Tensile, lb./in. M.D.	Tensile, lb./in. C.D.	Tensile, lb./in. 30° to M.D.	Tensile, lb./in. 60° to M.D.	Stretch, % M.D.	Stretch, % C.D.	Stretch, % 30° to M.D.	Stretch, % 60° to M.D.	Tensile Modulus, p.s.i. M.D.	Tensile Modulus, p.s.i. C.D.	Tensile Modulus, p.s.i. 30° to M.D.	Tensile Modulus, p.s.i. 60° to M.D.
1	4.9	93.8	31.1	3.0	142	152.7	32.0	73.7	39.8	2.0	2.7	2.0	2.5	589600	122330	306620	163050
2	4.6	111.8	32.4	3.4	259	236.0	50.7	112.8	63.5	2.9	3.5	2.8	3.2	728800	196420	454010	256010
3	4.9	100.7	31.4	3.2	196	208.0	41.4	99.6	52.9	2.3	3.7	2.6	3.3	687240	165000	406810	217040
4	3.1	80.7	27.1	3.0	139	156.5	38.6	87.1	49.6	1.4	3.2	1.9	2.5	702470	179100	405900	238440
5	3.8	70.1	27.0	2.6	104	107.9	26.7	60.5	34.0	1.5	2.2	1.7	1.9	518470	128470	308330	169450
6	5.8	82.9	25.5	3.2	182	190.0	41.0	101.0	52.1	1.8	3.2	2.3	2.5	826190	219820	531900	279350
7	7.8	99.7	30.4	3.3	137	158.4	40.6	90.8	50.7	1.4	3.0	1.7	2.3	702100	180020	464710	235410
8	4.4	102.9	31.7	3.2	195	225.1	55.8	125.1	71.7	1.8	4.9	2.4	3.6	766470	199590	506480	272990
9	8.6	111.0	31.5	3.5	186	190.6	51.6	118.3	62.2	1.7	3.4	2.2	2.6	695460	192450	489160	242420
10	7.6	98.2	30.0	3.3	150	160.0	43.7	96.9	53.7	1.3	3.2	1.9	2.4	701630	189170	474780	249800
11	6.2	77.6	30.8	2.5	86	86.6	45.7	69.1	52.1	1.0	1.8	1.2	1.5	411610	210890	319600	246040
12	2.8	109.8	34.5	3.2	142	143.9	35.8	79.9	45.0	2.0	4.1	2.3	3.5	476340	107980	264290	148700
13	2.6	105.9	33.1	3.2	154	141.3	36.9	77.5	46.7	2.3	5.0	2.6	3.9	474520	113053	267900	162660
14	3.4	106.4	31.6	3.4	145	128.9	44.8	91.0	57.0	1.4	3.4	2.3	2.9	542630	173900	379700	223950
15	3.3	98.5	32.0	3.1	172	165.2	45.2	97.9	57.8	1.9	3.8	2.3	3.2	547730	162490	372510	219930
16	3.5	104.7	33.9	3.1	183	190.9	47.8	108.6	59.8	1.8	3.8	2.4	3.1	596980	165500	393660	216250
17	6.4	90.5	28.0	3.2	190	178.2	49.4	104.7	62.6	2.1	2.9	2.4	2.9	606940	200590	397700	253590
18	1.9	105.2	32.4	3.2	172	166.6	48.2	97.5	60.3	2.0	4.2	2.4	3.8	548030	145990	339050	200180
19	1.9	90.7	26.2	3.5	172	163.2	43.2	99.4	51.8	2.2	3.9	2.5	3.3	645840	189060	434680	248450
20	2.8	93.1	31.7	3.0	101	119.1	32.2	75.5	38.3	1.5	3.3	1.6	2.7	487320	117740	306670	137130
21	6.5	96.9	30.0	3.2	113	101.8	34.7	68.0	41.4	1.7	2.8	1.9	2.5	446060	151330	298600	189190

TABLE VI (Continued)

CORE STOCK PROPERTIES

Run No.	Tensile Stiffness, lb./in. M.D.	Tensile Stiffness, lb./in. C.D.	Tensile Stiffness, lb./in. 30° to M.D.	Tensile Stiffness, lb./in. 60° to M.D.	Modified Ring Compression, lb./in. M.D.	Modified Ring Compression, lb./in. C.D.	Modified Ring Compression, lb./in. 30° to M.D.	Modified Ring Compression, lb./in. 60° to M.D.	Taber Stiffness, g.cm. M.D.	Taber Stiffness, g.cm. C.D.	Tearing Strength, g. M.D.	Tearing Strength, g. C.D.	TAPPI Plybond, p.s.i.g.	Porosity, sec./100 cc.	Water Drop, sec.
1	18337	3804	9536	5071	50.0	24.8	38.5	29.1	684	148	348	488	114	62	584+
2	23613	6364	14710	8295	68.9	42.7	60.5	47.5	1031	272	560	771	167	228	129
3	21579	5181	12774	6815	61.0	34.1	48.4	39.1	854	194	500	694	153	131	64
4	19037	4854	11000	6462	48.2	26.7	39.0	30.8	570	136	351	516	127	62	252
5	13999	3469	8325	4575	42.0	19.9	30.4	23.8	360	86	242	343	109	63	410
6	21068	5605	13564	7123	54.9	31.8	45.7	36.0	546	133	392	594	137	126	600+
7	21344	5473	14127	7156	53.2	29.9	42.4	33.2	762	190	422	565	129	115	216
8	24297	6327	16055	8654	71.4	42.1	61.9	46.9	1027	255	499	665	177	132	113
9	21907	6062	15409	7636	68.0	39.7	56.0	44.6	828	242	556	769	145	115	36
10	21049	5675	14244	7494	54.7	32.6	43.4	36.5	739	197	409	580	144	165	388
11	12678	6496	9844	7578	42.0	30.6	34.6	31.5	419	190	285	318	110	11	600+
12	16434	3725	9118	5130	48.4	26.4	40.4	31.6	743	178	402	535	132	102	600+
13	15707	3742	8868	5384	50.5	26.6	39.5	33.2	648	172	380	523	136	111	313
14	17147	5495	11998	7077	65.4	39.2	50.3	43.6	732	202	423	587	173	188	600+
15	17528	5200	11920	7038	56.8	29.1	43.4	35.6	750	194	472	629	131	50	28
16	20238	5611	13345	7331	60.0	33.8	49.0	41.8	929	245	572	712	139	60	24
17	16994	5616	11136	7101	56.2	36.3	45.4	40.3	556	182	317	428	163	91	600+
18	17756	4730	10985	6486	55.8	32.6	44.8	38.4	705	200	410	536	141	96	160
19	16921	4953	11389	6509	54.5	32.9	44.6	36.2	476	129	311	439	162	173	150
20	15448	3732	9722	4347	44.6	23.1	34.8	27.0	551	134	252	354	121	95	270+
21	13382	4540	8958	5676	42.0	25.8	37.0	31.0	512	176	322	445	139	72	50

TABLE VII

AVERAGE PROPERTIES OF INNER AND OUTER LINERS

Property	Inner Liner	Outer Liner
Basis weight, lb./M ft.^{2}	51.5	53.0
Caliper, pt.	15.0	15.3
Density, lb./pt.	3.5	3.5
Bursting strength, p.s.i.g.	103	96
Tensile strength, lb./in.,		
M.D.	101.5	93.9
C.D.	19.1	18.6
30°	49.6	49.3
60°	23.4	22.0
Stretch, %, M.D.	2.1	1.9
C.D.	4.2	4.2
30°	2.5	2.4
60°	3.8	3.6
Tensile modulus (E), p.s.i.,		
M.D.	778,350	756,400
C.D.	130,490	115,740
30°	381,160	377,010
60°	167,910	151,220
Tensile stiffness (Et), lb./in.,		
M.D.	11,640	11,590
C.D.	1,948	1,773
30°	5,699	5,778
60°	2,510	2,317
Modified ring compression, lb./in.,		
M.D.	29.6	29.7
C.D.	15.2	14.9
30°	24.7	25.3
60°	18.0	17.5
Taber stiffness, g.cm., M.D.	127	130
C.D.	23	23
Tearing strength, g., M.D.	179	171
C.D.	353	327
TAPPI plybond, p.s.i.g.	150	146
Porosity, sec./100 cc.	97	118
Water drop, sec.	66	133

the core performance tests using the data from the 17 runs where nominal 0.030-inch core stocks were employed.

With the above in mind the correlations between core stock properties and core stock performance are summarized in Table VIII. The intercorrelation coefficients between paper properties are shown in Appendix II.

Side Crush

The five properties which gave the highest correlation coefficients with side crush are listed below in order of decreasing correlation coefficient:

	Correlation Coefficient
1. Modified ring compression, 30° to M.D.	0.89
2. Modified ring compression, 60° to M.D.	0.89
3. Modified ring compression, M.D.	0.87
4. Modified ring compression, C.D.	0.87
5. Bursting strength	0.85

All of the above coefficients were statistically significant beyond the 0.01 level. As may be noted, the edgewise compression strength of the core stock as measured by the modified ring compression test was best related to side crush strength. The high coefficient obtained with the 30° orientation is explained by the fact that the bending and direct compression stresses generated in the side crush test are oriented at 30° to the M.D. for these cores, i.e., at the complement of the winding angle. It may be remarked that the correlation coefficients for the four modified ring compression orientations are nearly of the same magnitude. This is explained, in part at least, by the fact that the results for all four orientations are highly intercorrelated. For example, the results in Appendix II reveal that the intercorrelations between the four ring compression orientations are

TABLE VIII

RELATIONSHIP BETWEEN CORE PERFORMANCE AND CORE STOCK PROPERTIES FOR 0.030-INCH CORE STOCKS
(N = 17)

	Correlation Coefficient[a]					
			36-inch Beam		72-inch	
Core Stock Property	Side Crush	Axial Crush	First Peak	Maximum Load	Beam (Maximum)	Torque Strength
Weight	0.51	0.39	0.24	0.37	0.40	0.34
Caliper	0.17	-0.03	-0.18	-0.09	-0.07	-0.06
Density	0.44	0.44	0.34	0.46	0.48	0.40
Bursting strength	0.85	0.76	0.73	0.76	0.77	0.73
Tensile, M.D.	0.80	0.74	0.69	0.73	0.76	0.68
C.D.	0.69	0.85	0.90	0.89	0.88	0.87
30°	0.76	0.84	0.83	0.86	0.88	0.82
60°	0.75	0.87	0.91	0.90	0.90	0.90
Stretch, M.D.	0.57	0.29	0.23	0.26	0.25	0.29
C.D.	0.37	0.22	0.09	0.19	0.19	0.26
30°	0.72	0.52	0.44	0.52	0.50	0.54
60°	0.45	0.22	0.10	0.19	0.16	0.27
Tensile stiffness (Et), M.D.	0.68	0.71	0.64	0.69	0.75	0.60
C.D.	0.52	0.77	0.86	0.81	0.82	0.75
30°	0.60	0.79	0.77	0.79	0.84	0.71
60°	0.62	0.84	0.90	0.88	0.88	0.81
Modified ring compression, M.D.	0.87	0.90	0.83	0.90	0.92	0.87
C.D.	0.87	0.98	0.97	0.99	0.99	0.95
30°	0.89	0.93	0.87	0.91	0.94	0.88
60°	0.89	0.96	0.93	0.97	0.97	0.95
Taber stiffness, M.D.	0.75	0.71	0.61	0.67	0.72	0.63
C.D.	0.76	0.86	0.85	0.86	0.89	0.82
Tearing strength, M.D.	0.67	0.67	0.61	0.69	0.72	0.62
C.D.	0.68	0.67	0.58	0.68	0.72	0.60
TAPPI plybond	0.80	0.86	0.79	0.83	0.81	0.84
Porosity	0.66	0.63	0.49	0.58	0.61	0.54
Water drop	-0.18	-0.23	-0.22	-0.21	-0.24	-0.29

0.05 and 0.01 levels of significance are 0.482 and 0.605, respectively.

relatively high — ranging from 0.90 to 0.97. Further discussion of the effects of test orientation in terms of the behavior of orthotropic media may be found in the later sections of this report dealing with the engineering analyses of the various core tests.

Figure 7 illustrates the relationship between side crush and 30° modified ring compression for the 0.030-inch core stocks. The regression equation was as follows and observed and predicted values of side crush are shown in Table IX:

$$P_s = -0.605 + 1.215\, P_{m30} \qquad (24)$$

where

$\underline{P_s}$ = side crush, lb./in.

$\underline{P_{m30}}$ = modified ring compression, 30° to M.D., lb./in.

Thus, for the core size and construction employed in this study, it appears that the single property best related to side crush strength is the modified ring compression strength, preferably oriented at the complement of the winding angle.

As discussed in later pages the modified ring compression strength at any angle Θ to the M.D. appears to be well related to the M.D. and C.D. strengths by the following equation:

$$1/P_{m\Theta}^2 = (\cos^2\Theta/P_{mx}^2) + (\sin^2\Theta/P_{my}^2) \qquad (25)$$

where

$\underline{P_{m\Theta}}$ = modified ring compression strength at angle Θ, lb./in.

$\underline{P_{mx}}$ = modified ring compression strength in the machine direction, lb./in.

$\underline{P_{my}}$ = modified ring compression strength in the cross direction, lb./in.

Θ = angle from machine direction, deg.

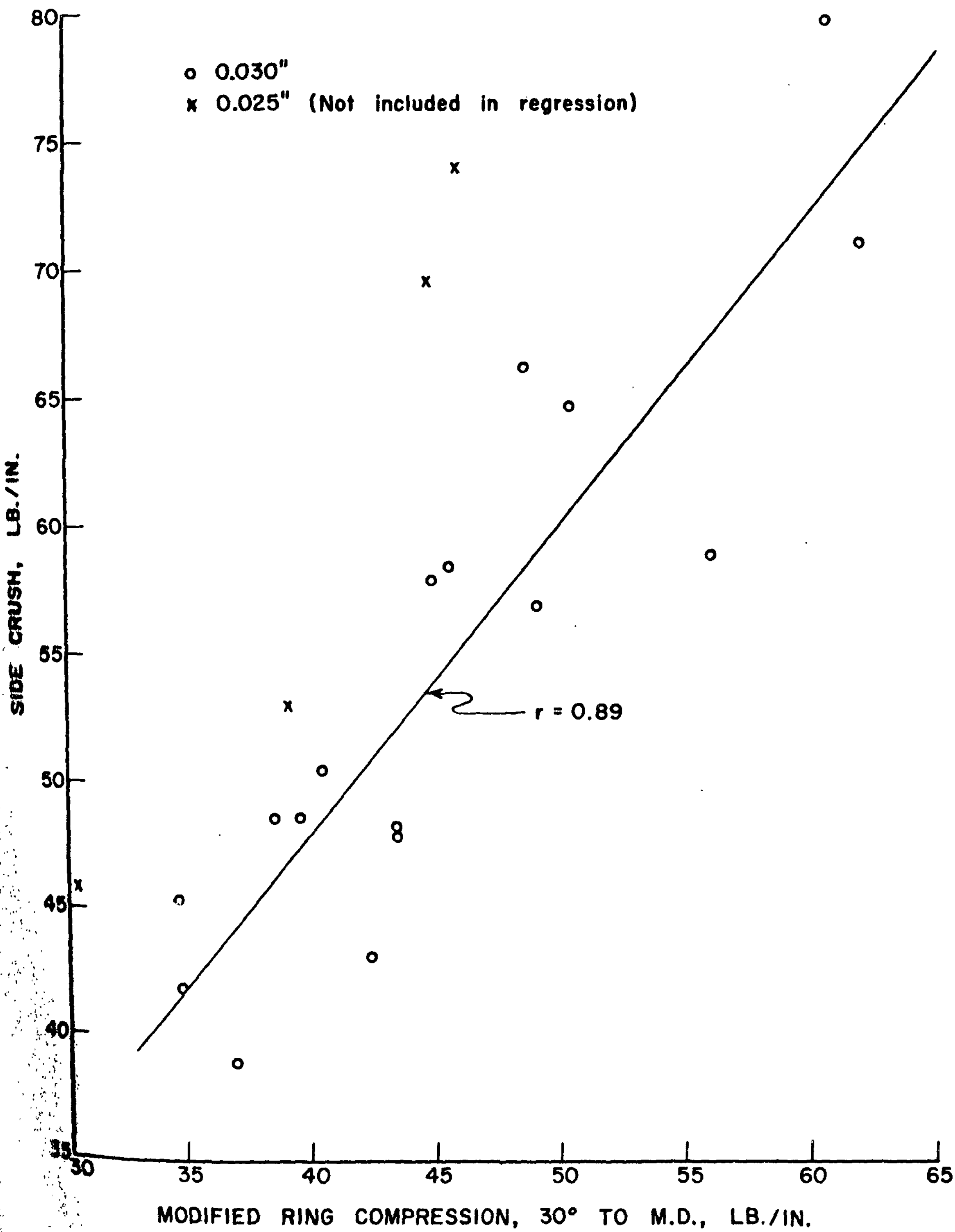

Figure 7. Relationship Between Side Crush and 30° Modified Ring Compression Load

TABLE IX

COMPARISON OF PREDICTED AND OBSERVED SIDE CRUSH VALUES USING STATISTICAL EQUATIONS

Run	Observed	Predicted Eq. (24)	Diff., %[a]	Predicted Eq. (26)	Diff., %[a]
1	48.5	46.2	- 4.8	45.9	- 5.3
2	79.8	72.9	- 8.6	73.7	- 7.7
3	66.2	58.2	- 12.1	58.4	-11.8
4	52.9	--	--	58.9	11.3
5	45.8	--	--	45.3	- 1.1
6	74.0	--	--	69.4	- 6.2
7	43.0	50.9	18.4	50.8	18.2
8	71.0	74.6	5.1	75.4	6.3
9	58.8	67.4	14.7	68.0	15.6
10	48.4	52.1	7.7	52.1	7.7
11	45.3	41.4	- 8.5	41.0	- 9.5
12	50.4	48.5	- 3.8	48.3	- 4.1
13	48.5	47.4	- 2.3	47.2	- 2.7
14	64.7	60.5	- 6.5	60.8	- 6.0
15	47.7	52.1	9.3	52.1	9.2
16	56.8	58.9	3.8	59.2	4.2
17	58.3	54.6	- 6.4	54.6	- 6.3
18	57.8	53.8	- 6.9	53.9	- 6.8
19	69.6	--	--	67.7	- 2.8
20	41.7	41.7	0.0	41.3	- 1.1
21	38.8	44.4	14.3	44.0	13.5
Av.			7.8		7.5

[a] Based on observed values as reference.

Note: Regression equations were as follows:

Eq. (24): $\underline{P}_{\underline{s}} = -0.605 + 1.215\ \underline{P}_{\underline{m}30}$

Eq. (26): $\underline{P}_{\underline{s}} = -2.64 + 0.158\ \underline{N}\ \underline{P}_{\underline{m}30}$

Using the above equation, the modified ring compression strengths at various angles may be estimated from the M.D. and C.D. modified ring compression strengths. Thus, the effect of improvements in M.D. and C.D. ring strengths on side crush may be estimated using Equations (24) and (25), although it is emphasized that Equation (24) strictly holds only for the particular core diameter and construction used herein. Equations of more general application are discussed in connection with the engineering analyses in later pages.

In Fig. 7 it may be noted that the four points representing 0.025-inch core stocks are located above and to the left of the regression line for the 0.030-inch core stocks. If the ring compression values are multiplied by the number of plies of core stock, a single regression line is obtained for both the 0.025 and 0.030-inch core stock runs. The resulting regression equation is shown below:

$$P_s = -2.64 + 0.158\ N\ P_{m30} \qquad (26)$$

where

P_s = side crush, lb./in.

P_{m30} = modified ring compression strength at 30° to M.D., lb./in.

N = number of plies of core stock

Equation (26) is a more general form of Equation (24) inasmuch as it ensated for the number of core stock plies for a core of a given diameter and thickness. While a more general equation which takes into account core geometry iscussed in the engineering analyses section, it may be of interest to compare prediction accuracies of Equations (24) and (26). These results are summarized ble IX. It may be noted that for the runs made with 0.030-inch core stock, the prediction error using Equation (24) was 7.8%. When both 0.025 and 0.030-re stocks were included in Equation (26), the resulting average error was 7.5%.

Thus, the results indicate that side crush strength is highly dependent on the modified ring compression strength of the core stock.

Generally speaking, natural phenomena often depend on more than one factor or variable. Mechanics of structures is no exception. For example, the bending deflection of a beam fabricated from fibrous materials depends on both the flexural stiffness and shear stiffness of the beam. There are essentially two ways to proceed in an empirical study of multiple-property relationships. One is to utilize theory as much as possible and explore those relationships suggested by theory. For example, theoretical considerations suggest the possible importance of edgewise compression and shear or edgewise compression and modulus in the case of side crush.

Another approach is to try all or a large number of combinations of properties through the use of statistical techniques such as stepwise multiple regression. This approach was believed to have disadvantages in the case of this study because of the large number of high intercorrelations between properties - a situation which can result in relationships having little or no basis in engineering theory.

For such reasons the study of multifactor relationships was limited to a few combinations of properties involving one additional factor along with 30° modified ring compression. The additional properties considered in conjunction with modified ring compression were: 30° tensile strength, 30° tensile stiffness, 30° stretch, bursting strength, TAPPI plybond, and porosity.

The two-factor regressions involving 30° modified ring compression and (a) 30° tensile strength, (b) 30° stretch, (c) bursting strength, (d) TAPPI plybond, and (e) porosity did not give statistically significant improvements in correlation or prediction accuracy; and in no case were the regression coefficients for the second property significant at the 0.05 level.

Some improvement in correlation was obtained using 30° modified ring and 30° tensile stiffness $(\underline{Et})_{30}$. The multiple correlation coefficient of 0.93 was higher than the coefficient for 30° modified ring alone (0.891). The average prediction accuracy for the two-factor relationship was 6.1% as compared to 7.8% for the 30° modified ring alone [Equation (24), Table IX]. The regression equation was as follows:

$$P_s = 1.31 + 1.74\, P_{m_{30}} - 0.00215(Et)_{30} \qquad (27)$$

In Equation (27) both factors were statistically significant at the 0.05 level or greater.

From a physical standpoint, tensile stiffness may be involved in side crush because the stress distribution will depend in part on the modulus of elasticity and its inelastic equivalent when the stress exceeds the proportional limit. Also, under side crush load there is some flattening of core cross section where the load is applied and the degree of flattening and resulting redistribution of stresses could depend, in part, on the tensile stiffness.

While additional multifactor statistical correlations could be investigated it was believed that further work along these lines should be held in abeyance until the results of the second phase are available. Therefore, to briefly summarize, the statistical analyses indicated that side crush was best related to 30° modified ring compression strength of the core stock. Small but significant improvements in predictive accuracy may be achieved by also considering the 30° tensile stiffness.

In addition to the above, it may be noted that close inspection of the side crush $\underline{vs}$. 30° ring results suggests that some property of the core stock — other than those evaluated for this study — may be involved. In this connection it may be recalled that observations of core failure in the side crush test indicate that ply delamination is evident as the initial peak load is approached. This suggests that the shear properties of the core stock may be a factor in side crush. Unfortunately, this is a difficult property to measure directly and none of the common paperboard tests directly measure either shear modulus or shear strength.

As one approach to indirectly investigate the possible importance of shear effects, the 36- and 72-in. beam data were utlized to obtain estimates of the ratio $(\underline{E}/\underline{G})_{60}$ — i.e., the ratio of bending modulus to shear modulus corresponding to the 60° angle of wind. This orientation, of course, does not match the 30° orientation which is believed to be directly involved in the side crush test for the cores of this study. However, it would be expected that $(\underline{E}/\underline{G})_{60}$ is probably fairly well related to $(\underline{E}/\underline{G})_{30}$.

With this in mind, the calculated ratios of $(\underline{E}/\underline{G})_{60}$ together with [illegible]$_{30}$ and $(\underline{Et})_{30}$ were correlated against side crush. The results are summarized in Table X. As may be noted, a significant improvement in correlation and prediction accuracy was obtained using the bending to shear modulus ratio $(\underline{E}/\underline{G})_{60}$ together with $\underline{N}\ \underline{P}_{\underline{m}30}$. A small additional improvement was achieved with the three-[illegible] regression involving $(\underline{Et})_{30}$ with the other two properties.

It is speculated that the above results indicate that the shear charac[illegible] of the core stock — modulus or perhaps more appropriately, shear [illegible] affect side crush though to a lesser extent than edgewise compression

TABLE X

COMPARISON OF SIDE CRUSH REGRESSION EQUATIONS INVOLVING THE BENDING TO SHEAR MODULUS RATIO

No.	Regression Equation	Multiple Correlation Coefficient	Average Prediction Error, %
1	$P_s = -2.64 + 0.158\ N\ P_{m30}$	0.908[a]	7.5
2	$P_s = 16.91 + 0.152\ N\ P_{m30} - 1.22\ (E/G)_{60}$	0.946[a]	5.6
3	$P_s = 16.62 + 0.183\ N\ P_{m30} - 1.09\ (E/G)_{60} - 0.00112\ (Et)_{30}$	0.956[b]	4.7

[a] Factor or factors significant at the 0.01 level.

[b] $N\ P_{m30}$ and $(E/G)_{60}$ significant at the 0.01 level; $(Et)_{30}$ significant at the 0.10 level.

strength. Consequently, it appears that investigation of ways of measuring shear properties of core stock would have merit.

Axial Crush

For the runs made with 0.030-inch core stocks the five properties which gave the highest correlation coefficients with axial crush are listed below in order of decreasing correlation coefficient.

		Correlation Coefficient
1.	Modified ring compression, C.D.	0.98
2.	Modified ring compression, 60° to M.D.	0.96
3.	Modified ring compression, 30° to M.D.	0.93
4.	Modified ring compression, M.D.	0.90
5.	Tensile strength, 60° to M.D.	0.87

The above coefficients were highly significant — beyond the 0.01 level. Other properties which also were highly correlated though to a lesser extent than the above included TAPPI plybond, tensile strength, tensile stiffness, and Taber stiffness.

It may be noted that axial crush was best related to the modified ring compression strength in the C.D. direction followed closely by the 60° to the M.D. orientation. In the axial test the compression stresses are applied at an angle corresponding to the angle of wind — i.e., 60° to the M.D. direction in the case of the cores of this study. Thus, on physical grounds it would be anticipated that the 60° orientation — i.e., the orientation corresponding to the angle of wind — would be best related to axial crush; however, the statistical results appear to indicate that the C.D. orientation is slightly better related to axial crush than the 60° ring compression orientation. The differences in correlation coefficient

(0.98 and 0.96) are quite small, however, and may result from test variability. Tenzer's (3) results also confirmed that axial crush is dependent on the orientation of the core stock. For these reasons it is believed that regression equations based on the modified ring compression oriented at the angle of wind may have more general application.

Figures 8 and 9 illustrate the relationship between axial crush and modified ring compression in the C.D. and 60° orientations, respectively, for the 0.030-inch core stocks. The regression equations are shown below and the prediction errors are summarized in Table XI:

$$P_a = 96.4 + 80.60\, P_{m60} \qquad (28)$$

$$P_a = 336.9 + 85.12\, P_{my} \qquad (29)$$

where

P_a = axial crush, lb.

P_{m60} = modified ring compression, 60° to M.D., lb./in.

P_{my} = modified ring compression, C.D., lb./in.

Thus, the above results indicate that the single property best related [illegible]al crush for the 0.030-inch core stocks is the modified ring compression [illegible] in either the C.D. direction or the direction corresponding to the angle [illegible].

In Fig. 8 and 9, the four points representing 0.025-inch core stock are [illegible] from the other points. As in the case of side crush a single regression [illegible] approximately fits the results for both core stock thicknesses may be [illegible] multiplying the ring compression values by the number of plies of core [illegible] resulting regression equations are shown below and the results are illustrated in Fig. 10 and 11:

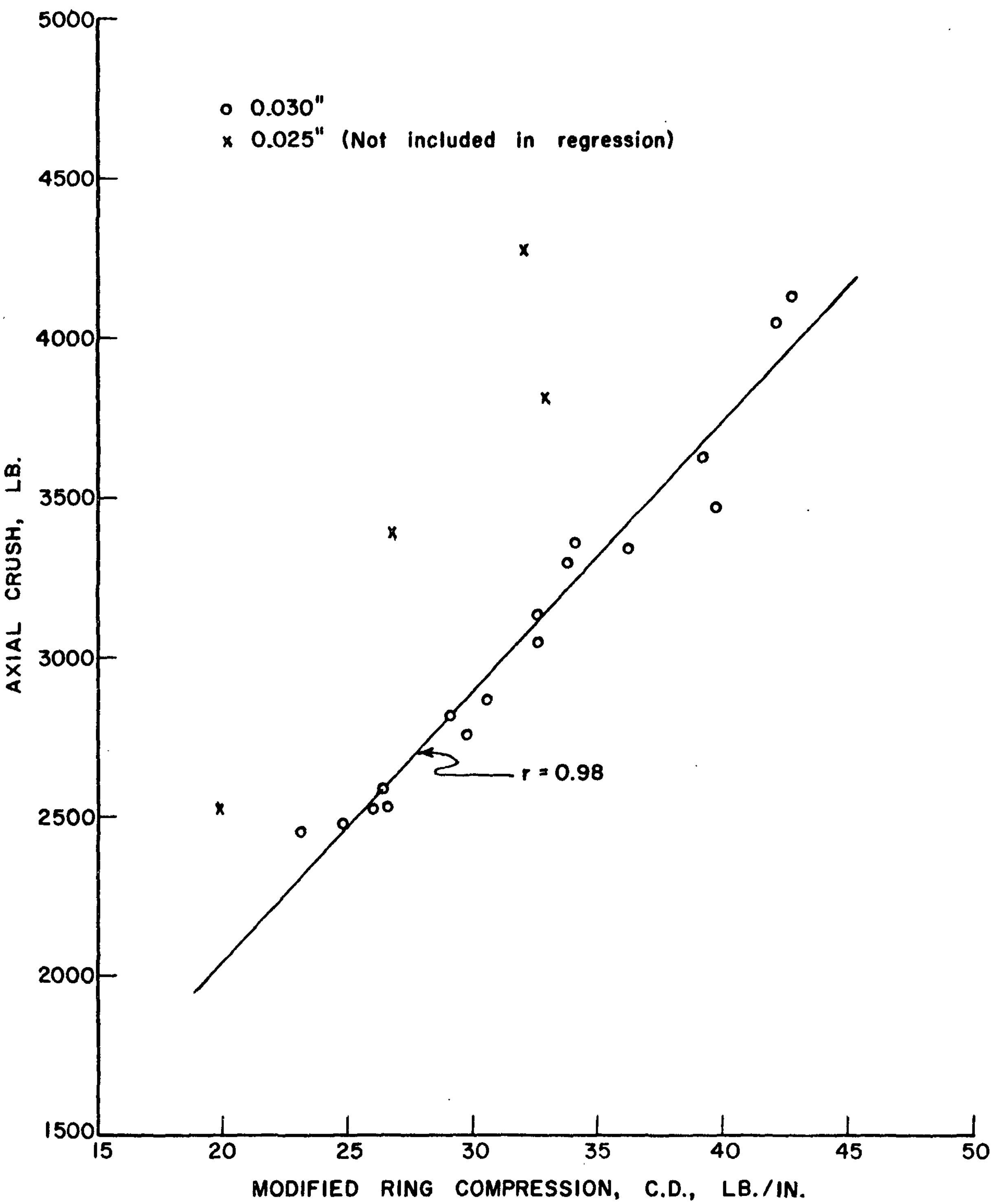

Figure 8. Relationship Between Axial Crush and C.D. Modified Ring Compression Strength

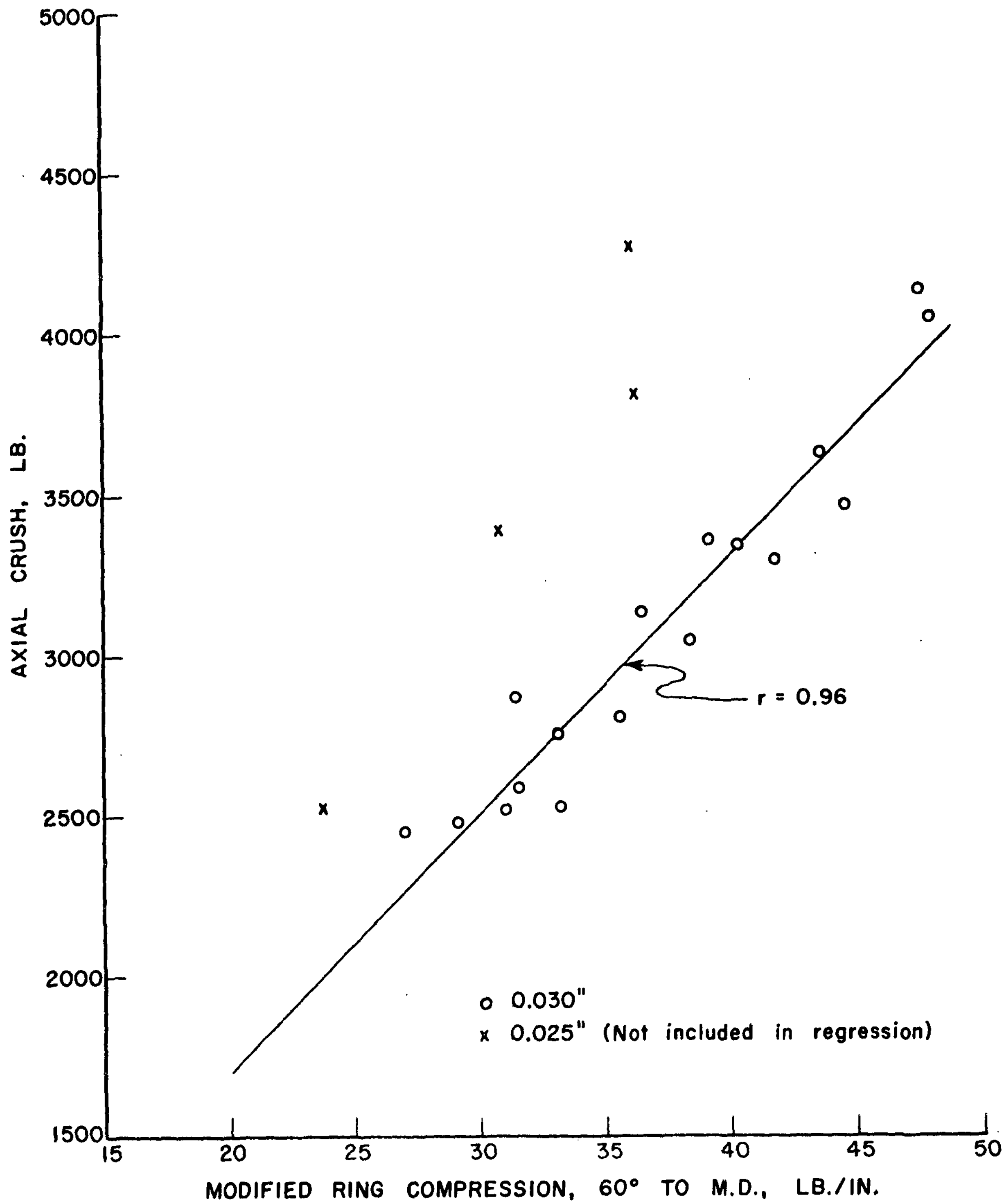

Figure 9. Relationship Between Axial Crush and 60° Modified Ring Compression

TABLE XI

COMPARISON OF OBSERVED AND PREDICTED AXIAL CRUSH LOADS BASED ON STATISTICAL EQUATIONS FOR 0.030-INCH CORE STOCKS

		Axial Crush, lb.							
Run	Observed	Predicted (Eq. 28)	Diff., %[a]	Predicted (Eq. 29)	Diff., %[a]	Predicted (Eq. 30)	Diff., %[a]	Predicted (Eq. 31)	Diff., %[a]
1	2483	2442	- 1.7	2448	- 1.4	2435	- 1.9	2454	- 1.2
2	4135	3925	- 5.1	3971	- 4.0	4021	- 2.8	4052	- 2.0
3	3360	3248	- 3.3	3239	- 3.6	3297	- 1.9	3284	- 2.3
4	3392	--	--	--	--	3245	- 4.3	3219	- 5.1
5	2527	--	--	--	--	2491	- 1.4	2460	- 2.6
6	4277	--	--	--	--	3805	-11.0	3788	-11.4
7	2756	2772	0.6	2882	4.6	2788	1.2	2909	5.6
8	4046	3877	- 4.2	3920	- 3.1	3969	- 1.9	3998	- 1.2
9	3468	3691	6.4	3716	- 7.2	3771	8.7	3784	9.1
10	3136	3038	- 3.1	3112	- 0.8	3073	- 2.0	3150	0.4
11	2867	2635	- 8.1	2941	2.6	2642	- 7.9	2972	3.6
12	2590	2643	2.1	2583	- 0.2	2650	2.3	2597	0.3
13	2533	2772	9.4	2601	2.7	2788	10.1	2614	3.2
14	3630	3611	- 0.5	3673	1.2	3685	1.5	3739	3.0
15	2814	2966	5.4	2814	0.0	2995	6.4	2838	0.8
16	3298	3466	5.1	3214	- 2.6	3530	7.0	3257	- 1.2
17	3344	3345	0.0	3427	2.5	3400	1.7	3480	4.1
18	3054	3191	4.5	3111	1.9	3237	6.0	3150	3.1
19	3816	--	--	--	--	3827	0.3	3911	2.5
20	2454	2273	- 7.4	2303	- 6.1	2254	- 8.2	2302	- 6.2
21	2522	2595	2.9	2532	0.4	2599	3.0	2543	0.8
Av.			4.1		2.6		4.4		3.3

[a] Based on observed values as reference.

Note: Eq. (28): $\underline{P}_{\underline{a}} = 96.4 + 80.60\ \underline{P}_{\underline{m}60}$

Eq. (29): $\underline{P}_{\underline{a}} = 336.9 + 85.12\ \underline{P}_{\underline{my}}$

Eq. (30): $\underline{P}_{\underline{a}} = -73.2 + 10.77\ \underline{N}\ \underline{P}_{\underline{m}60}$

Eq. (31): $\underline{P}_{\underline{a}} = 239.9 + 11.16\ \underline{N}\ \underline{P}_{\underline{my}}$

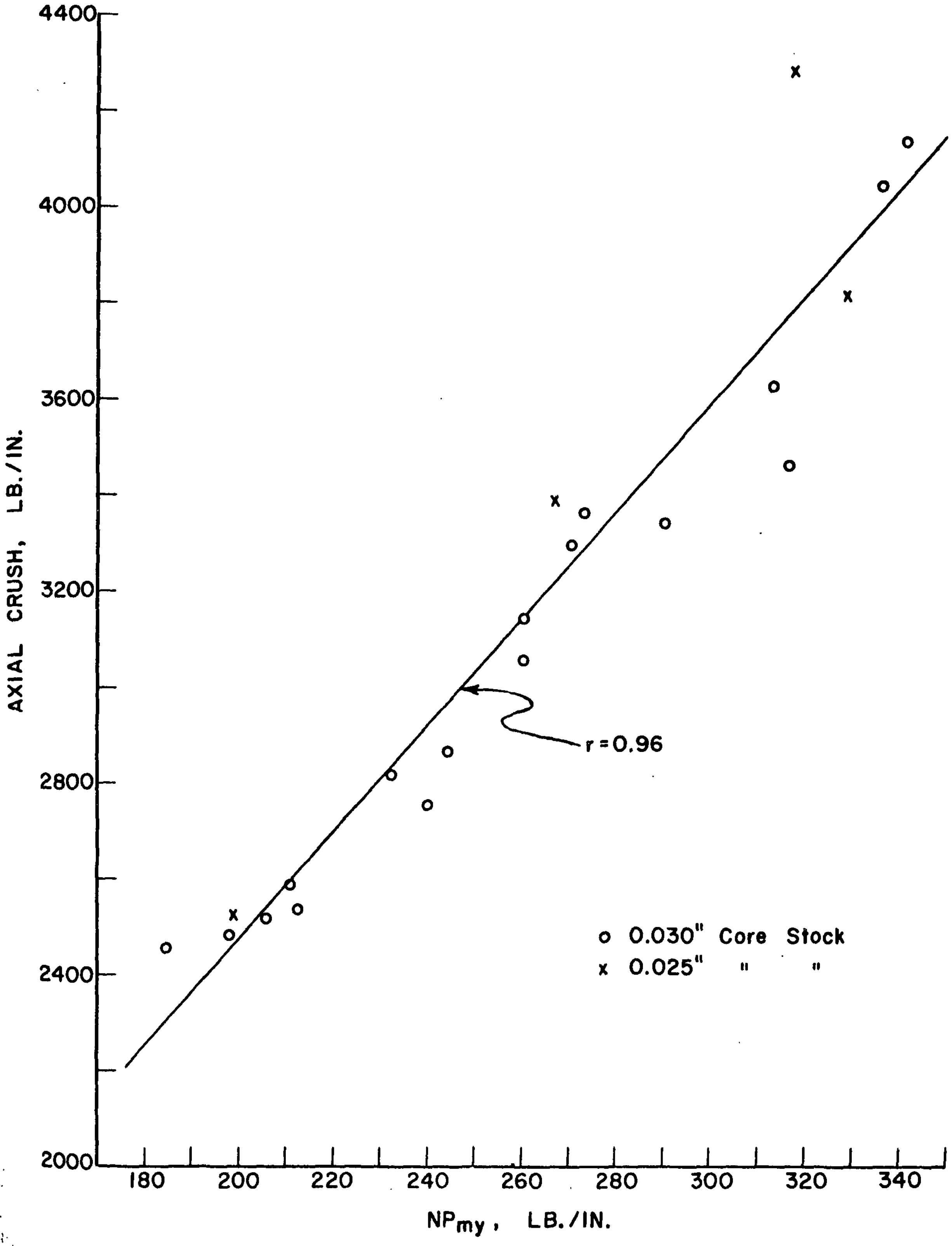

Figure 10. Relationship Between Axial Crush and NP_{my}

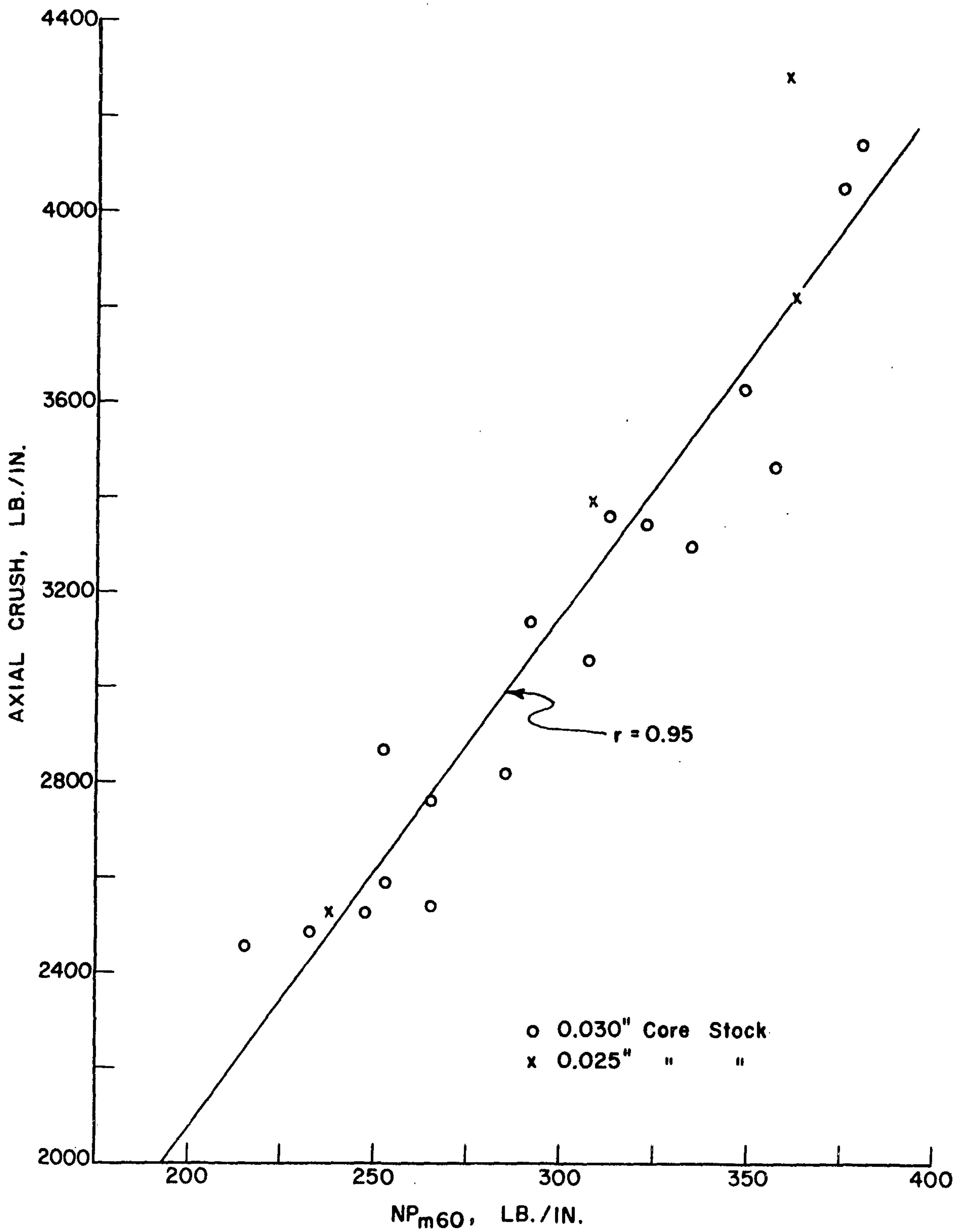

Figure 11. Relationship Between Axial Crush and NP_{m60}

$$P_a = -73.2 + 10.77\ N\ P_{m60} \qquad (30)$$

$$P_a = 239.9 + 11.16\ N\ P_{my} \qquad (31)$$

where

P_a = axial crush, lb.

P_{m60} = 60° modified ring compression, lb./in.

P_{my} = C.D. modified ring compression, lb./in.

N = number of core stock plies

As may be noted in Table XI, the average prediction errors for Equations (30) and (31) were only slightly greater than the average prediction errors obtained with Equations (28) and (29).

Two-factor multiple regressions were also investigated following the approach described previously in connection with the side crush results. However, none of the two-factor equations gave a statistically significant improvement in correlation with axial crush.

Beam Strength

For the runs made with 0.030-inch core stocks, the five properties which gave the highest correlation coefficients with beam strength are listed below in order of decreasing correlation coefficient.

	Correlation Coefficient	
	36-in. Beam	72-in. Beam
1. Modified ring compression, C.D.	0.99	0.99
2. Modified ring compression, 60° to M.D.	0.97	0.97
3. Modified ring compression, 30° to M.D.	0.91	0.94
4. Modified ring compression, M.D.	0.90	0.92
5. Tensile strength, 60° to M.D.	0.90	0.90

The above coefficients were highly significant and indicate that maximum beam strength is strongly dependent on the modified ring compression strength of the core stock. Other properties which were highly correlated with beam strength though to a lesser extent included C.D. Taber stiffness, plybond, tensile strength (C.D. and 30°), and tensile stiffness (C.D. and 60°).

It may be noted that beam strength was best related to the modified ring compression strength in the C.D. direction followed closely by the 60° to the M.D. orientation. On physical grounds it might be expected that the 60° orientation would be best related to beam strength; however, the above results indicate that the C.D. orientation is slightly better related to beam strength than the 60° orientation. The differences in correlation coefficient (0.99 and 0.97) are quite small, however, and may result from chance fluctuations due to test variability. On the other hand, it may be recalled that the same situation occurred in the case of axial crush. This may indicate there is an unknown factor involved — either in the ring tests or core tests — which favors the C.D. direction.

Figures 12 and 13 illustrate the relationship between 36-inch beam strength and modified ring compression in the C.D. and 60° orientations, respectively. Figures 14 and 15 show the corresponding results for the 72-inch beams. Inspection of the figures reveals that, in general, the data points for the 0.030-inch core stocks are closely clustered about the line of best fit — the least scatter being evident on the graphs of beam strength vs. C.D. ring compression.

The regression equations for the 0.030-inch core stocks are shown below and the prediction errors are summarized in Table XII:

36-inch beam

$$P_{36} = 53.10 + 8.395\,P_{m_{60}} \qquad (32)$$

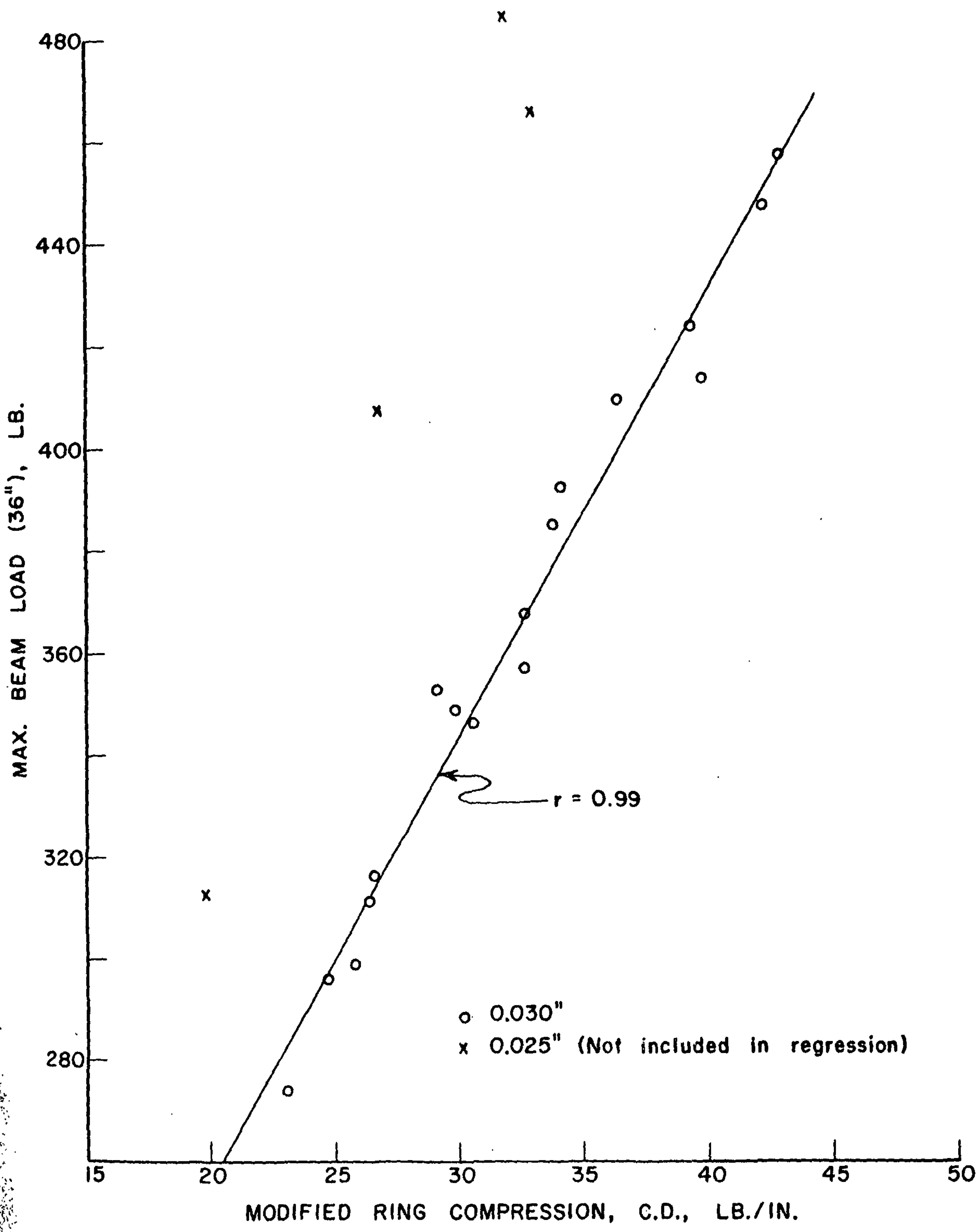

Figure 12. Relationship Between 36-Inch Beam Strength and C.D. Modified Ring Compression Strength

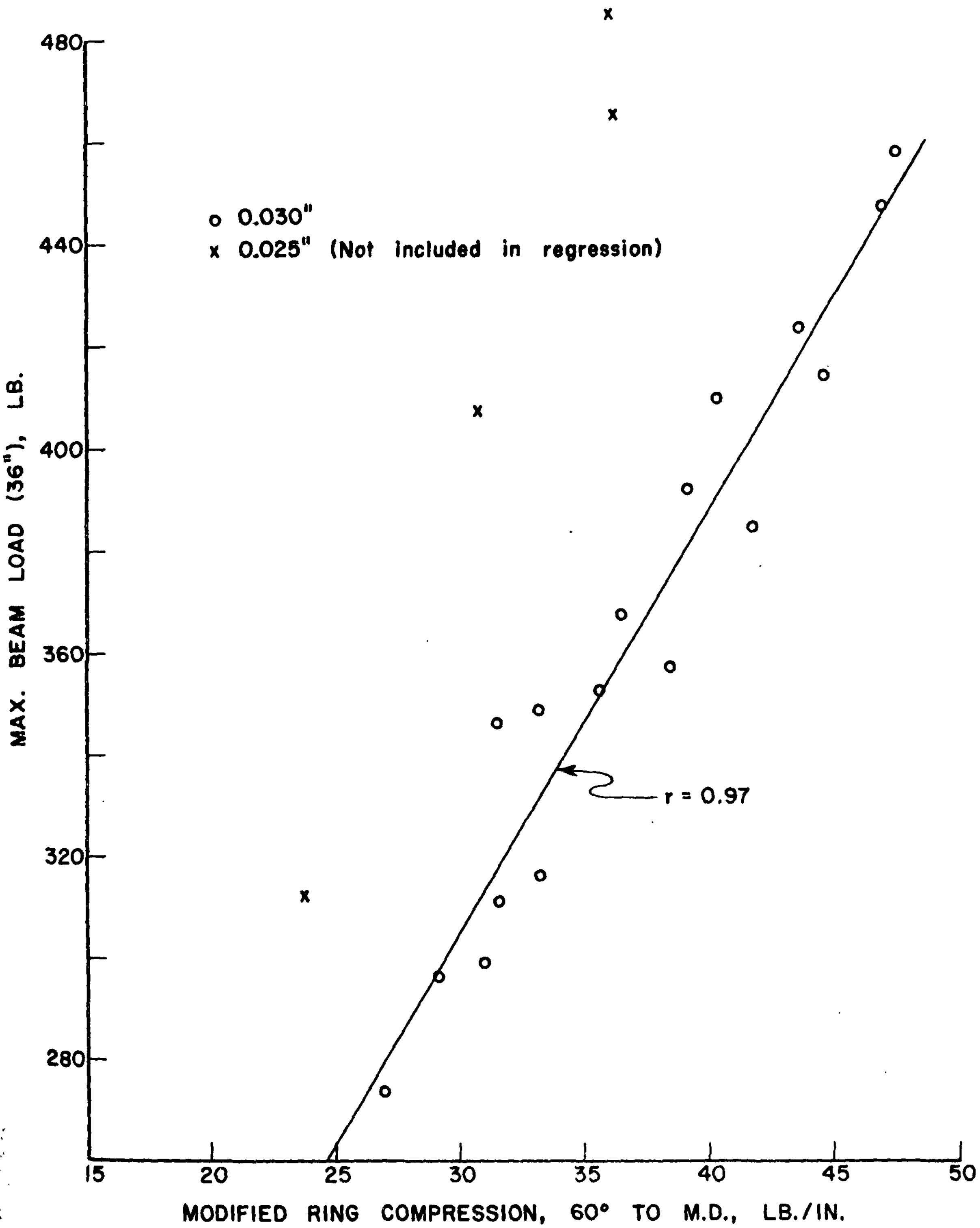

Figure 13. Relationship Between 36-Inch Beam Strength and 60° Modified Ring Compression Strength

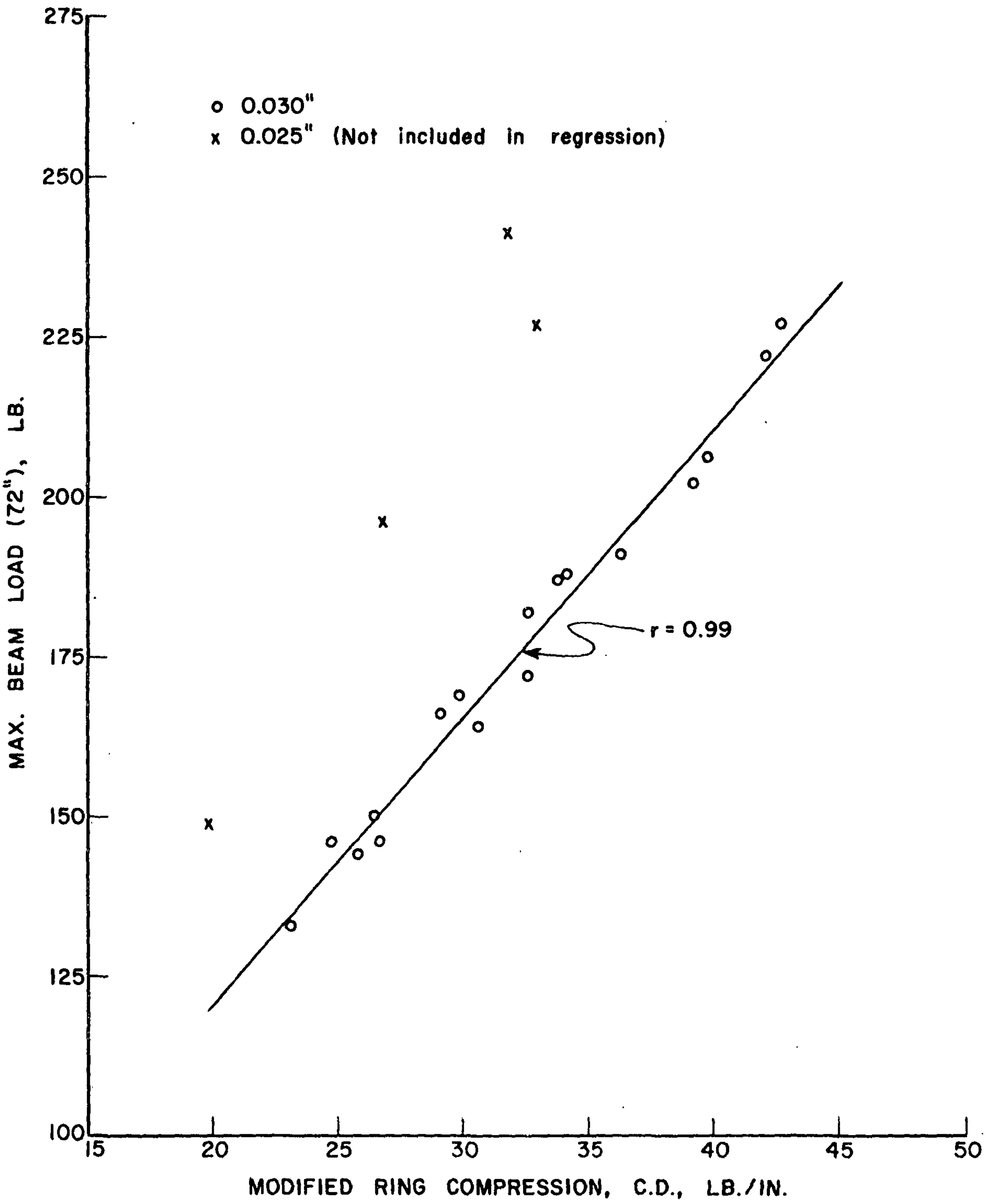

Figure 14. Relationship Between 72-Inch Beam Strength and C.D. Modified Ring Compression Strength

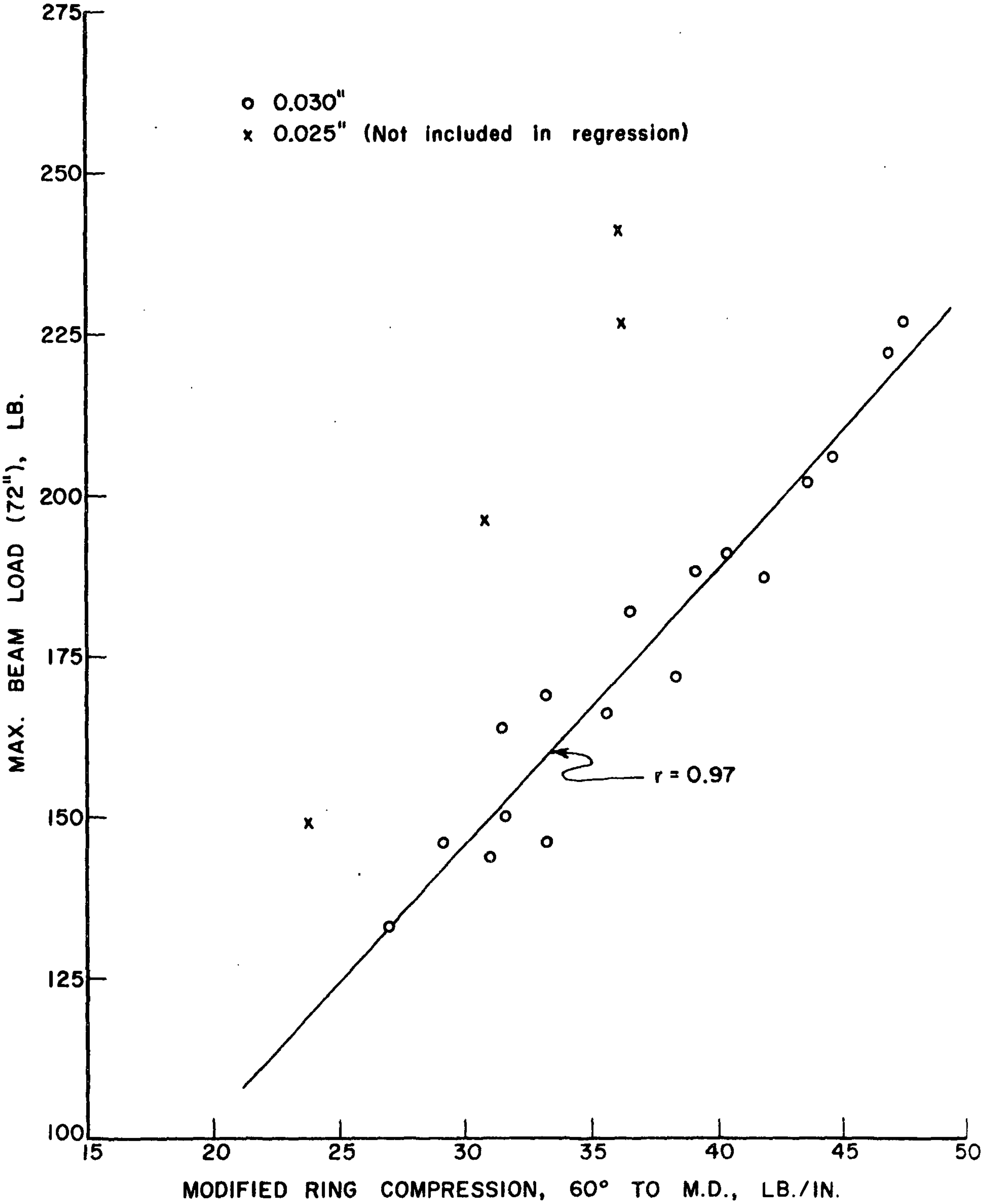

Figure 15. Relationship Between 72-Inch Beam Strength and 60° Modified Ring Compression Strength

TABLE XII

COMPARISON OF OBSERVED AND PREDICTED VALUES OF BEAM STRENGTH USING STATISTICAL EQUATIONS FOR 0.030-INCH CORE STOCKS

	36-in. Beam Strength, lb.					72-in. Beam Strength, lb.				
Run	Observed	Predicted (Eq. 32)	Diff., %[a]	Predicted (Eq. 33)	Diff., %[a]	Observed	Predicted (Eq. 34)	Diff., %[a]	Predicted (Eq. 35)	Diff., %[a]
1	296	297.4	0.5	298.0	0.7	146	141.9	- 2.8	142.2	- 2.6
2	458	451.9	- 1.3	456.7	- 0.3	227	220.6	- 2.8	223.1	- 1.7
3	392	381.3	- 2.7	380.4	- 2.9	188	184.7	- 1.8	184.2	- 2.0
4	407	--	--	--	--	196	--	--	--	--
5	312	--	--	--	--	149	--	--	--	--
6	485	--	--	--	--	241	--	--	--	--
7	349	331.9	- 4.9	343.2	- 1.7	169	159.5	- 5.6	165.2	- 2.2
8	448	446.8	- 0.3	451.4	0.8	222	218.0	- 1.8	220.4	- 0.7
9	414	427.5	- 3.3	430.1	3.9	206	208.2	1.1	209.6	1.7
10	367	359.5	- 2.0	367.2	0.0	182	173.6	- 4.6	177.5	- 2.5
11	346	317.5	- 8.2	349.4	1.0	164	152.2	- 7.2	168.4	2.7
12	311	318.4	2.4	312.2	0.4	150	152.6	- 1.7	149.4	- 0.4
13	316	331.8	5.0	314.0	- 0.7	146	159.5	9.2	150.3	3.0
14	424	419.1	- 1.2	425.7	0.4	202	203.9	0.9	207.3	2.6
15	353	352.0	- 0.3	336.1	- 4.8	166	169.7	2.2	161.6	- 2.6
16	385	404.0	4.9	377.8	- 1.9	187	196.2	4.9	182.9	- 2.2
17	410	391.4	- 4.5	400.0	- 2.5	191	189.8	- 0.6	194.2	1.7
18	357	375.5	5.2	367.2	2.8	172	181.7	5.6	177.5	3.2
19	466	--	--	--	--	227	--	--	--	--
20	274	279.8	2.1	282.9	3.3	133	133.0	0.0	134.5	1.1
21	299	313.3	4.8	306.9	2.6	144	150.1	4.2	146.7	1.9
Av.			3.2		1.8			3.4		2.0

[a]Based on observed values as reference.

Note: Regression equations were as follows:

Eq. (32): $\underline{P}_{36} = 53.10 + 8.395\ \underline{P}_{\underline{m}60}$

Eq. (33): $\underline{P}_{36} = 78.12 + 8.866\ \underline{P}_{\underline{my}}$

Eq. (34): $\underline{P}_{72} = 17.57 + 4.274\ \underline{P}_{\underline{m}60}$

Eq. (35): $\underline{P}_{72} = 29.97 + 4.524\ \underline{P}_{\underline{my}}$

$$P_{36} = 78.12 + 8.866\ P_{my} \quad (33)$$

72-inch beam

$$P_{72} = 17.57 + 4.274\ P_{m60} \quad (34)$$

$$P_{72} = 29.97 + 4.524\ P_{my} \quad (35)$$

where

P_{36} and P_{72} = beam strengths for 36- and 72-inch spans, respectively, lb.

P_{m60} = modified ring compression strength at 60° to M.D., lb./in.

P_{my} = modified ring compression strength, C.D., lb./in.

In Table XII it may be noted that the average prediction errors for the 0.030-inch core stock runs were 1.8 and 2.0% for the 36- and 72-inch beam strengths, respectively, when the C.D. ring compression was used [Equations (33) and (35)]. Slightly greater average prediction errors (3.2 and 3.4%) were obtained using the 60° modified ring strengths [Equations (32) and (34)]. As mentioned previously, there is no obvious explanation for the fact that slightly better predictions were obtained using C.D. ring strength rather than the ring strength oriented at the angle of wind. It is known, however, that beam strength varies as the angle of wind is changed (9). This implies that the strength property governing failure should be measured in the direction corresponding to the angle of wind. For this reason it appears that the equations based on modified ring compression at 60° to the M.D. should be favored.

The primary value of the above regression equations is to indicate what properties of the core stock are important inasmuch as they are strictly applicable to the particular core size construction used herein. More general equations which take into account core geometry are discussed in the engineering analyses.

While Equations (32)-(35) were restricted to the 0.030-inch core stock runs, the equations may be generalized to also include the 0.025-inch core stocks. This may be done by multiplying the modified ring strength by the number of core plies involved, namely, eight for 0.030-inch core stocks and ten for 0.025-inch core stocks. The following regression equations were obtained and the results for Equations (36) and (38) are graphed in Fig. 16 and 17:

36-inch beams

$$P_{36} = 31.1 + 1.143\ N\ P_{m60} \tag{36}$$

$$P_{36} = 63.6 + 1.186\ N\ P_{my} \tag{37}$$

72-inch beams

$$P_{72} = 5.41 + 0.585\ N\ P_{m60} \tag{38}$$

$$P_{72} = 21.84 + 0.608\ N\ P_{my} \tag{39}$$

where

P_{36} and P_{72} = maximum beam strength for 36- and 72-inch spans, respectively, lb.

P_{m60} = modified ring compression strength at 60° to M.D., lb./in.

P_{my} = modified ring compression strength, C.D., lb./in.

N = number of plies of core stock

For the twenty-one runs involving both 0.025- and 0.030-inch core stocks the correlation coefficients for Equations (36)-(39) ranged from 0.95 to 0.97 — nearly as high as obtained in the first correlations involving only 0.030-inch core stocks. The average prediction errors in Table XIII for Equations (36)-(39) range from 2.9 to 4.2% — only slightly greater than the average errors obtained in Table XII for the 0.030-inch core stock runs only. Thus, for the core diameter and

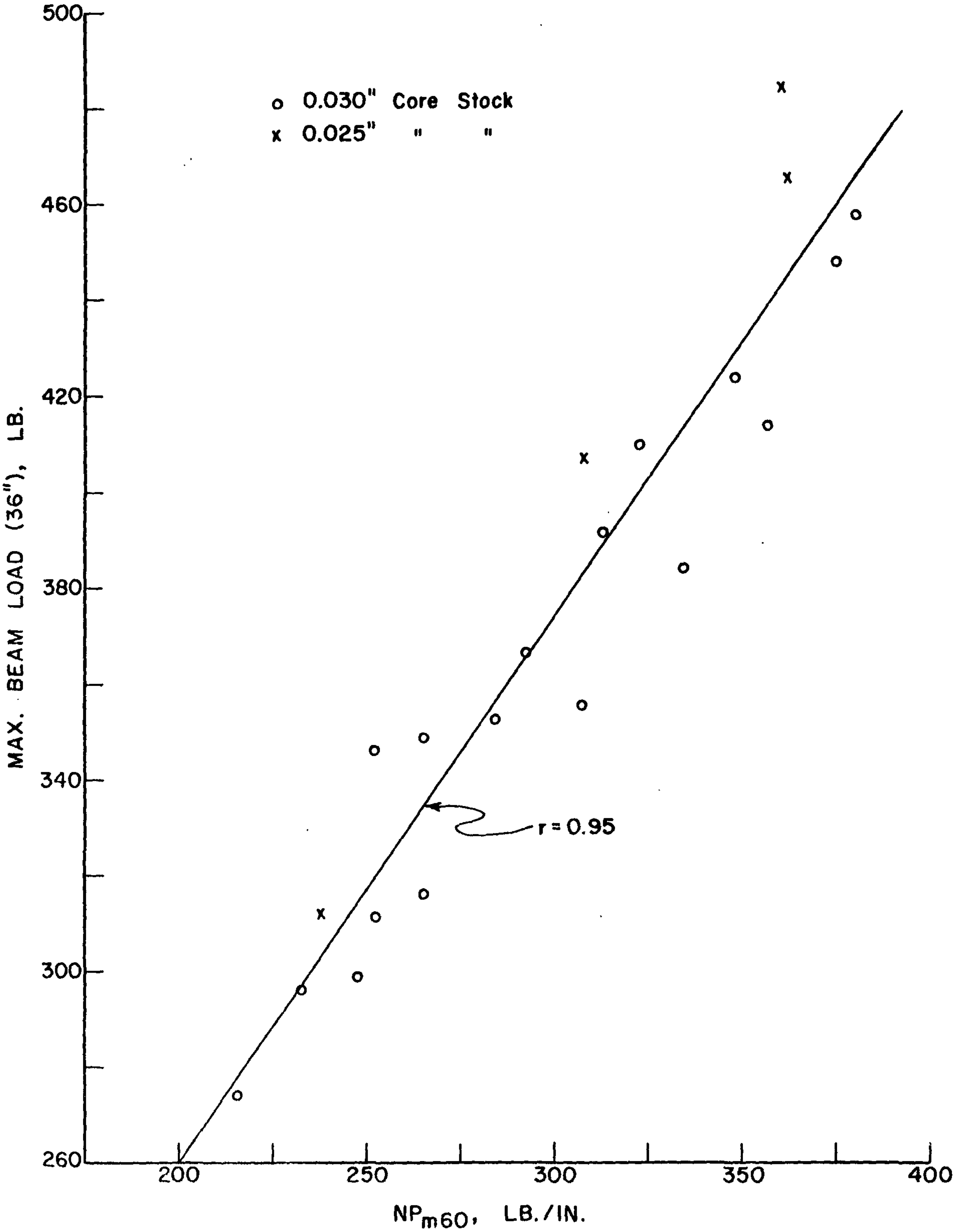

Figure 16. Relationship Between 36-Inch Beam Strength and $\underline{N}$ $\underline{P}_{m60}$

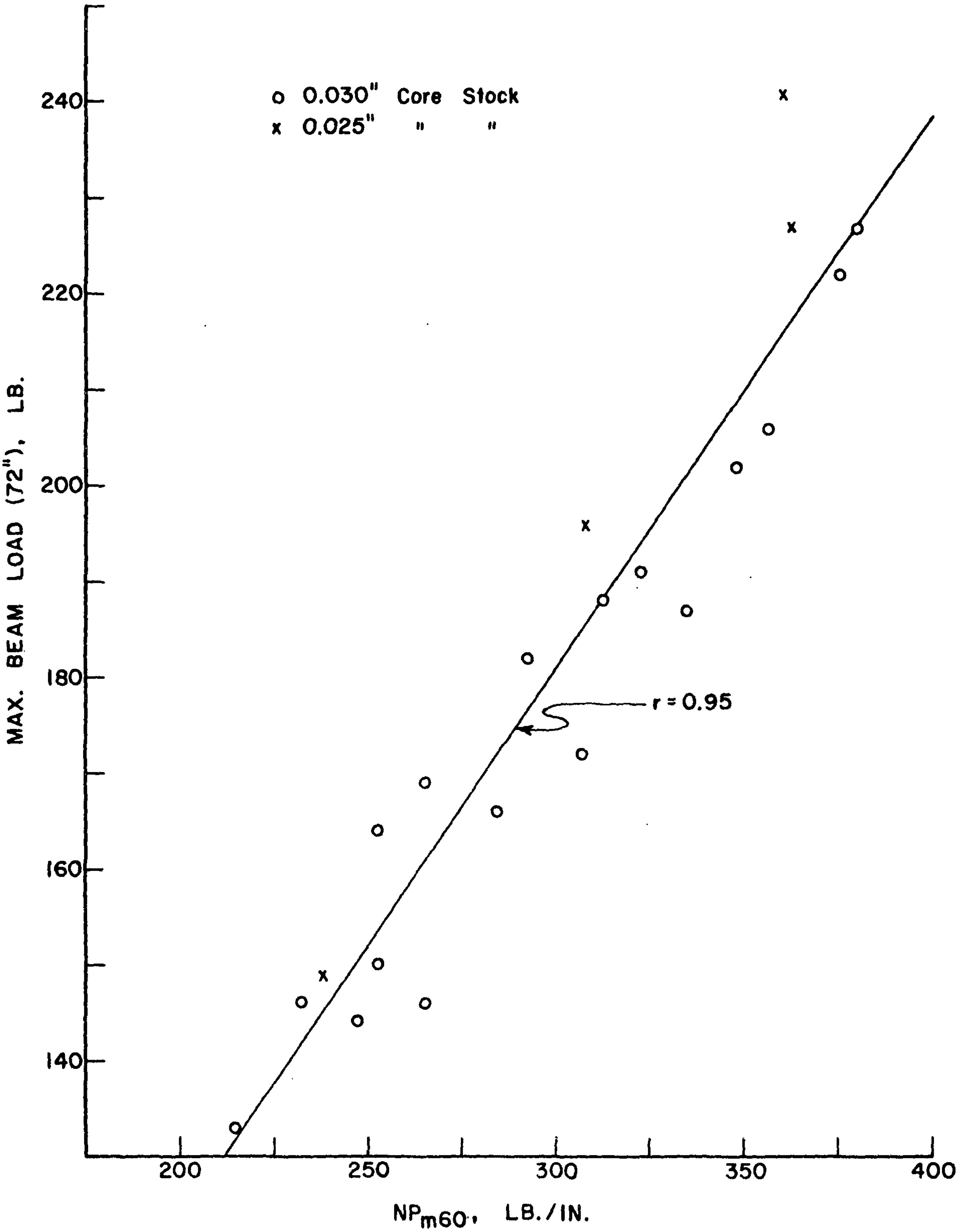

Figure 17. Relationship Between 72-Inch Beam Strength and NP_{m60}

TABLE XIII

COMPARISON OF OBSERVED AND PREDICTED VALUES OF BEAM STRENGTH CORRECTING FOR NUMBER OF PLIES

Run	36-in. Beam Strength, lb. Observed	Predicted (Eq. 36)	Diff., %[a]	Predicted (Eq. 37)	Diff., %[a]	72-in. Beam Strength, lb. Observed	Predicted (Eq. 38)	Diff., %[a]	Predicted (Eq. 39)	Diff., %[a]
1	296	297.1	0.4	298.9	1.0	146	141.6	- 3.0	142.5	- 2.4
2	458	465.3	1.6	468.8	2.4	227	227.7	0.3	229.6	1.1
3	392	388.5	- 0.9	387.2	- 1.2	188	188.4	0.2	187.7	- 0.1
4	407	383.0	- 5.9	380.3	- 6.6	196	185.6	- 5.3	184.2	- 6.0
5	312	303.0	- 2.9	299.6	- 4.0	149	144.6	- 2.9	142.8	- 4.1
6	485	442.4	- 8.8	440.8	- 9.1	241	216.0	-10.4	215.2	-10.7
7	349	334.6	- 4.1	347.3	- 0.5	169	160.8	- 4.9	167.3	- 1.0
8	448	459.8	2.6	463.1	3.4	222	224.9	1.3	226.6	2.1
9	414	438.8	6.0	440.3	6.4	206	214.1	4.0	215.0	4.4
10	367	364.7	- 0.6	372.9	1.6	182	176.2	- 3.2	180.4	- 0.9
11	346	319.0	- 7.8	354.0	2.3	164	152.8	- 6.8	170.7	4.1
12	311	320.0	2.9	314.1	1.0	150	153.3	2.2	150.3	0.2
13	316	334.6	5.9	316.0	0.0	146	160.8	10.1	151.2	3.6
14	424	429.6	1.3	435.6	2.7	202	209.5	3.7	212.5	5.2
15	353	356.5	1.0	339.7	- 3.8	166	172.0	3.6	163.4	- 1.6
16	385	413.2	7.3	384.3	- 0.2	187	201.0	7.5	186.3	- 0.4
17	410	399.5	- 2.6	408.0	- 0.5	191	194.0	1.6	198.4	3.9
18	357	382.1	7.0	372.9	4.5	172	185.1	7.6	180.4	4.9
19	466	444.7	- 4.6	453.8	- 2.6	227	217.1	- 4.3	221.9	- 2.2
20	274	277.9	1.4	282.8	3.2	133	131.8	- 0.9	134.2	0.9
21	299	314.5	5.2	308.4	3.2	144	150.5	4.5	147.3	2.3
Av.			3.8		2.9			4.2		3.0

[a] Based on observed values as reference.

Note: Regression equations were as follows:

Eq. (36): $\underline{P}_{36} = 31.1 + 1.143\ \underline{N}\ \underline{P}_{\underline{m}60}$

Eq. (37): $\underline{P}_{36} = 63.6 + 1.186\ \underline{N}\ \underline{P}_{\underline{my}}$

Eq. (38): $\underline{P}_{72} = 5.41 + 0.585\ \underline{N}\ \underline{P}_{\underline{m}60}$

Eq. (39): $\underline{P}_{72} = 21.84 + 0.608\ \underline{N}\ \underline{P}_{\underline{my}}$

constructions used in this study, the results indicate that beam strength is best related to the modified ring compression strength of the core stock.

A number of two-factor multiple regressions were also investigated following the approach described previously in connection with the side crush results. However, none of the two-factor equations appeared to result in a statistically significant improvement in correlation with beam strength.

Torque Strength

For the runs made with 0.030-inch core stocks the seven properties which exhibited the highest correlation coefficients with torque strength were as follows (listed in order of decreasing correlation coefficient):

	Correlation Coefficient
1. Modified ring compression, C.D.	0.95
2. Modified ring compression, 60° to M.D.	0.95
3. Tensile strength, 60° to M.D.	0.90
4. Modified ring compression, 30° to M.D.	0.88
5. Modified ring compression, M.D.	0.87
6. Tensile strength, C.D.	0.87
7. Tensile stiffness, 60° to M.D.	0.87

The above coefficients were highly significant and indicate that torque strength is most highly dependent on the modified ring compression strength of the core stock. Other properties which were highly correlated with torque strength though to a lesser extent included plybond and C.D. Taber stiffness.

As mentioned previously, in the torque test equal shear stresses are induced on the plane of the section and on radial planes. At intermediate angles the stresses may be resolved, in general, into shear and "normal" (tension and compression) stresses. According to Roark (4) torque failure modes depend on the material — i.e., for some materials a shear failure mode is observed; for others failure occurs due to the "normal" stresses. For the latter case the fracture surface is usually helicoidal. As mentioned previously in the case of the cores evaluated for this study, the failure wrinkles followed the spiral pattern associated with the angle of wind. It appears quite possible that failure occurs when the "normal" compression stresses induced in the core walls exceed the compression strength of the material under combined stresses. Inasmuch as the edgewise compression strength of the core stock is a minimum in the cross direction this may be the limiting strength for this particular angle of wind (58°) and this would explain the high correlation coefficient obtained with C.D. modified ring compression. An equally high coefficient was obtained for the 60° orientation and this may result because of the relatively high intercorrelation between the C.D. and 60° orientations.

Figures 18 and 19 illustrate the relationship between torque strength and modified ring compression strength. As may be noted, the data for the runs made with 0.030-inch core stock are closely clustered about the regression line shown in the figures.

The regression equations for the 0.030-inch core stock runs are shown below and the prediction errors are summarized in Table XIV:

$$T = 495.04 + 105.84\, P_{my} \qquad (40)$$

$$T = 116.44 + 102.37\, P_{m60} \qquad (41)$$

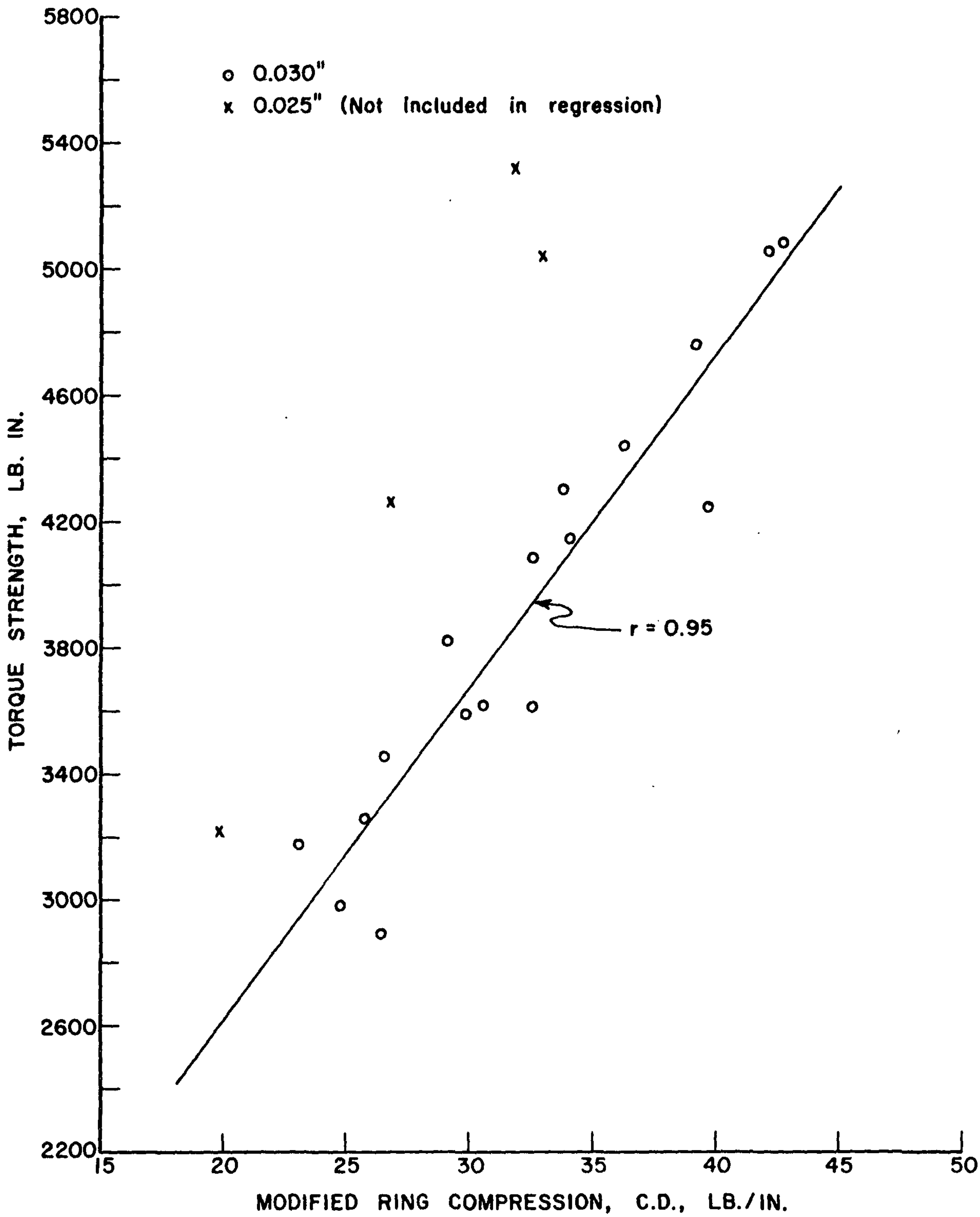

Figure 18. Relationship Between Torque Strength and C.D. Modified Ring Compression

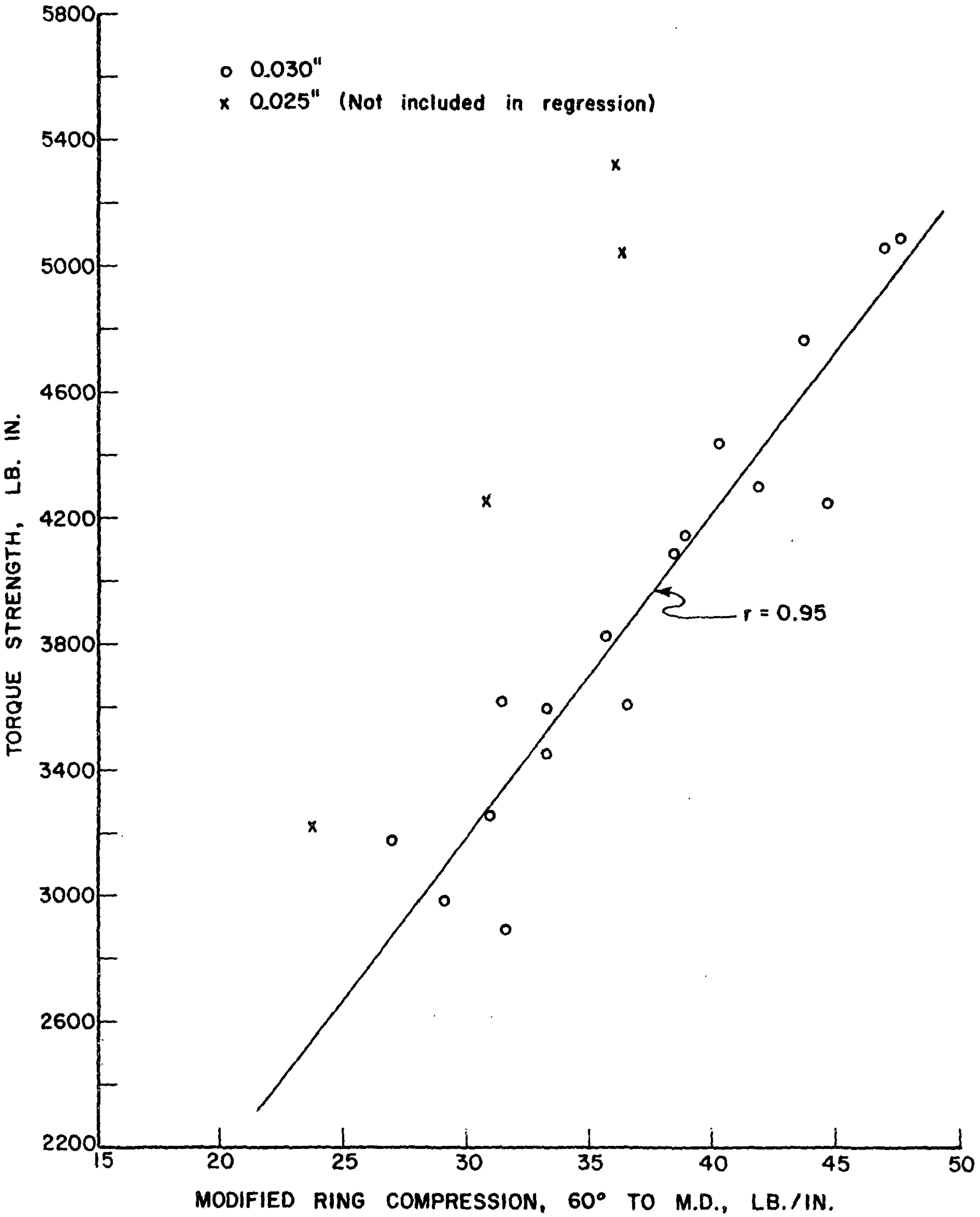

Figure 19. Relationship Between Torque Strength and 60° Modified Ring Compression

TABLE XIV

COMPARISON OF PREDICTED AND OBSERVED VALUES OF TORQUE STRENGTH

	Torque Strength, lb. in.								
Run	Observed	Predicted (Eq. 40)[b]	Diff., %[a]	Predicted (Eq. 41)[b]	Diff., %[a]	Predicted (Eq. 42)	Diff., %[a]	Predicted (Eq. 43)	Diff., %[a]
1	2982	3120	4.6	3095	3.8	3119	4.6	3084	3.4
2	5094	5014	- 1.6	4979	- 2.3	5138	0.9	5114	0.4
3	4152	4104	- 1.2	4119	- 0.8	4168	0.4	4187	0.8
4	4260	--	--	--	--	4087	- 4.1	4121	- 3.3
5	3222	--	--	--	--	3127	- 2.9	3155	- 2.1
6	5334	--	--	--	--	4806	- 9.9	4838	- 9.3
7	3594	3660	1.8	3515	- 2.2	3695	2.8	3536	- 1.6
8	5064	4951	- 2.2	4918	- 2.9	5071	0.1	5047	- 0.3
9	4254	4697	10.4	4682	10.1	4800	12.8	4794	12.7
10	3606	3945	9.4	3853	6.8	3999	10.9	3900	8.2
11	3618	3733	3.2	3342	- 7.7	3774	4.3	3348	- 7.5
12	2886	3289	14.0	3351	16.1	3300	14.3	3359	16.4
13	3456	3310	- 4.2	3515	1.7	3322	- 3.9	3536	2.3
14	4764	4644	- 2.5	4580	- 3.9	4744	- 0.4	4683	- 1.7
15	3822	3575	- 6.5	3761	- 1.6	3604	- 5.7	3801	- 0.6
16	4302	4072	- 5.3	4395	2.2	4135	- 3.9	4485	4.2
17	4440	4337	- 2.3	4242	- 4.5	4417	- 0.5	4319	- 2.7
18	4092	3945	- 3.6	4047	- 1.1	3999	- 2.3	4110	0.4
19	5046	--	--	--	--	4961	- 1.7	4865	- 3.6
20	3180	2940	- 7.5	2880	- 9.4	2928	- 7.9	2852	-10.3
21	3258	3226	- 0.1	3290	1.0	3232	- 0.8	3293	1.1
Av.			4.8		4.6		4.5		4.4

[a] Based on observed values as reference.
[b] For runs made with 0.030 in. core stocks.

Note: Regression equations were as follows:

Eq. (40) $\underline{T} = 495.04 + 105.84\ \underline{P}_{\underline{m}y}$

Eq. (41) $\underline{T} = 116.44 + 102.37\ \underline{P}_{\underline{m}60}$

Eq. (42) $\underline{T} = 321.9 + 14.10\ \underline{N}\ \underline{P}_{\underline{m}y}$

Eq. (43) $\underline{T} = 127.2 + 13.79\ \underline{N}\ \underline{P}_{\underline{m}60}$

where

$\underline{T}$ = torque strength, lb. in.

$\underline{P}_{\underline{my}}$ = modified ring compression strength, C.D., lb./in.

$\underline{P}_{\underline{m60}}$ = modified ring compression strength, 60° to M.D., lb./in.

The average prediction errors for Equations (40) and (41) were 4.8 and 4.6%, respectively. Thus, for a given diameter core and construction, torque strength is highly dependent on the modified ring compression strength of the core stock.

More general equations are discussed in the engineering analyses in later pages. However, as in the case of the other core performance tests the above equations may be generalized to include the 0.025-inch core stocks by multiplying the ring strength by the number of core plies involved, namely, eight for 0.030-inch core stocks and ten for 0.025-inch core stocks. The following regression lines were obtained.

$$T = 321.9 + 14.10 \; N \; P_{my} \qquad (42)$$

$$T = -127.2 + 13.79 \; N \; P_{m60} \qquad (43)$$

...re $\underline{N}$ = number of plies of core stock and the other symbols are as previously ...ined.

The above relationships are graphically illustrated in Fig. 20 and 21 and ...prediction errors are summarized in Table XIV. Referring to the table and ...o it may be noted that the average prediction errors over all twenty-one ...es were 4.5 and 4.4% for Equations (42) and (43), respectively. In comparison, ...erage prediction errors for Equations (40) and (41) for the seventeen 0.030- ...ore stock runs were 4.8 and 4.6%, respectively. Thus, for the core diameter ...structions used in this study, torque strength is best related to the modi- ...ing compression strength of the core stock.

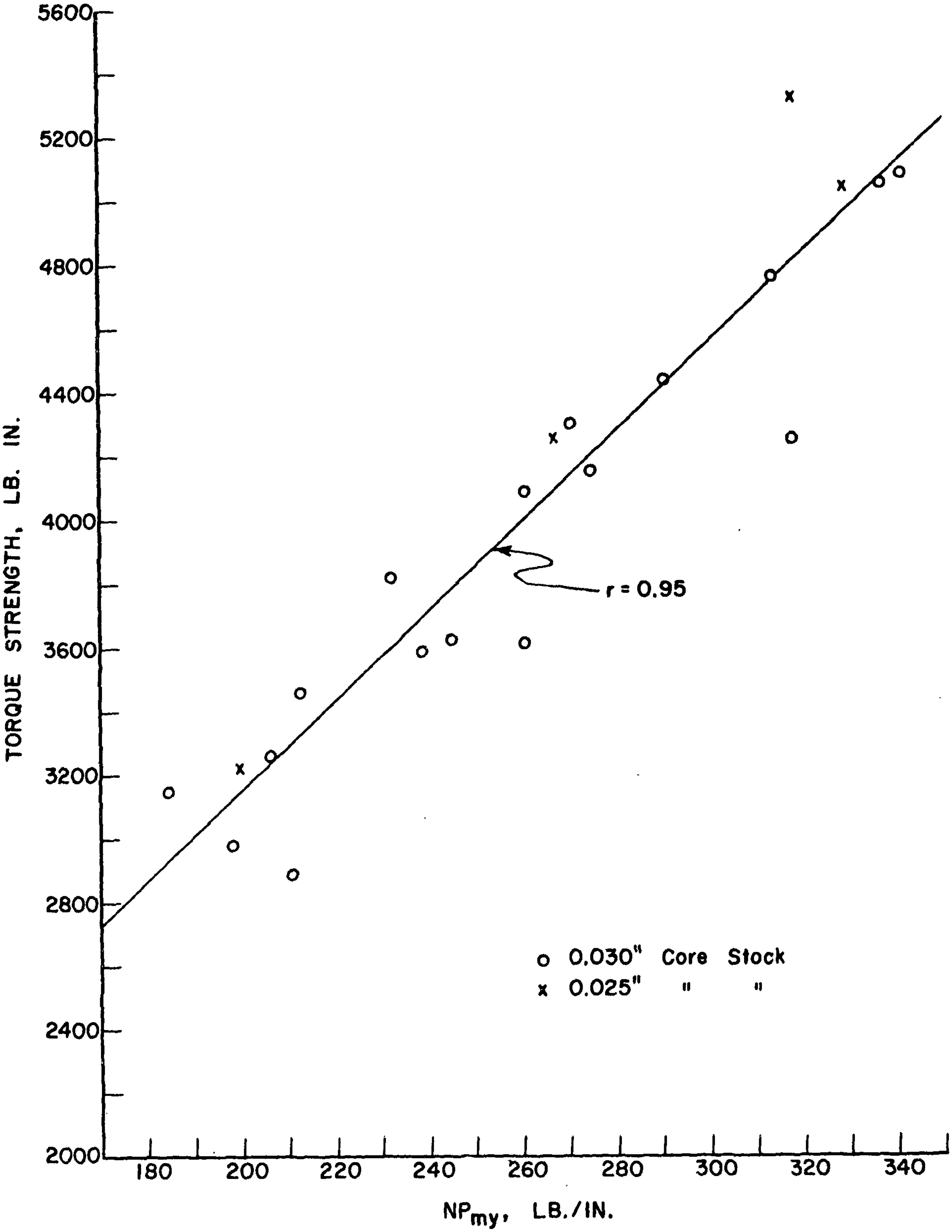

Figure 20. Relationship Between Torque Strength and NP_{my}

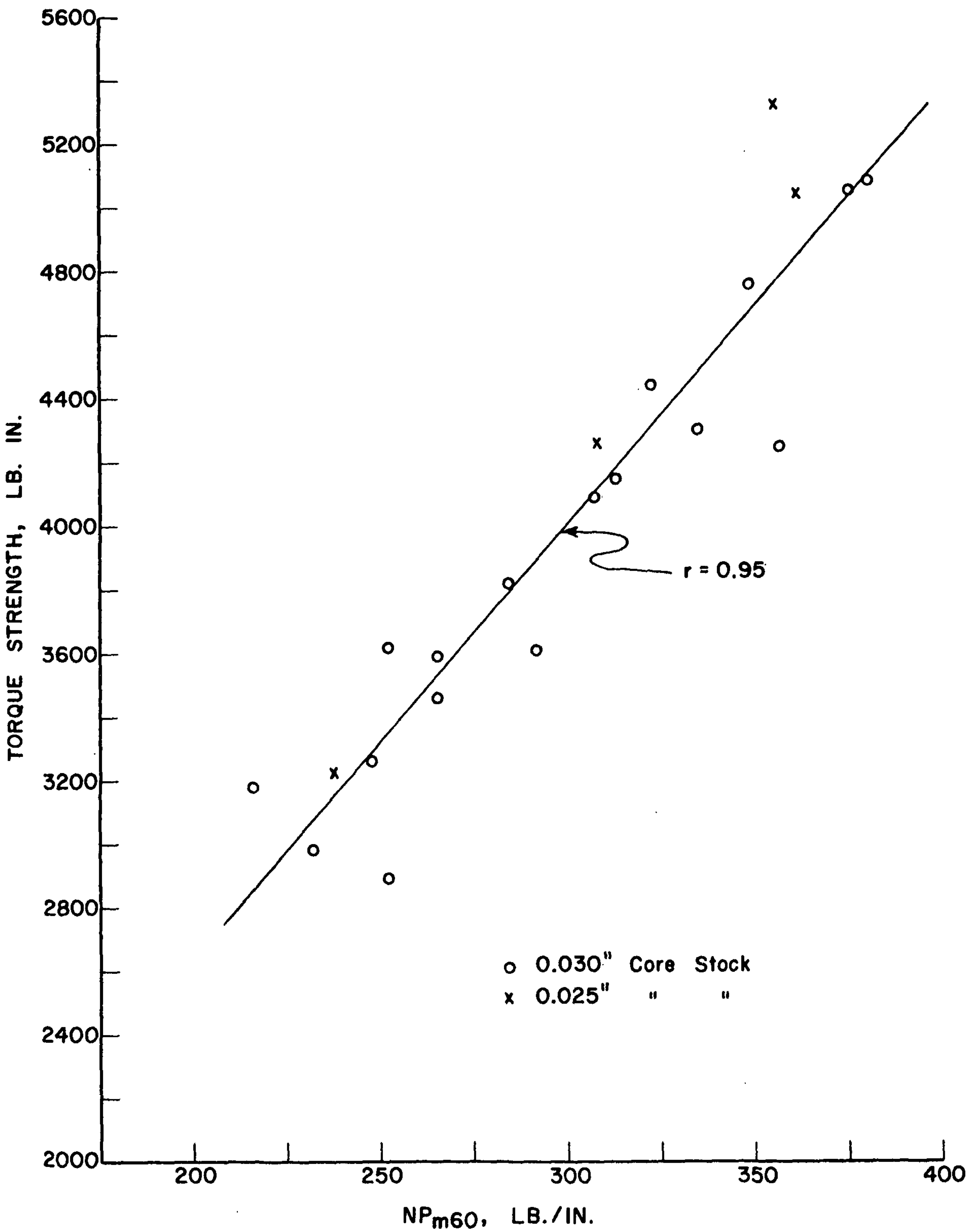

Figure 21. Relationship Between Torque Strength and NP_{m60}

ENGINEERING ANALYSES

AXIAL CRUSH

Assuming that the failure mode is one in which core failure occurs when the material compressive strength is reached, the axial stress at failure is determined by the following equation:

$$\sigma_x = \frac{P_a}{A} \tag{44}$$

where

σ_x = normal stress in the axial direction, p.s.i.

P_a = maximum axial load, lb.

A = core cross-sectional area, sq. in.

If the effects of the core liners are neglected, the cross-sectional area may be simply related to the core geometry as follows:

$$A = \frac{\pi}{4} (D_o^2 - D_i^2) \tag{45}$$

where

D_o = core outside diameter, in.

D_i = core inside diameter, in.

From the core geometry, we know that the axial direction makes an angle of 60° with the core stock machine direction, so that

$$\sigma_x = P_{m60}/h_c \tag{46}$$

where

P_{m60} = core stock strength per unit length when tested uniaxially at an angle of 60° from the machine direction, lb./in.

h_c = core stock thickness, in.

Rewriting the above equations and solving for the maximum axial load, the following equation is obtained:

$$P_a = \frac{P_{m_{60}} \pi (D_o^2 - D_i^2)}{4h_c} \qquad (47)$$

Inasmuch as all quantities on the right-hand side of Equation (47) were measured directly, estimates of the maximum axial load can be made without further analysis. A comparison of the theoretically estimated loads using Equation (47) with the observed maximum loads is displayed in Table XV. The average algebraic error was found to be +0.97%, indicating Equation (45) tends to overestimate the failure load by a very slight amount. The average absolute error, which is an indication of the error, without regard to sign, one might expect to make in using Equation (47), was found to be 5.35%.

SIDE-TO-SIDE CRUSH

Judging from the literature, very little theoretical analysis of spiral-wound fiber cores has been accomplished. Cylindrical structures fabricated from metals and other nonmetallics are very common structural elements, on the other hand, and have been analyzed extensively with respect to their behavior under a variety of types of applied load. Despite a number of differences in regard to material characteristics and fabrication, it might be anticipated that theoretical analysis of nonpaperboard cylinders would serve as a first approximation for fiber tubes and cores.

A relationship between the side-to-side crush load and the edgewise compression strength of the core stock is derived in Appendix III, starting

TABLE XV

COMPARISON OF THEORETICAL AND OBSERVED AXIAL LOADS

Sample Number	Axial Crush, lb. Theoretical	Axial Crush, lb. Observed	Error, %[a]
1	2459	2483	-0.95
2	4100	4135	-0.84
3	3371	3360	0.34
4	3231	3392	-4.74
5	2399	2527	-5.08
6	3760	4277	-12.08
7	2854	2756	3.54
8	3989	4046	-1.40
9	3794	3468	9.40
10	3100	3136	-1.15
11	2452	2867	-14.49
12	2704	2590	4.41
13	2816	2533	11.18
14	3811	3630	4.99
15	3024	2814	7.46
16	3543	3298	7.44
17	3467	3344	3.69
18	3209	3054	5.08
19	3831	3816	0.40
20	2324	2454	-5.29
21	2734	2522	8.42
		Average algebraic error	+0.97
		Average absolute error	5.35

[a]Based on observed results as reference.

from well-known relationships from strength of materials theory. The following side-to-side crush equation was derived:

$$P_s = \frac{P_{m\theta}}{[0.9549(D_i/t + 1)(t - 2h_l - h_c)h_c/t^2]} \tag{48}$$

where

α = angle of wind, degree

P_s = side-to-side crush, lb./in.

$P_{m\theta}$ = edgewise compression strength of core stocks in the θ direction, lb./in.

D_i = inside core diameter, in.

t = core wall thickness, in.

h_l = thickness of inner liner, in.

h_c = thickness of core stock, in.

The simplifying assumptions and approximations which were employed in deriving Equation (48) were the following (see Appendix III):

(1) Core failure is caused by bending stress developed at the point of loading,

(2) Core failure occurs when the normal stress on the outermost ply of core stock reaches the compression strength of the core stock,

(3) Plane cross sections remain plane in bending,

(4) Materials exhibit linear stress-strain behavior,

(5) "Thin tube" theory applies,

(6) Application of adhesive does not affect core stock properties,

(7) Moduli of liners and core stocks are equal,

(8) Applied load is a line load and not one distributed over an area,

(9) Tensile and compressive moduli of elasticity of a ply are equal.

A comparison of the loads computed with Equation (48) with the observed maximum loads is shown in Table XVI. The average algebraic error was found to be -24.7% indicating that the use of Equation (48) results in a serious underestimation of load. In view of assumptions (2), (8), and (9) (discussed in detail in Appendix III) these results are not too surprising. As a temporary corrective measure, adjusting constants were determined such that a minimum error existed between the observed failure loads and the adjusted estimated failure loads. The adjusting equation was the following:

$$P_{obs} = a_1 P_{est} + a_o \qquad (49)$$

where

P_{obs} = observed failure load, lb.

P_{est} = estimated failure load, lb.

a_1 = adjusting multiplying factor

a_o = adjusting additive term, lb.

Satisfactory results were obtained by assuming that $a_o = 0$. For this case the value of a_1 was found to be 1.335 and the average algebraic and absolute errors were found to be +0.52% and 8.74%, respectively. These results are summarized in Table XVI, in which the original unadjusted estimates computed from Equation (48) also are shown.

It is believed that assumptions (2), (8), and (9) are the major contributors to the error inherent in Equation (46). These assumptions state something about the postfailure behavior of the materials, the degree of load

TABLE XVI

COMPARISON OF THEORETICAL AND OBSERVED SIDE CRUSH LOADS

Sample Number	Side Crush, lb./in. Theoretical	Side Crush, lb./in. Observed	Error, %[a]	Side Crush, lb./in. Theoretical X1.335	Side Crush, lb./in. Observed	Error, %[a]
1	34.2	48.5	-29.37	45.7	48.5	-5.73
2	56.9	79.7	-28.62	76.0	79.6	-4.71
3	44.5	66.2	-32.78	59.4	66.2	-10.28
4	43.7	52.9	-17.37	58.3	52.9	10.29
5	31.9	45.8	-30.31	42.6	45.8	-6.99
6	48.9	74.0	-33.85	65.3	74.0	-11.69
7	38.2	43.0	-11.26	50.9	43.0	18.46
8	56.1	71.0	-20.97	74.9	71.0	5.49
9	50.8	58.8	-13.57	67.8	58.8	15.37
10	38.0	48.4	-21.49	50.7	48.4	4.77
11	26.9	45.3	-40.48	36.0	45.3	-20.55
12	39.0	50.4	-22.53	52.1	50.4	3.40
13	36.6	48.5	-24.52	48.8	48.5	0.73
14	47.3	64.7	-26.83	63.1	64.7	-2.32
15	39.4	47.7	-17.40	52.6	47.7	10.26
16	46.0	56.8	-18.95	61.4	56.8	8.20
17	38.5	58.3	-33.88	51.5	58.3	-11.73
18	40.0	57.8	-30.67	53.5	57.8	-7.45
19	49.6	69.6	-28.66	66.3	69.6	-4.77
20	32.0	41.7	-23.15	42.8	41.7	2.56
21	34.2	38.8	-11.92	45.6	38.8	17.59
	Average algebraic error		-24.70	Average algebraic error		+0.52
	Average absolute error		24.70	Average absolute error		8.74

[a]Based on observed results as reference.

distribution at the application point, and the relationship between tension and compressive moduli. It should be noted that all of these factors tend to underestimate the failure load and taken together could account for the 33.5% increase which was required for a minimum error condition. In addition, each of the errors introduced by these three assumptions could be slightly different for each material, indicating that an improvment on the 8.74% average error is a possibility.

BEAM BENDING

When a core is simply supported at two points and loaded by a concentrated load midway between those points, the response of the core will simulate that of a beam undergoing bending deformation (Fig. 22). Equations which relate the maximum load supported by the core to core stock strengths and core dimensions are as follows (see Appendix IV):

$$P_B = \frac{\pi(D_o^4 - D_i^4)}{8\ L\ D_o\ h} P_{m\alpha} \qquad (50)$$

$$P_B = \frac{\pi(D_o^4 - D_i^4)}{8\ L\ D_o\ h_o} \frac{P_{my}}{\sin^2\alpha} \qquad (51)$$

where

P_B = maximum applied bending load, lb.

$P_{m\alpha}$ = core stock modified ring strength, tested uniaxially at an angle α from the stock machine-direction (60° for present case), lb./in.

P_{my} = core stock modified ring strength in the cross-machine direction, lb./in.

h_o = core stock thickness, in.

L = length of tube between support points, in.

$\underline{D}_o$ = outer tube of diameter, in.

$\underline{D}_i$ = inner tube diameter, in.

α = angle of wind; angle between core axial direction and core stock machine-direction (approximately 60° for present cores), degree

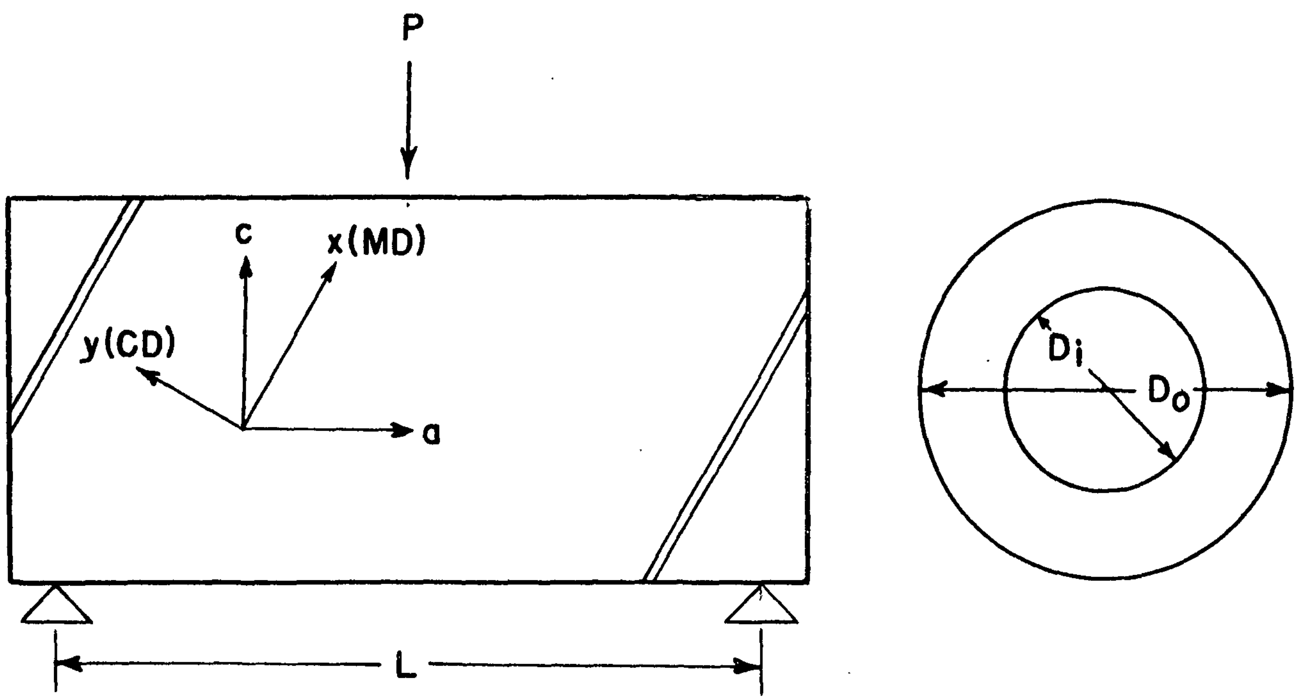

Figure 22. Cylindrical Core Loaded as a Beam

The assumptions made in deriving Equations (50) and (51) are slightly different. The most logical and straightforward approach results in Equation (50) and involves assuming that core failure will occur when the normal compressive stress in the axial direction, $\sigma_{\underline{a}}$ (Fig. 23), exceeds the compressive strength of core stock in the axial direction ($\underline{P}_{\underline{m}60}$ for a 60° wind angle). Equation (51) on the other hand is based on the assumption that core failure will occur when the normal compressive stress in a direction corresponding to the core stock cross-machine direction exceeds the strength of the stock in that direction (-30° or 150° from the axial direction for a 60° angle of wind).

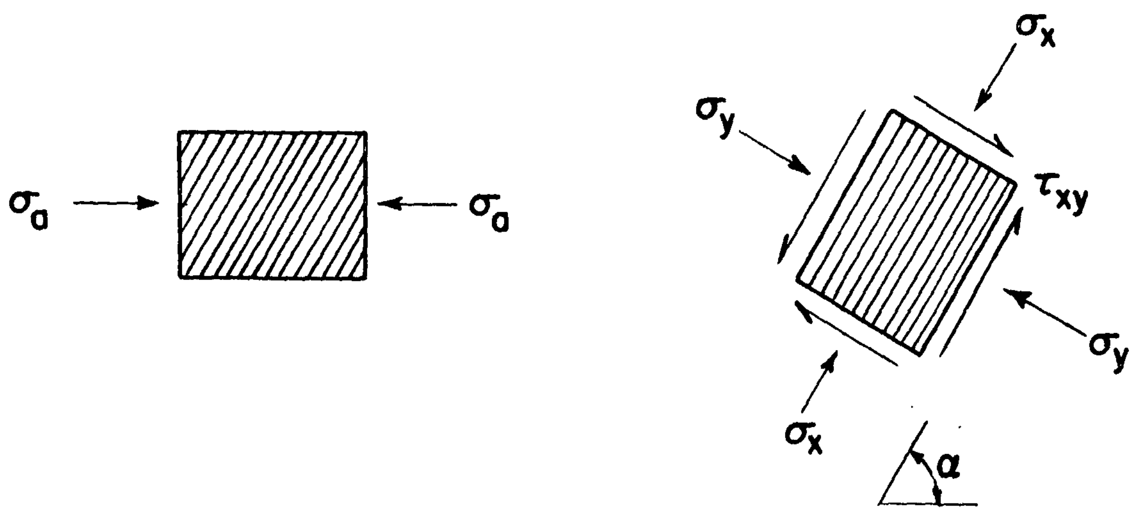

Figure 23. Stresses on Tube Elements Oriented With the Tube Axis and With the Core Stock Orthotropic Axes

Additional assumptions which apply to both of Equations (50) and (51) are as follows:

(1) The beam is cylindrical and straight but of arbitrary cross section.

(2) Plane sections in the unstressed beam remain plane during bending deformations.

(3) The deflection of each beam element is in the form of an arc.

(4) Shearing stresses are distributed uniformly across the width of the beam.

(5) Materials exhibit linear stress-strain behavior.

(6) Application of adhesive does not affect core stock properties.

(7) Moduli of liners and core stocks are equal.

(8) Tensile and compressive moduli of elasticity of a ply are equal.

The results of using Equation (50) are shown in Tables XVII and XVIII, along with the observed values, for the 36-in. and 72-in. cores, respectively. In each of these tables, three estimates are shown. The first estimate (Column 3) is obtained directly from Equation (50) and results in an average underestimation of 27.88 and 25.38% for the 36-in. and 72-in. cores, resp. These errors being quite substantial, adjustments were made to the estimates from Equation (50) by using the following equation:

$$P'_B = b_1 P_B + b_o \tag{52}$$

where

P'_B = adjusted estimated maximum bending load, lb.

P_B = load defined by Equation (50) or (51), lb.

b_1 = adjusting factor

b_o = adjusting constant, lb.

Columns 5 and 7 list the adjusted estimates using constants b_1 and both b_1 and b_o, respectively. It may be seen that, by using the term b_o in addition to b_1, the average errors are improved from 5.07 to 4.82% and 5.53 to 5.18% for the 36-in. and 72-in. cores, respectively.

Tables XIX and XX illustrate similar results but reflect the use of Equation (51) (failure governed by C.D. strength) to compute the estimates, P_B. The unadjusted estimates are again too conservative, resulting in average errors

TABLE XVII

ESTIMATES OF MAXIMUM BEAM BENDING LOAD FOR 36 INCH CORE USING P_{m60}
[Based on Equations (50) and (52)]

No.	Observed, lb.	$P'_B = P_B$ Theoretical, lb.	Error, %[a]	$P'_B = (1.380)P_B$ Theoretical, lb.	Error, %[a]	$P'_B = (1.188)P_B + 53.50$ Theoretical, lb.	Error, %[a]
1	296	208	-29.61	288	-2.84	301	1.70
2	458	348	-24.02	480	4.88	467	1.96
3	392	286	-27.06	395	0.68	393	0.31
4	407	274	-32.55	379	-6.90	380	-6.71
5	312	204	-34.73	281	-9.91	295	-5.30
6	485	319	-34.26	440	-9.25	432	-10.85
7	349	241	-30.87	333	-4.57	340	-2.53
8	448	338	-24.49	467	4.22	455	1.66
9	414	321	-22.46	443	7.02	435	5.05
10	367	262	-28.59	362	-1.42	365	-0.57
11	346	207	-40.09	286	-17.30	300	-13.35
12	311	230	-26.14	317	1.94	326	4.96
13	316	239	-24.36	330	4.41	337	6.80
14	424	323	-23.76	446	5.23	437	3.20
15	353	256	-27.36	354	0.26	358	1.46
16	385	301	-21.87	415	7.83	410	6.72
17	410	293	-28.46	405	-1.25	402	-1.95
18	357	272	-23.75	376	5.25	377	5.58
19	466	325	-30.27	449	-3.74	440	-5.66
20	274	197	-28.08	272	-0.72	288	4.98
21	299	231	-22.66	319	6.75	328	9.79
	Average absolute error		27.88		5.07		4.82

[a]Based on observed results as reference.

TABLE XVIII

ESTIMATES OF MAXIMUM BEAM BENDING LOAD FOR A 72 INCH CORE USING P_{m60}
[Based on Equations (50) and (52)]

No.	Observed, lb.	$P'_B = P_B$ Theoretical, lb.	$P'_B = P_B$ Error, %[a]	$P'_B = (1.338)P_B$ Theoretical, lb.	$P'_B = (1.338)P_B$ Error, %[a]	$P'_B = (1.217)P_B + 16.85$ Theoretical, lb.	$P'_B = (1.217)P_B + 16.85$ Error, %[a]
1	146	104	-28.65	139	-4.54	144	-1.63
2	227	174	-23.35	233	2.55	229	0.69
3	188	143	-23.95	191	1.74	191	1.49
4	196	137	-29.97	184	-6.31	184	-6.18
5	149	102	-31.67	136	-8.57	141	-5.53
6	241	160	-33.85	213	-11.49	211	-12.51
7	169	120	-28.62	161	-4.50	164	-3.16
8	222	169	-23.81	226	1.93	223	0.30
9	206	160	-22.08	215	4.24	212	2.99
10	182	131	-28.00	175	-3.66	176	-3.12
11	164	104	-36.80	139	-15.44	143	-12.81
12	150	115	-23.43	154	2.43	157	4.40
13	146	119	-18.14	160	9.52	162	11.15
14	202	162	-19.99	216	7.04	214	5.70
15	166	128	-22.77	172	3.33	173	4.13
16	187	150	-19.58	201	7.59	200	6.87
17	191	147	-23.22	196	2.72	195	2.25
18	172	136	-20.87	182	5.87	182	6.08
19	227	162	-28.42	217	-4.24	215	-5.48
20	133	98	-25.92	132	-0.88	137	2.81
21	144	115	-19.70	154	7.42	157	9.41
	Average absolute error		25.38		5.53		5.18

[a]Based on observed results as reference.

TABLE XIX

ESTIMATES OF MAXIMUM BENDING LOAD FOR 36 INCH CORE USING P_{my}
[Based on Equations (51) and (52)]

		$P'_B = P_B$		$P'_B = (1.184)P_B$		$P'_B = (0.947)P_B + 77.23$	
No.	Observed, lb.	Theoretical, lb.	Error, %[a]	Theoretical, lb.	Error, %[a]	Theoretical, lb.	Error, %[a]
1	296	237	-20.02	280	-5.34	301	1.78
2	458	417	-8.93	493	7.78	472	3.06
3	392	332	-15.18	393	0.38	391	-0.01
4	407	317	-22.04	375	-7.73	377	-7.23
5	312	227	-27.24	268	-13.88	292	-6.37
6	485	376	-22.57	444	-8.36	432	-10.79
7	349	290	-16.99	342	-1.75	351	0.69
8	448	405	-9.63	479	6.95	460	2.77
9	414	381	-7.97	450	8.91	437	5.75
10	367	312	-14.96	369	0.64	372	1.53
11	346	268	-22.40	317	-8.16	331	-4.23
12	311	256	-17.73	302	-2.63	319	2.70
13	316	255	-19.19	302	-4.36	318	0.92
14	424	387	-8.61	458	8.15	443	4.71
15	353	279	-20.83	330	-6.30	341	-3.19
16	385	324	-15.77	383	-0.31	384	-0.21
17	410	352	-14.08	416	1.68	410	0.15
18	357	308	-13.69	364	2.14	368	3.32
19	466	394	-15.50	466	0.00	449	-3.44
20	274	225	-17.96	266	-2.90	289	5.83
21	299	257	-14.17	303	1.57	320	7.06
	Average absolute error		16.46		4.76		3.61

[a]Based on observed results as reference.

TABLE XX

ESTIMATES OF MAXIMUM BENDING LOAD FOR 72 INCH CORE USING P_{my}
[Based on Equations (51) and (52)]

		$P'_B = P_B$		$P'_B = (1.147)P_B$		$P'_B = (0.971)P_B + 28.80$	
No.	Observed, lb.	Theoretical, lb.	Error, %[a]	Theoretical, lb.	Error, %[a]	Theoretical, lb.	Error, %[a]
1	146	118	-18.93	135	-6.97	143	-1.58
2	227	208	-8.13	239	5.41	231	1.86
3	188	166	-11.57	190	1.45	190	1.14
4	196	158	-19.06	182	-7.13	182	-6.74
5	149	113	-23.82	130	-12.59	138	-6.73
6	241	187	-22.09	215	-10.60	211	-12.43
7	169	144	-14.29	166	-1.65	169	0.23
8	222	202	-8.81	232	4.62	225	1.48
9	206	190	-7.53	218	6.10	213	3.73
10	182	156	-14.26	179	-1.61	180	-0.95
11	164	134	-18.14	154	-6.07	159	-2.98
12	150	127	-14.71	146	-2.14	152	1.98
13	146	127	-12.55	146	0.33	152	4.60
14	202	193	-4.09	222	10.04	216	7.35
15	166	139	-15.82	160	-3.41	164	-0.94
16	187	162	-13.29	186	-0.51	186	-0.43
17	191	176	-7.79	202	5.80	199	4.58
18	172	154	-10.43	176	2.77	178	3.68
19	227	196	-13.27	225	-0.48	219	-3.12
20	133	112	-15.49	128	-3.03	137	3.67
21	144	128	-10.90	147	2.23	153	6.48
	Average absolute error		13.57		4.53		3.66

[a]Based on observed results as reference.

of 16.46 and 13.57% for the 36-in. and 72-in. cores, respectively. The average errors resulting from the use of $\underline{b}_1$ alone are 4.76 and 4.53% for the 36-in. and 72-in. cores. These errors improve to 3.61 and 3.66% if both constants, $\underline{b}_o$ and $\underline{b}_1$, are used.

It should be pointed out that while estimates made from Equation (51) were more accurate than those made from Equation (50), the range of applicability of these two equations is markedly different. Because Equation (50) requires knowledge of a uniaxial core stock property which is measured in the same direction as the known uniaxial stress (axial bending stress), it can be expected that Equation (50) would result in reasonably accurate estimates for tubes of varying geometry, and in particular, for all angles of wind between zero and ninety degrees. On the other hand, Equation (51) is obviously limited to those tubes with angles of wind such that the component of the axial stress in the stock cross-machine direction is the one which governs failure. As an extreme example, consider the case where $\alpha = 0^{\circ}$ (core stock machine-direction in axial direction). Equation (51) predicts an infinitely large maximum bending load since the component of the axial stress in the cross-machine direction (circumferential direction) is zero. Obviously, a core stock strength in some other direction would govern failure and Equation (51) would be grossly incorrect.

Use of Equation (51), then, must be restricted to use on tubes with geometries similar to those tested for this report. In particular, the tubes should have angles of wind close to 60°. The use of Equation (50) is, therefore, recommended for general use. Although for the present core geometries, estimates made from Equation (50) were less accurate than the best obtainable, it is believed that the accuracy of Equation (50) may remain substantially the same when applied to cores of different dimensions and angles of wind.

The adjusted recommended equations are:

for 36-in. cores,

$$P_B' = (1.188)\ \frac{\pi}{8}\ \frac{(D_o^{\ 4} - D_i^{\ 4})}{L\ D_o\ h}\ P_{m\alpha} + 53.50 \qquad (53)$$

and for 72-in. cores

$$P_B' = (1.217)\ \frac{\pi}{8}\ \frac{(D_o^{\ 4} - D_i^{\ 4})}{L\ D_o\ h}\ P_{m\alpha} + 16.85 \qquad (54)$$

The large corrective factors, $\underline{b}_1$, necessary to adjust the estimates to a minimum error condition should not necessarily be viewed with alarm. As was discussed in a previous section, for many materials beam rupture frequently and consistently occurs at a stress level significantly higher than one would expect from a computation of the bending stress. Multiplying constants are traditionally computed experimentally to account for a particular cross-sectional shape for a given material. The additive constant, $\underline{b}_o$, however, is less easily explained. Whether this term arises from an oversimplification of the analysis and varies significantly with tube geometry or arises from a systematic error which is independent of tube geometry, is a question which will be answered when data from the tubes of different geometry have been incorporated into the analysis.

TORQUE

The following equations were used to estimate the torque strength of cores twisted at the ends (see Appendix V):

$$T = \frac{\pi}{16}\ \frac{(D_o^{\ 4} - D_i^{\ 4})}{D_o}\ \tau_{ac} \qquad (55a)$$

$$\left(\frac{1}{\tau_{ac}}\right)^2 = \left(\frac{h_c}{P_{mx}}\right)^2 \left[1 + \left(\frac{P_{mx}}{P_{my}}\right)\right] + \left(\frac{h_c}{P_{my}}\right)^2 \qquad (55b)$$

or alternatively,

$$T = \frac{\pi}{16} \frac{(D_o{}^4 - D_i{}^4)}{D_o h_c} \frac{P_{my}}{\sin^2\alpha} \qquad (56)$$

where

$\underline{T}$ = maximum applied torque, in.-lb.

$\underline{D_i}$ = inner core diameter, in.

$\underline{D_o}$ = outer core diameter, in.

τ_{ac} = shear stress induced in the a-c plane, p.s.i.

$\underline{h_c}$ = core stock thickness, in.

$\underline{P_{mx}}$ = core stock machine-direction tensile strength, lb./in.

$\underline{P_{my}}$ = core stock cross-direction modified ring strength, lb./in.

α = angle of wind; angle between core axial direction and core stock machine-direction, degrees

Equations (55) are based on the assumptions that core stock shear strength is independent of orientation and that core failure is due to excessive shear stress. Equation (56) is based on the assumption that the core stock cross-direction normal stress component governs failure. Other assumptions on which both equations are based are listed in Appendix V.

The results of estimating torques with Equations (55) and (56) along with the corresponding observed values and errors are shown in Tables XXI and XXII. The first four columns in each table pertain to the unadjusted estimates made directly from Equations (55) and (56). The average errors were 7.38 and

TABLE XXI

ESTIMATES OF TORQUE STRENGTH BASED ON CONSTANT SHEAR STRENGTH
[Equations (55) and (57)]

	$T' = T$			$T' = (1.052)T$			$T' = (0.925)T + 501.1$		
No.	Theoretical, in.-lb.	Observed, in.-lb.	Error, %[a]	Theoretical, in.-lb.	Observed, in.-lb.	Error, %[a]	Theoretical, in.-lb.	Observed, in.-lb.	Error, %[a]
1	2931	2982	-1.70	3082	2982	3.35	3211	2982	7.68
2	5111	5094	0.33	5374	5094	5.50	5226	5094	2.61
3	4113	4152	-0.93	4325	4152	4.16	4304	4152	3.66
4	3910	4260	-8.20	4111	4260	-3.47	4116	4260	-3.36
5	2776	3222	-13.83	2919	3222	-9.39	3068	3222	-4.77
6	4636	5334	-13.07	4875	5334	-8.59	4788	5334	-10.23
7	3534	3594	-1.65	3716	3594	3.40	3769	3594	4.87
8	4944	5064	-2.36	5198	5064	2.66	5072	5064	0.17
9	4597	4254	8.06	4833	4254	13.63	4751	4254	11.69
10	3775	3606	4.70	3970	3606	10.09	3992	3606	10.70
11	2981	3618	-17.60	3134	3618	-13.35	3257	3618	-9.96
12	3130	2886	8.48	3292	2886	14.07	3395	2886	17.66
13	3116	3456	-9.83	3276	3456	-5.18	3382	3456	-2.13
14	4426	4764	-7.09	4654	4764	-2.30	4593	4764	-3.57
15	3433	3822	-10.16	3610	3822	-5.53	3675	3822	-3.82
16	3982	4302	-7.43	4187	4302	-2.66	4183	4302	-2.75
17	4261	4440	-4.02	4480	4440	0.92	4441	4440	0.02
18	3744	4092	-8.49	3937	4092	-3.77	3963	4092	-3.14
19	4769	5046	-5.48	5015	5046	-0.61	4910	5046	-2.67
20	2734	3180	-14.01	2875	3180	-9.58	3029	3180	-4.73
21	3017	3258	-7.37	3173	3258	-2.59	3291	3258	1.02
	Average absolute error		7.38			5.95			5.30

[a]Based on observed results as reference.

TABLE XXII

ESTIMATES OF TORQUE STRENGTH BASED ON CORE STOCK C.D. STRENGTH, $\underline{P}_{\underline{my}}$
[Equations (56) and (57)]

No.	$\underline{T}' = \underline{T}$ Theoretical, in.-lb.	Observed, in.-lb.	Error, %[a]	$\underline{T}' = (0.817)\underline{T}$ Theoretical, in.-lb.	Observed, in.-lb.	Error, %[a]	$\underline{T} = (0.726)\underline{T} + 463.6$ Theoretical, in.-lb.	Observed, in.-lb.	Error, %[a]
1	3690	2982	23.74	3015	2982	1.13	3142	2982	5.38
2	6501	5094	27.63	5313	5094	4.30	5183	5094	1.76
3	5182	4152	24.82	4235	4152	2.01	4226	4152	1.78
4	4945	4260	16.09	4041	4260	-5.12	4054	4260	-4.83
5	3538	3222	9.82	2891	3222	-10.24	3032	3222	-5.88
6	5853	5334	9.73	4783	5334	-10.31	4713	5334	-11.64
7	4515	3594	25.65	3690	3594	2.68	3741	3594	4.11
8	6311	5064	24.62	5157	5064	1.84	5045	5064	-0.37
9	5938	4254	39.60	4853	4254	14.08	4774	4254	12.24
10	4865	3606	34.91	3975	3606	10.25	3995	3606	10.80
11	4185	3618	15.67	3420	3618	-5.46	3501	3618	-3.20
12	3988	2886	38.19	3259	2886	12.93	3359	2886	16.38
13	3980	3456	15.17	3252	3456	-5.87	3353	3456	-2.97
14	6040	4764	26.78	4936	4764	3.61	4848	4764	1.77
15	4356	3822	13.97	3560	3822	-6.85	3626	3822	-5.12
16	5054	4302	17.50	4131	4302	-3.97	4133	4302	-3.92
17	5490	4440	23.66	4487	4440	1.06	4449	4440	0.21
18	4803	4092	17.37	3925	4092	-4.07	3950	4092	-3.45
19	6137	5046	21.63	5016	5046	-0.59	4919	5046	-2.50
20	3503	3180	10.18	2863	3180	-9.94	3007	3180	-5.42
21	4000	3258	22.77	3268	3258	0.33	3367	3258	3.36
Average absolute error			21.89			5.56			5.10

[a]Based on observed results as reference.

21.89% for estimates based on Equations (55) and (56), respectively. Improvement resulted when adjustments of the data of the following form were made:

$$T' = b_1 T + b_o \tag{57}$$

where

T' = adjusted estimated maximum torque, in.-lb.

b_1 = adjusting multiplying constant

b_o = adjusting additive constant, in.-lb.

In Tables XXI and XXII, Columns 5 and 8 reflect the effects of using adjusting constant b_1 only, and both b_1 and b_o, respectively. The average errors using only b_1 to adjust the data were 5.95 and 5.56% for Equations (55) and (56), respectively. The errors improved to 5.30 and 5.10% for Equations (55) and (56) if both adjusting constants b_o and b_1 were used.

It should be pointed out that a more complicated expression could have been used to estimate core stock shear strength instead of Equation (55b). This expression is not based on the assumption of constant shear strength and so would not be independent of angle of wind. The expression is complex, however (see Appendix VI), so only the comparative results of torque strength estimates will be monitored. The average errors were 8.75, 5.37, and 5.40% for the nonadjusted estimates, and the estimates adjusted with one and two constants, respectively.

It is evident that, for the cores tested for this report, the use of the stress in the core stock cross-direction and the strength P_{my} as a failure criteria, results in somewhat less error than the use of a formula to estimate core stock shear strength. It is also apparent, however, that the range of applicability of Equation (56) is very limited, particularly with regard to the core angle of wind. For the case of $\alpha = 0$, for example, Equation (56) predicts an infinitely large failure torque, since the normal stress component in the cross-direction is zero. Obviously, a strength at some other angle would govern failure for this case, and estimates based on Equation (56) would be grossly in error. The use of Equation (56) then must be restricted to cores similar to the present cores.

Although Equation (53) predicts that core torque strength will be independent of wind, it is felt that the errors resulting from application to cores of different angles of wind would probably not be too large. Accordingly, the equations recommended for general use to estimate core strength are:

$$T' = (0.925)\ T + 501.1 \qquad (58)$$

where $\underline{T}$ is defined by Equation (55).

LITERATURE CITED

1. Gerard, G., and Becker, H. Handbook of structural stability. Part III. Buckling of curved plates and shells. Washington, NACA TN3783, Aug., 1957.

2. March, H. W. Buckling of long thin plywood cylinders in axial compression. Madison, Wis., USDA, Forest Products Laboratory Report No. 1322.

3. Tenzer, H. The strength of wound cylindrical tubes. Papier Druck (Buchbind. Papierverarb.) 14, no. 6:89-94 (June, 1965).

4. Roark, R. J. Formulas for stress and strain. 4th Ed. New York, McGraw-Hill Book Co., 1965.

5. American Society for Testing Materials. Method of test for flexural strength of concrete. Standards C:78-59 (1961).

6. Kuenzi, E. W. Flexure of structural sandwich constructions. Madison, Wis., USDA, Forest Products Laboratory Report No. 1829, Dec., 1951.

7. Marks, L. S. Mechanical engineers handbook. p. 426. New York, McGraw-Hill Co., 1957.

8. McKee, R. C., Gander, J. W., and Wachuta, J. R. Flexural stiffness of corrugated board. Paperboard Pkg. 47, no. 12:111-16, 118 (Dec., 1962).

9. Biggs, W. A., Jr., and Dunlap, C. K., Jr. U.S. pat. 3,194,275 (July, 1965).

10. Dryssen, G. Arch. Drucktech. 104, no. 7:55-9 (Sept., 1967) [Ger., Engl. and Fr. sum].

11. Ish-Horowicz, M. Aircraft Eng. 23, no. 263 (Jan., 1951).

12. Cozzone, F. P. J. Aero. Sci. 10:137 (May, 1943).

13. Phillips, A. J. Appl. Mech. 18, no. 4 (Dec., 1951).

14. Eulenstein, ____. Papier Druck (Buchbind. Papierverarb.) 13, no. 4:61-2 (April, 1964).

15. Jones, W. C. U.S. pat. 3,164,010 (Jan. 5, 1965).

16. Wagenhals, R. E. U.S. pat. 2,618,963 (Nov. 25, 1952).

17. Bigger, R. P. Fibre Containers 29, no. 9:34, 36, 38, 42, 44, 46, 48, 53-4 (Sept., 1944).

18. Brosnan, E. G. Paper, Film, Foil Converter 11, no. 9:100-4 (Sept., 1967).

19. Norris, C. B. USDA, Forest Products Laboratory Report No. 1816, July, 1950.

20. Van den Akker, J. A. Unpublished work, 1963.

21. Craver, J. K., and Taylor, D. L. Tappi 48, no. 3:142 (1965).

22. Kubat, J., and Lindbergson, B. Svensk Papperstid. 68, no. 21:743 (Nov. 15, 1965).

23. Jones, A. R. Tappi 51, no. 5:203-9 (May, 1968).

24. Love, A.E.H. Mathematical theory of elasticity. 4th Ed. p. 160-2, New York, Dover Publications, 1944.

25. March, H. W. USDA, Forest Products Laboratory Report No. R1503, 1944.

26. Horio, M., and Onogi, S. J. Appl. Phys. 22, no. 7:971 (July, 1951).

27. Campbell, J. G. Australian J. Appl. Sci. 12, no. 3:356 (1961).

28. Tsai, S. W. Strength characteristics of composite materials. NASA CR-224.

29. Timoshenko, S. P., and Goodier, J. N. Theory of elasticity. 3rd Ed. New York, McGraw-Hill Book Co., 1970.

30. Mauer, E. R., and Withey, M. O. Strength of materials. p. 152. New York, John Wiley & Sons, 1946.

31. Timoshenko, S. Strength of materials. Part II. Advanced theory and problems. p. 362. New York, D. Van Nostrand Co., 1940.

THE INSTITUTE OF PAPER CHEMISTRY

Michael J. Laughlin

Michael J. Laughlin, Research Associate

W J Whitsitt

William J. Whitsitt, Research Associate

R C McKee by WJW

Robert C. McKee, Chairman
Contain Section

APPENDIX I

PROPERTIES OF INNER AND OUTER LINERS

TABLE XXIII

INNER LINER PROPERTIES

Run No.	Basis Weight, lb./M ft.^{2}	Caliper, pt.	Density, lb./pt.	Bursting Strength, p.s.i.g.	Tensile, lb./in. M.D.	Tensile, lb./in. C.D.	Tensile, lb./in. 30° to M.D.	Tensile, lb./in. 60° to M.D.	Stretch, % M.D.	Stretch, % C.D.	Stretch, % 30° to M.D.	Stretch, % 60° to M.D.	Tensile Modulus, p.s.i. M.D.	Tensile Modulus, p.s.i. C.D.	Tensile Modulus, p.s.i. 30° to M.D.	Tensile Modulus, p.s.i. 60° to M.D.
1	56.7	15.3	3.6	105	109.0	20.2	54.8	24.6	2.1	4.2	2.6	3.9	806350	123820	387140	150000
2	58.5	15.3	3.8	108	110.5	21.0	55.2	25.4	2.1	4.6	2.6	4.1	830060	122780	388650	158150
3	53.1	15.1	3.6	107	105.4	20.0	51.1	24.5	2.0	4.2	2.4	4.0	842660	132880	375660	157700
4	50.6	15.0	3.4	101	99.6	18.7	46.7	23.4	2.0	3.9	2.4	3.9	788260	131570	354480	166170
5	50.3	14.9	3.4	100	99.1	18.6	46.9	22.9	2.0	4.1	2.5	3.4	771310	120420	355200	168700
6	49.9	15.0	3.4	99	99.6	18.6	46.7	23.0	2.1	4.2	2.6	3.8	777250	123880	351600	165870
7	50.1	15.0	3.4	102	101.4	18.9	48.6	23.0	2.1	4.3	2.6	4.0	772660	136040	359000	166100
8	50.3	15.1	3.4	105	103.9	18.8	50.2	22.8	2.1	4.1	2.5	4.0	778060	133650	382510	163770
9	50.8	15.1	3.4	106	104.2	19.0	49.8	23.2	2.1	3.9	2.5	3.8	780440	126130	383050	170110
10	52.2	15.0	3.5	109	102.4	19.5	49.8	24.2	2.1	4.0	2.5	3.8	766600	132850	374360	171840
11	50.9	14.9	3.4	102	104.8	18.9	49.1	23.3	2.2	4.1	2.5	3.8	784810	127700	396960	172990
12	51.3	15.0	3.4	105	101.2	19.3	49.6	24.3	2.1	4.4	2.5	4.0	730830	136540	384570	174580
13	50.0	14.9	3.4	102	98.6	18.8	48.1	23.6	2.1	4.5	2.4	3.9	755560	131980	387980	180380
14	50.2	14.9	3.4	103	97.8	18.7	47.8	23.2	2.0	4.1	2.4	3.9	782700	123620	384810	172270
15	50.2	14.8	3.4	102	99.8	18.8	50.0	22.6	2.1	4.1	2.4	4.0	754870	143730	402980	165260
16	49.4	14.7	3.4	102	101.2	18.6	49.7	22.2	2.2	4.1	2.4	3.8	761140	147540	409470	162010
17	50.1	14.9	3.4	102	103.2	18.7	49.6	22.7	2.2	4.0	2.4	3.7	791920	129170	404660	162630
18	51.7	15.0	3.4	102	102.8	19.5	49.4	23.8	2.0	4.5	2.4	4.0	790200	126930	386880	177130
19	51.1	14.9	3.4	102	99.3	19.3	52.3	22.9	2.0	4.4	2.6	3.8	772280	130950	396270	174040
20	49.2	14.8	3.3	102	98.3	18.8	52.3	21.8	2.2	4.2	2.6	3.6	736460	133950	391110	172280
21	55.4	14.6	3.8	95	89.3	18.5	44.5	23.0	1.8	3.7	2.1	3.6	771020	124120	347020	174200

TABLE XXIII (Continued)

INNER LINER PROPERTIES

Run No.	Tensile Stiffness, lb./in. M.D.	Tensile Stiffness, lb./in. C.D.	Tensile Stiffness, lb./in. 30° to M.D.	Tensile Stiffness, lb./in. 60° to M.D.	Modified Ring Compression, lb./in. M.D.	Modified Ring Compression, lb./in. C.D.	Modified Ring Compression, lb./in. 30° to M.D.	Modified Ring Compression, lb./in. 60° to M.D.	Taber Stiffness, g./cm. M.D.	Taber Stiffness, g./cm. C.D.	Tearing Strength, g./sheet M.D.	Tearing Strength, g./sheet C.D.	TAPPI Plybond, p.s.i.g.	Porosity, sec./100 cc.	Water Drop, sec.
1	12295	1888	5903	2289	31.0	16.7	26.6	19.6	133	24	194	368	153	108	59
2	12694	1879	5945	2419	31.7	16.9	27.2	20.2	142	25	199	378	156	123	49
3	12683	1999	5655	2373	31.2	16.2	26.2	19.1	135	25	194	366	152	113	54
4	11786	1968	5300	2484	29.6	15.2	24.2	17.6	129	23	175	346	149	99	60
5	11492	1770	5292	2514	28.7	14.8	23.8	17.4	130	22	173	342	146	92	55
6	11619	1828	5256	2480	28.4	14.5	23.4	17.3	128	22	174	346	143	86	56
7	11629	2048	5404	2500	29.2	14.9	23.5	17.6	125	22	168	350	150	96	66
8	11749	2018	5776	2473	30.0	15.3	24.6	18.5	124	22	169	350	155	102	70
9	11745	1898	5765	2560	29.8	15.2	24.9	18.7	127	23	175	352	152	97	61
10	11499	1993	5615	2578	30.2	15.2	25.2	18.6	134	24	180	364	150	96	51
11	11734	1909	5935	2586	30.2	15.3	24.8	17.8	128	22	182	360	154	87	57
12	10962	2048	5769	2619	30.0	15.0	25.1	18.0	128	24	183	362	150	88	56
13	11294	1973	5801	2697	29.0	14.6	24.6	17.7	123	23	177	349	150	82	63
14	11662	1842	5734	2567	29.2	15.0	24.6	18.0	124	23	168	354	149	85	64
15	11173	2125	5963	2446	29.5	15.3	24.4	17.8	120	23	175	359	148	89	68
16	11189	2169	6019	2381	29.2	14.8	24.0	17.5	118	22	174	348	152	97	74
17	11762	1918	6010	2416	29.6	15.0	24.2	17.6	124	22	176	345	155	97	66
18	11855	1904	5803	2657	29.6	15.2	25.1	17.7	128	23	187	370	146	85	53
19	11515	1950	5903	2594	29.0	15.2	25.1	17.4	122	22	183	353	147	86	64
20	10900	1982	5787	2550	29.2	15.1	25.1	17.3	118	21	174	336	154	84	71
21	11205	1809	5050	2534	27.8	14.4	22.6	16.9	124	25	175	318	134	142	161

TABLE XXIV

OUTER LINER PROPERTIES

Run No.	Basis Weight, lb./M ft.²	Caliper, pt.	Density lb./pt.	Bursting Strength, p.s.i.g.	Tensile, lb./in. M.D.	Tensile, lb./in. C.D.	Tensile, lb./in. 30° to M.D.	Tensile, lb./in. 60° to M.D.	Stretch, % M.D.	Stretch, % C.D.	Stretch, % 30° to M.D.	Stretch, % 60° to M.D.	Tensile Modulus, p.s.i. M.D.	Tensile Modulus, p.s.i. C.D.	Tensile Modulus, p.s.i. 30° to M.D.	Tensile Modulus, p.s.i. 60° to M.D.
1	54.6	15.3	3.6	100	92.1	18.6	50.3	22.4	1.7	4.6	2.4	3.7	733330	111510	366170	148720
2	54.4	15.3	3.6	98	93.8	18.2	50.4	22.3	1.8	4.4	2.4	3.6	747300	110080	356010	145430
3	54.0	15.3	3.5	92	93.8	18.3	50.1	22.1	1.8	4.3	2.4	3.8	772880	111730	357730	147410
4	53.2	15.2	3.5	91	89.8	18.5	48.3	21.8	1.8	4.4	2.4	3.8	772310	117000	357780	143550
5	52.0	15.2	3.4	90	88.7	18.3	47.8	20.9	1.8	4.2	2.4	3.4	735790	115780	358310	147040
6	53.5	15.3	3.5	94	93.1	18.4	50.6	21.5	1.9	4.1	2.5	3.4	724460	109340	388990	148920
7	54.9	15.4	3.6	99	94.8	18.8	51.0	22.3	1.9	4.4	2.4	3.5	724660	105530	396730	146540
8	55.1	15.5	3.6	100	96.2	19.3	51.2	22.8	1.9	4.4	2.4	3.5	735910	104150	395280	152780
9	53.9	15.4	3.6	97	95.9	18.9	50.7	22.6	1.8	4.1	2.4	3.7	758900	108720	403000	154260
10	53.1	15.2	3.5	93	97.1	18.1	48.3	22.1	1.9	4.1	2.4	3.7	810260	111230	389380	149050
11	53.2	15.4	3.4	99	90.4	18.9	50.1	22.5	1.9	4.0	2.4	4.0	786220	123750	385860	157020
12	53.6	15.2	3.5	95	95.8	18.4	47.7	22.2	1.8	4.3	2.4	3.4	822820	109310	381060	145480
13	53.1	15.3	3.5	96	96.0	18.1	47.1	21.6	1.8	4.1	2.4	3.3	788890	111410	384130	152110
14	51.3	15.3	3.4	95	96.4	18.1	47.4	21.2	2.0	4.0	2.4	3.3	759980	114600	382310	153360
15	51.4	15.4	3.4	96	94.8	18.6	48.8	21.4	2.1	4.0	2.3	3.3	718520	117210	369860	150580
16	51.7	15.4	3.4	95	95.1	18.7	49.2	21.4	2.2	4.1	2.4	3.6	707960	120440	355890	152890
17	52.5	15.5	3.4	98	91.4	18.7	50.3	21.9	2.1	4.1	2.4	3.9	760310	126010	377450	154340
18	52.0	15.3	3.4	93	92.0	18.7	48.4	22.3	1.9	4.1	2.3	4.0	767050	119020	368860	159310
19	52.3	15.3	3.4	93	95.2	19.0	49.6	22.2	2.0	4.1	2.2	3.9	781980	124140	385540	153560
20	53.0	15.3	3.4	96	95.4	19.0	51.3	21.8	2.2	4.0	2.4	3.9	748240	124540	391120	148840
21	49.8	14.9	3.4	98	93.7	18.6	47.6	22.3	2.3	4.3	2.4	3.8	726560	134960	365830	164490

TABLE XXIV (Continued)

OUTER LINER PROPERTIES

Run No.	Tensile Stiffness, lb./in. M.D.	C.D.	30° to M.D.	60° to M.D.	Modified Ring Compression, lb./in. M.D.	C.D.	30° to M.D.	60° to M.D.	Taber Stiffness, g./cm. M.D.	C.D.	Tearing Strength, g./sheet M.D.	C.D.	TAPPI Plybond, p.s.i.g.	Porosity, sec./100 cc.	Water Drop, sec.
1	11184	1701	5584	2268	29.2	14.9	25.2	17.0	136	22	169	322	142	109	151
2	11471	1690	5464	2232	29.1	15.0	25.0	17.2	137	23	169	322	140	113	93
3	11863	1715	5491	2263	29.4	15.0	25.2	17.2	134	23	174	325	140	118	95
4	11779	1784	5457	2189	28.8	14.6	25.1	17.0	122	23	172	323	141	112	93
5	11220	1766	5465	2243	28.2	14.6	24.9	16.9	116	21	170	324	144	115	96
6	11121	1678	5972	2286	29.5	15.0	25.2	17.4	130	23	171	329	142	133	97
7	11196	1630	6129	2264	30.4	15.1	25.2	17.8	143	25	174	338	142	135	103
8	11444	1620	6147	2376	30.2	15.4	25.4	18.0	141	24	182	341	148	136	110
9	11686	1673	6206	2376	29.6	15.1	25.0	17.9	136	23	179	334	148	121	136
10	12316	1691	5919	2266	29.7	14.7	24.7	17.6	133	22	175	326	145	109	135
11	12148	1912	5962	2426	30.4	15.1	25.8	18.1	132	26	167	334	148	114	143
12	12507	1662	5792	2211	30.8	14.8	25.5	17.6	133	22	174	324	143	116	120
13	12030	1699	5858	2320	30.4	15.0	26.3	17.6	130	22	168	318	148	122	133
14	11628	1753	5849	2346	29.9	14.7	25.2	17.4	128	21	168	319	154	124	228
15	11028	1799	5677	2312	30.4	14.6	24.4	17.4	130	23	165	326	155	125	231
16	10938	1861	5498	2362	30.2	14.8	25.1	17.6	127	23	162	327	153	120	138
17	11785	1953	5851	2392	29.8	15.0	25.5	18.0	128	23	166	334	149	108	143
18	11736	1821	5644	2437	30.1	14.8	26.1	17.6	124	24	166	324	148	123	136
19	11966	1900	5900	2349	29.8	14.6	26.4	17.8	126	23	170	326	149	114	126
20	11488	1912	6004	2285	29.0	14.7	26.2	17.7	126	24	168	326	152	108	128
21	10863	2016	5469	2459	28.4	14.5	23.5	17.2	123	21	174	322	143	111	148

APPENDIX II

INTERCORRELATIONS BETWEEN CORE STOCK PROPERTIES
FOR NOMINAL 0.040-INCH CORE STOCKS

TABLE XXV

INTERCORRELATIONS BETWEEN CORE STOCK PROPERTIES
($\underline{N}$ = 17)

Property	Caliper	Density	Bursting Strength	Tensile				Stretch				Tensile Stiffness	
				M.D.	C.D.	30°	60°	M.D.	C.D.	30°	60°	M.D.	C.D.
Basis Weight	0.58	0.82	0.61	0.56	0.22	0.50	0.31	0.53	0.69	0.73	0.67	0.54	0.06
Caliper	1.00	0.04	0.15	0.15	-0.07	0.04	-0.03	0.29	0.59	0.36	0.55	0.09	-0.29
Density		1.00	0.59	0.53	0.25	0.55	0.33	0.38	0.43	0.61	0.43	0.58	0.07
Bursting Strength			1.00	0.94	0.63	0.82	0.71	0.77	0.45	0.85	0.55	0.76	0.41
Tensile, M.D.				1.00	0.62	0.89	0.70	0.64	0.48	0.73	0.50	0.90	0.41
C.D.					1.00	0.86	0.98	0.10	0.20	0.36	0.16	0.56	0.85
30°						1.00	0.90	0.32	0.42	0.58	0.37	0.84	0.64
60°							1.00	0.19	0.32	0.48	0.29	0.62	0.79
Stretch, M.D.								1.00	0.47	0.84	0.68	0.35	-0.15
C.D.									1.00	0.70	0.92	0.36	-0.22
30°										1.00	0.84	0.49	-0.01
60°											1.00	0.27	-0.31
Tensile Stiffness, M.D.												1.00	0.48
C.D.													1.00

APPENDIX II

INTERCORRELATIONS BETWEEN CORE STOCK PROPERTIES FOR NOMINAL 0.040-INCH CORE STOCKS

TABLE XXV

INTERCORRELATIONS BETWEEN CORE STOCK PROPERTIES
(N = 17)

Property	Caliper	Density	Bursting Strength	Tensile M.D.	Tensile C.D.	Tensile 30°	Tensile 60°	Stretch M.D.	Stretch C.D.	Stretch 30°	Stretch 60°	Tensile Stiffness M.D.	Tensile Stiffness C.D.
Bssis Weight	0.58	0.82	0.61	0.56	0.22	0.50	0.31	0.53	0.69	0.73	0.67	0.54	0.06
Caliper	1.00	0.04	0.15	0.15	-0.07	0.04	-0.03	0.29	0.59	0.36	0.55	0.09	-0.29
Density		1.00	0.59	0.53	0.25	0.55	0.33	0.38	0.43	0.61	0.43	0.58	0.07
Bursting Strength			1.00	0.94	0.63	0.82	0.71	0.77	0.45	0.85	0.55	0.76	0.41
Tensile, M.D.				1.00	0.62	0.89	0.70	0.64	0.48	0.73	0.50	0.90	0.41
C.D.					1.00	0.86	0.98	0.10	0.20	0.36	0.16	0.56	0.85
30°						1.00	0.90	0.32	0.42	0.58	0.37	0.84	0.64
60°							1.00	0.19	0.32	0.48	0.29	0.62	0.79
Stretch,. M.D.								1.00	0.47	0.84	0.68	0.35	-0.15
C.D.									1.00	0.70	0.92	0.36	-0.22
30°										1.00	0.84	0.49	-0.01
60°											1.00	0.27	-0.31
Tensile Stiffness, M.D.												1.00	0.48
C.D.													1.00

TABLE XXV (Continued)

INTERCORRELATIONS BETWEEN CORE STOCK PROPERTIES
(N = 17)

Property	Tensile Stiffness 30°	Tensile Stiffness 60°	Modified Ring Compression M.D.	Modified Ring Compression C.D.	Modified Ring Compression 30°	Modified Ring Compression 60°	Taber Stiffness M.D.	Taber Stiffness C.D.	Tearing Strength M.D.	Tearing Strength C.D.	TAPPI Plybond	Porosity	Water Drop
Basis Weight	0.39	0.12	0.62	0.39	0.62	0.54	0.72	0.51	0.72	0.77	0.50	0.63	-0.39
Caliper	-0.07	-0.19	0.13	-0.08	0.13	0.06	0.43	0.22	0.42	0.36	-0.10	0.04	-0.20
Density	0.51	0.21	0.64	0.47	0.61	0.56	0.56	0.41	0.56	0.68	0.65	0.75	-0.33
Bursting Strength	0.63	0.56	0.83	0.73	0.84	0.81	0.81	0.74	0.78	0.81	0.69	0.57	-0.41
Tensile, M.D.	0.75	0.57	0.84	0.69	0.86	0.77	0.89	0.72	0.80	0.82	0.62	0.51	-0.47
C.D.	0.75	0.91	0.76	0.89	0.79	0.88	0.53	0.85	0.61	0.54	0.64	0.27	-0.29
30°	0.88	0.76	0.91	0.86	0.91	0.90	0.80	0.83	0.80	0.79	0.71	0.45	-0.47
60°	0.76	0.88	0.83	0.90	0.84	0.91	0.61	0.84	0.65	0.60	0.71	0.33	-0.30
Stretch; M.D.	0.04	-0.01	0.37	0.22	0.41	0.34	0.48	0.28	0.41	0.46	0.36	0.38	-0.27
C.D.	0.19	0.01	0.44	0.18	0.42	0.35	0.56	0.29	0.45	0.47	0.42	0.31	-0.37
30°	0.27	0.21	0.66	0.48	0.64	0.64	0.66	0.48	0.64	0.69	0.67	0.51	-0.31
60°	0.03	-0.08	0.40	0.17	0.38	0.34	0.49	0.21	0.39	0.41	0.45	0.31	-0.29
Tensile Stiffness,													
M.D.	0.90	0.62	0.83	0.68	0.83	0.70	0.91	0.70	0.79	0.83	0.55	0.60	-0.44
C.D.	0.75	0.96	0.58	0.81	0.63	0.71	0.37	0.77	0.48	0.41	0.46	0.23	-0.20
30°	1.00	0.83	0.83	0.79	0.83	0.78	0.78	0.80	0.76	0.76	0.57	0.51	-0.47
60°		1.00	0.71	0.87	0.75	0.81	0.55	0.85	0.62	0.56	0.58	0.33	-0.28

TABLE XXV (Continued)

INTERCORRELATIONS BETWEEN CORE STOCK PROPERTIES
(N = 17)

Property	Tensile Stiffness		Modified Ring Compression				Taber Stiffness		Tearing Strength		TAPPI		Water
	30°	60°	M.D.	C.D.	30°	60°	M.D.	C.D.	M.D.	C.D.	Plybond	Porosity	Drop
Basis Weight	0.39	0.12	0.62	0.39	0.62	0.54	0.72	0.51	0.72	0.77	0.50	0.63	-0.39
Caliper	-0.07	-0.19	0.13	-0.08	0.13	0.06	0.43	0.22	0.42	0.36	-0.10	0.04	-0.20
Density	0.51	0.21	0.64	0.47	0.61	0.56	0.56	0.41	0.56	0.68	0.65	0.75	-0.33
Bursting Strength	0.63	0.56	0.83	0.73	0.84	0.81	0.81	0.74	0.78	0.81	0.69	0.57	-0.41
Tensile, M.D.	0.75	0.57	0.84	0.69	0.86	0.77	0.89	0.72	0.80	0.82	0.62	0.51	-0.47
C.D.	0.75	0.91	0.76	0.89	0.79	0.88	0.53	0.85	0.61	0.54	0.64	0.27	-0.29
30°	0.88	0.76	0.91	0.86	0.91	0.90	0.80	0.83	0.80	0.79	0.71	0.45	-0.47
60°	0.76	0.88	0.83	0.90	0.84	0.91	0.61	0.84	0.65	0.60	0.71	0.33	-0.30
Stretch, M.D.	0.04	-0.01	0.37	0.22	0.41	0.34	0.48	0.28	0.41	0.46	0.36	0.38	-0.27
C.D.	0.19	0.01	0.44	0.18	0.42	0.35	0.56	0.29	0.45	0.47	0.42	0.31	-0.37
30°	0.27	0.21	0.66	0.48	0.64	0.64	0.66	0.48	0.64	0.69	0.67	0.51	-0.31
60°	0.03	-0.08	0.40	0.17	0.38	0.34	0.49	0.21	0.39	0.41	0.45	0.31	-0.29
Tensile Stiffness,													
M.D.	0.90	0.62	0.83	0.68	0.83	0.70	0.91	0.70	0.79	0.83	0.55	0.60	-0.44
C.D.	0.75	0.96	0.58	0.81	0.63	0.71	0.37	0.77	0.48	0.41	0.46	0.23	-0.20
30°	1.00	0.83	0.83	0.79	0.83	0.78	0.78	0.80	0.76	0.76	0.57	0.51	-0.47
60°		1.00	0.71	0.87	0.75	0.81	0.55	0.85	0.62	0.56	0.58	0.33	-0.28

TABLE XXV (Continued)

INTERCORRELATIONS BETWEEN CORE STOCK PROPERTIES
(N = 17)

Property	Modified Ring Compression M.D.	Modified Ring Compression C.D.	Modified Ring Compression 30°	Modified Ring Compression 60°	Taber Stiffness M.D.	Taber Stiffness C.D.	Tearing Strength M.D.	Tearing Strength C.D.	TAPPI Plybond	Porosity	Water Drop
Modified Ring Compression, M.D.	1.00	0.90	0.97	0.94	0.85	0.81	0.83	0.85	0.80	0.63	-0.36
C.D.		1.00	0.92	0.97	0.65	0.87	0.67	0.66	0.83	0.59	-0.20
30°			1.00	0.95	0.86	0.89	0.82	0.83	0.81	0.63	-0.40
60°				1.00	0.74	0.90	0.78	0.77	0.85	0.59	-0.33
Taber Stiffness, M.D.					1.00	0.78	0.90	0.91	0.58	0.58	-0.50
C.D.						1.00	0.85	0.79	0.63	0.44	-0.47
Tearing Strength, M.D.							1.00	0.98	0.50	0.43	-0.60
C.D.								1.00	0.55	0.54	-0.59
TAPPI Plybond									1.00	0.72	-0.17
Porosity										1.00	-0.07

TABLE XXV (Continued)

INTERCORRELATIONS BETWEEN CORE STOCK PROPERTIES
(N = 17)

Property	Modified Ring Compression				Taber Stiffness		Tearing Strength		TAPPI Plybond	Porosity	Water Drop
	M.D.	C.D.	30°	60°	M.D.	C.D.	M.D.	C.D.			
Modified Ring Compression,											
M.D.	1.00	0.90	0.97	0.94	0.85	0.81	0.83	0.85	0.80	0.63	-0.36
C.D.		1.00	0.92	0.97	0.65	0.87	0.67	0.66	0.83	0.59	-0.20
30°			1.00	0.95	0.86	0.89	0.82	0.83	0.81	0.63	-0.40
60°				1.00	0.74	0.90	0.78	0.77	0.85	0.59	-0.33
Taber Stiffness, M.D.					1.00	0.78	0.90	0.91	0.58	0.58	-0.50
C.D.						1.00	0.85	0.79	0.63	0.44	-0.47
Tearing Strength, M.D.							1.00	0.98	0.50	0.43	-0.60
C.D.								1.00	0.55	0.54	-0.59
TAPPI Plybond									1.00	0.72	-0.17
Porosity										1.00	-0.07

APPENDIX III

DERIVATION OF THEORETICAL RELATIONSHIP FOR SIDE-TO-SIDE CRUSH

The following assumptions will be made for the case of a multiple-ply spiral wound paperboard cylinder loaded in the side-to-side crush mode:

(1) Core failure is caused by bending stress developed at the points of loading,

(2) Core failure occurs when the normal stress on the outermost ply of core stock reaches the compression strength of the core stocks,

(3) Plane cross section remain plane in bending,

(4) Materials exhibit linear stress-strain behavior,

(5) "Thin tube" theory applies,

(6) Application of adhesive does not affect core stock properties,

(7) Moduli of liners and core stocks are equal,

(8) Applied load is a line load and not one distributed over an area, and

(9) Tensile and compressive moduli of elasticity of a ply are equal.

Utilizing these assumptions, the stress on the outermost ply of core stock is computed from the following equation:

$$\sigma_s = \frac{MZ}{I} \qquad (59)$$

where the symbols are defined at the end of this Appendix. Equation (59) will be applied to the cross section immediately under the load, since analysis (4) indicates that the bending moment $\underline{M}$ is a maximum at that point. The magnitude of the bending moment at the points of load application is related to the load as follows:

APPENDIX III

DERIVATION OF THEORETICAL RELATIONSHIP FOR SIDE-TO-SIDE CRUSH

The following assumptions will be made for the case of a multiple-ply spiral wound paperboard cylinder loaded in the side-to-side crush mode:

(1) Core failure is caused by bending stress developed at the points of loading,

(2) Core failure occurs when the normal stress on the outermost ply of core stock reaches the compression strength of the core stocks,

(3) Plane cross section remain plane in bending,

(4) Materials exhibit linear stress-strain behavior,

(5) "Thin tube" theory applies,

(6) Application of adhesive does not affect core stock properties,

(7) Moduli of liners and core stocks are equal,

(8) Applied load is a line load and not one distributed over an area, and

(9) Tensile and compressive moduli of elasticity of a ply are equal.

Utilizing these assumptions, the stress on the outermost ply of core stock is computed from the following equation:

$$\sigma_s = \frac{MZ}{I} \tag{59}$$

where the symbols are defined at the end of this Appendix. Equation (59) will be applied to the cross section immediately under the load, since analysis (4) indicates that the bending moment $\underline{M}$ is a maximum at that point. The magnitude of the bending moment at the points of load application is related to the load as follows:

$$M = +0.3183\ WR \tag{60}$$

For a rectangular cross section we have,

$$I = Lt^3/12 \tag{61}$$

and

$$Z = -(t - 2h_1 - h_c)/2 \tag{62}$$

Substitutions of Equations (60)-(62) into (59) results in:

$$\sigma_s = -1.9098\ R(t - 2h_{i1} - h_c)\ w/t^3 \tag{63}$$

Using

$$\sigma_s = -P_s/h_c \tag{64}$$

and

$$R/t = 1/2(D_i/t + 1) \tag{65}$$

the side-to-side crush load corresponding to compressive failure of the first inner core ply is found to be

$$P_s = \frac{P_{me}}{0.9549(D_i/t + 1)(t - 2h_1 - h_c)h_c/t^2} \tag{66}$$

The significance and possible consequences of the assumptions which were made in deriving Equation (66) will now be discussed in more detail.

Assumption (1) is, of course, basic to the development of Equation (59). An alternative assumption, that of failure being caused by excessive shearing stress, was not pursued in detail for two reasons. First, the magnitude of the calculated shearing stress is relatively low and second, the shearing strength in the appropriate X-Z plane is extremely difficult to

$$M = +0.3183\ WR \tag{60}$$

or a rectangular cross section we have,

$$I = Lt^3/12 \tag{61}$$

nd

$$Z = -(t - 2h_1 - h_c)/2 \tag{62}$$

stitutions of Equations (60)-(62) into (59) results in:

$$\sigma_s = -1.9098\ R(t - 2h_{i1} - h_c)\ w/t^3 \tag{63}$$

ing

$$\sigma_s = -P_s/h_c \tag{64}$$

d

$$R/t = 1/2(D_i/t + 1) \tag{65}$$

side-to-side crush load corresponding to compressive failure of the first er core ply is found to be

$$P_s = \frac{P_{me}}{0.9549(D_i/t + 1)(t - 2h_1 - h_c)h_c/t^2} \tag{66}$$

The significance and possible consequences of the assumptions which made in deriving Equation (66) will now be discussed in more detail.

Assumption (1) is, of course, basic to the development of Equation). An alternative assumption, that of failure being caused by excessive ring stress, was not pursued in detail for two reasons. First, the magni- of the calculated shearing stress is relatively low and second, the ring strength in the appropriate X-Z plane is extremely difficult to measure if indeed it ever has been reliably measured. On the other hand, ply delaminations were observed in the specimens near the regions of highest shearing stress, suggesting that interlaminar shear stress may indeed be a contributor to core failure. The side-to-side crush tests of cores of different geometry should afford an opportunity to examine the possibility of shear failure in more detail.

Assumption (2) is expected to lead to an underestimation error of side-to-side crush strength. The assumption states that the maximum load on the core is reached when the stress on the outermost core ply reaches its edgewise compression strength. It seems more likely based on the reported behavior of wood flexural members (30), that the ply will not fail completely but continue to support some load so that the next ply will reach its compression strength as the load is increased. In this way the critical stress (edgewise compression strength) will progress some further distance into the core wall before the maximum load is reached. The depth of penetration of the critical stress is, of course, unknown and presents a difficult problem in stress analysis, since it requires knowledge of the postfailure behavior of those plies which have attained failure stress.

Assumption (3) is traditional and has been verified by experiment for a wide variety of structures (31). Assumptions (4) and (5) have been discussed in a previous section together with their possible effects on maximum crush load. Assumption (6) probably introduces an error because in the present study the materials were evaluated from the parent roll and thus do not reflect any stiffening or strengthening from the adhesive. This assumption can be expected to lead to an underestimation of side-to-side crush load.

Assumption (7) is an approximation which lends considerable simplification to the stiffness calculations but which is expected to have a negligible effect on maximum crush load.

Assumption (8) was made because of the unavailability of a more realistic solution involving flat plates at the load-application points. When flat platens are used to apply the side-to-side load, as was done in our tests, the assumption of a line load is exact only for zero load, when the contact surface between plate and cylinder is a line. As load is applied the core flattens somewhat in the vicinity of the line of loading, and the load is then distributed over a small area. As the loading increases, further flattening and load redistribution occur. To estimate the importance of this effect, the solution for a cylinder compressed by a distributed load of constant contact area (as opposed to a steadily increasing one) was examined. The effect of load distribution was seen to be a more even distribution of the bending moment thus reducing the maximum bending moment. Figure 24 shows a plot of the ratio of the expected failure load for a distributed load to the expected failure load for a point load (for equal stresses) as a function of the amount of load distribution. It may be seen that for a distribution of 10°, a 15% increase in load and a 2% increase in stiffness (force/deflection) are to be expected. It is not possible, however, to use Fig. 24 directly in a corrective factor for our particular case since the load distribution shape is undoubtedly not uniform and the effective contact width cannot be determined. Thus, Assumption (8) is expected to lead to a significant underestimation of core strength.

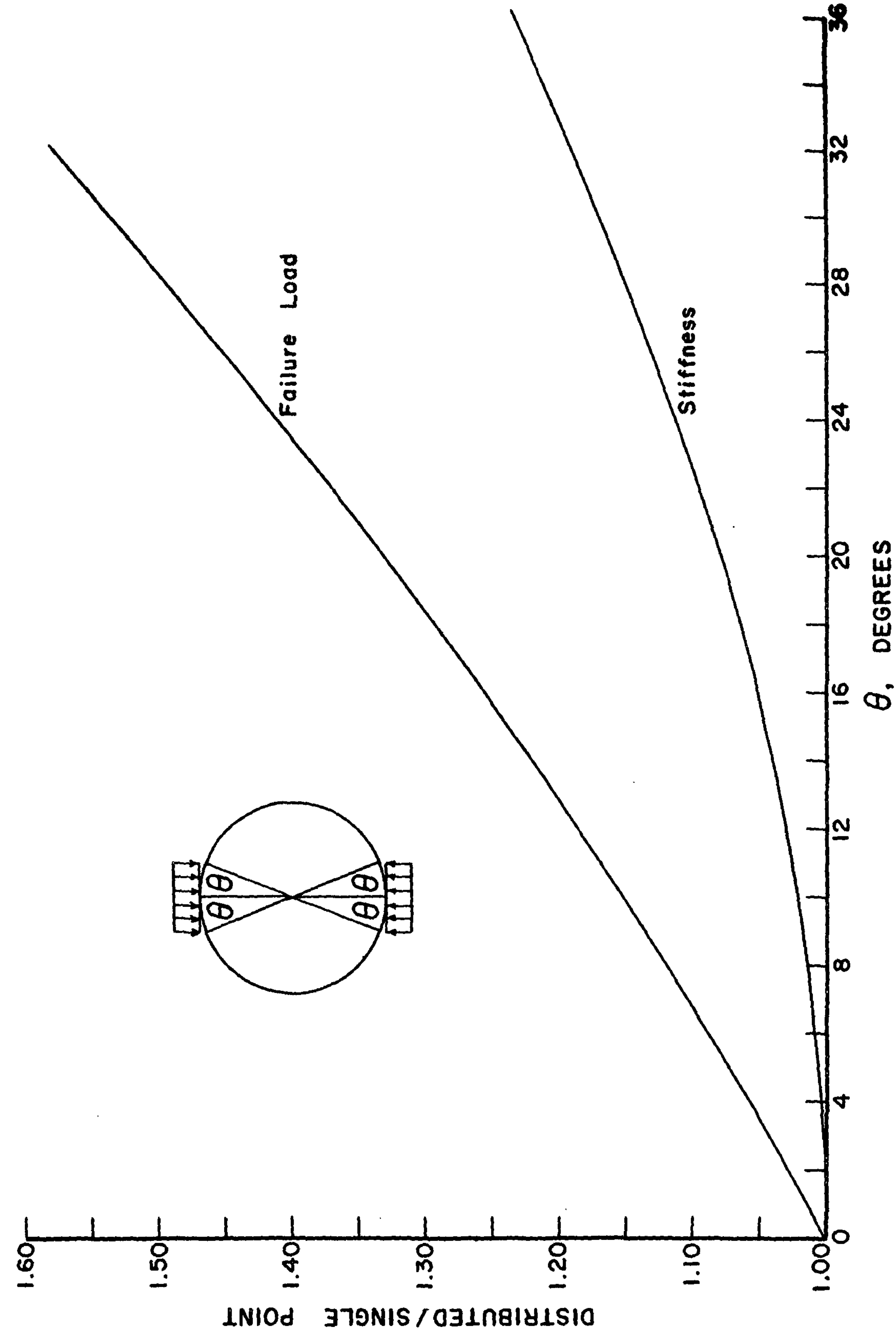

Figure 24. Effect of Load Distribution on Maximum Side Crush Load and Stiffness, Compared to the Effects from a Point Load

Assumption (9) states that the Young's modulus as measured while the material is under tension is identical to that measured while the material is being compressed. Whether or not there is any difference between the two moduli is controversial, there being evidence to support both a significant difference and no difference at all. To determine the effect on maximum side-to-side crush load from unequal tension and compression moduli, some theoretical calculations were made. The results indicate that (a) the neutral bending axis shifts toward the material of higher modulus, (b) the compressive stress is decreased while the tensile stress is increased, and (c) the core stiffness (force/deflection) decreases. These conclusions are illustrated by Fig. 25 in which the effects of tension to compression modulus ratios of from 1.0 (equal moduli) to 3.0 are displayed. Since the core stock tensile strength is generally about twice its compression strength, (average for all samples, 2.07) core failure would be governed by compressive stress. Thus, for a modulus ratio of 2.0 ($E_T = 2.0\ E_c$), a 15% increase in core strength would be expected from the 15% decrease in compressive stress. Similarly, a stiffness of only 68.5% of that for equal moduli would be expected for the same modulus ratio of 2.0. Assumption (9) then, if it were untrue, would be expected to lead to a significant underestimation of maximum core side-to-side crushing strength.

SYMBOLS

θ = complement of angle of wind, degree

D_i = inner diameter of core, in.

h_l = inner liner thickness, in.

h_c = core stock thickness, in.

I = moment of inertia of wall cross section about centroidal axis, in.^{4}

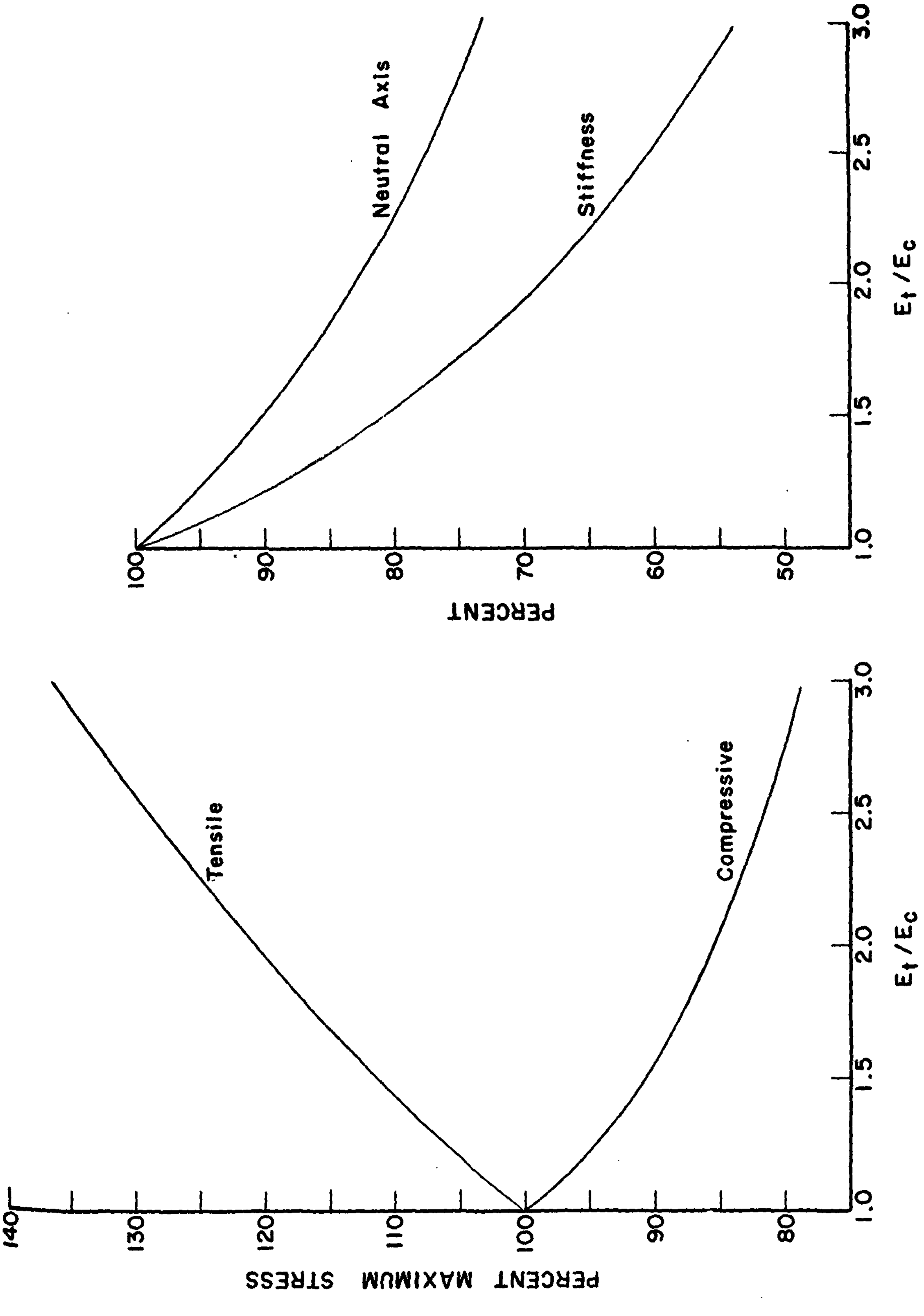

Figure 25. Effect of Unequal Elastic Tension and Compression Moduli on Maximum Stresses, Neutral Axis Position, and Stiffness

$\underline{L}$ = length of core, in.

$\underline{M}$ = bending moment, lb.-in.

$\underline{P}_{m\theta}$ = edgewise compression strength of core stock ply in a direction θ, lb.-in.

$\underline{R}$ = mean radius of core, in.

$\underline{t}$ = core wall thickness, in.

$\underline{W}$ = applied load, lb.

$\underline{P}_{s}$ = applied load per unit length, lb./in.

$\underline{Z}$ = distance from neutral bending axis of core wall cross section to centerline of outermost ply of core stock, in.

σ_{s} = stress in the outermost ply of core stock, lb./in.^{2}

APPENDIX IV

DERIVATION OF A THEORETICAL RELATIONSHIP FOR BEAM BENDING

The following assumptions will be made for the case of a multiple-ply spiral wound paperboard cylinder simply supported and loaded midway between the supports by a concentrated load (Fig. 22):

(1) Core failure is caused by bending stress.

(2a) Core failure occurs when the axial normal compressive stress exceeds the core stock axial compressive strength ($\underset{\sim}{P}_{m_{60}}$ for 60° wind angle), or

(2b) Core failure occurs when the normal compressive stress acting in a direction corresponding to the stock cross-machine direction exceeds the stock strength in that direction.

(3) The beam is cylindrical and straight but of arbitrary cross section.

(4) Plane sections in the unstressed beam remain plane during bending deformation.

(5) The deflection of each beam element is in the form of an arc.

(6) Shearing stresses are distributed uniformly across the width of the beam.

(7) Materials exhibit linear stress strain behavior.

(8) Application of adhesive does not affect core stock properties.

(9) Moduli of liners and core stocks are equal.

(10) Tensile and compressive moduli of elasticity of a ply are equal.

Based on Assumptions (1) and (3) through (10), the following equation relates the axial normal stress to the applied bending moment (see end of Appendix IV for symbols):

$$\sigma_a = \frac{MC}{I} \tag{67}$$

From equilibrium of forces we know that

$$M = PL/4 \tag{68}$$

The moment of inertia for a tube is given by

$$I = \frac{\pi}{64} (D_o^{\,4} - D_i^{\,4}) \tag{69}$$

Substituting Equations (68) and (69) into (67) and noting that $C = R_o$ gives

$$P = \frac{\pi}{8} \frac{(D_o^{\,4} - D_i^{\,4})}{L\,D_o} \sigma_a \tag{70}$$

By utilizing Assumption 2a we note that

$$\sigma_a = P_{m\alpha}/h_c \tag{71}$$

By combining Equations (70) and (71) we get

$$P = \frac{\pi}{8} \frac{(D_o^{\,4} - D_i^{\,4})}{L\,D_o\,h_c} P_{m\alpha} \tag{72}$$

If Assumption 2b is used, however, we must determine the magnitude of the stress acting in the core stock cross-machine direction in terms of the axial stress. Referring to Fig. 23 it is evident that a uniaxial stress field involving stresses acting along an axis different from the material natural axes may be resolved into an equivalent stress field which is aligned with the natural axes but in general contains all three stress components. The stress in the "y" direction is related to the stresses acting the a-c coordinate system as follows (29):

$$\sigma_y = \sigma_a \sin^2\alpha + \sigma_c \cos^2\alpha - \tau_{ac} \sin 2\alpha \tag{73}$$

where α is the angle between the axial direction and the machine-direction (angle of wind). In the case of bending stress, only the stress in the axial direction, $\sigma_{\underline{a}}$, is nonzero, so we have

$$\sigma_y = \sigma_a \sin^2\alpha \tag{74}$$

By using Assumption 2b we get

$$\sigma_y = P_{my}/h_c \tag{75}$$

Upon substituting Equations (74) and (75) into Equation (70), we get

$$P = \frac{\pi}{8} \frac{(D_o^4 - D_i^4)}{L\, D_o\, h_c} \frac{P_{my}}{\sin^2\alpha} \tag{76}$$

Equation (76) should be used to estimate maximum bending loads if it is thought that failure is governed by the stock cross-machine direction strength, while Equation (72) should be used where $P_{\underline{m}60}$ governs core failure. The latter case is probably safer for general use since its basic assumption is more generally applicable. The use of Equation (76), however, is limited to those cases involving core geometries and angles of wind such that the stress in the cross-machine governs core failure.

The possible effects of the simplifying assumptions on Equations (72) and (76) have been discussed in previous sections in connection with other equations, but the conclusions may be expected to apply to Equations (72) and (76) as well.

SYMBOLS

α = angle of wind; angle between core axial direction and core stock machine-direction, degrees

$\underline{C}$ = distance from core neutral bending axis to extreme beam fiber, in.

$\underline{D}_i$ = inner diameter of core, in.

$\underline{D}_o$ = outer diameter of core, in.

$\underline{h}_c$ = core stock thickness, in.

$\underline{I}$ = moment of inertia of core cross section about neutral bending axis, in.^{4}

$\underline{L}$ = length of core between supports, in.

$\underline{M}$ = maximum bending moment, in.-lb.

$\underline{P}$ = load applied to core midway between supports, lb.

$\underline{P}_{m\alpha}$ = core stock modified ring strength, tested uniaxially at an angle Θ from the stock machine-direction, lb./in.

$\underline{P}_{my}$ = core stock modified ring strength in the "y" direction (cross-direction) lb./in.

σ_a = normal stress in the axial direction, p.s.i.

σ_y = normal stress in the core stock cross-direction, p.s.i.

APPENDIX V

DERIVATION OF TORQUE ESTIMATING EQUATIONS

The following assumptions are necessary to derive a relationship between the torque applied to a core and the shear stress developed:

(1) Core failure is caused by shearing stress developed in the plane of the core stock; or

(2) Core failure occurs when the normal stress acting in the core stock cross-direction exceeds the strength in that direction.

(3) The core is straight and of uniform concentrically hollow section.

(4) The core is loaded only by equal and opposite twisting couples which are applied at its ends in planes normal to its axis.

(5) The core is not stressed beyond the elastic limit.

(6) Application of adhesive does not affect core stock properties.

(7) Moduli of liners and core stock are equal.

Utilizing Assumptions (3)-(7) the following equation relates the torque at failure to the core geometry and the shear stress developed (4):

$$T = \frac{\pi}{16} \frac{(D_o^4 - D_i^4)}{D_o} \tau_{ac} \tag{77}$$

An estimate of the strength is afforded by the simplified shear strength equation derived in Appendix VI, Equation (99). If the shear strength estimate, S_{xy}, were set equal to the shear stress, τ_{xy}, we have:

$$\left(\frac{1}{\tau_{xy}}\right)^2 = \left(\frac{h_c}{P_{mx}}\right)^2 \left[1 + \left(\frac{P_{mx}}{P_{my}}\right)^K\right] + \left(\frac{h_c}{P_{my}}\right)^2 \tag{78}$$

Thus, knowing the uniaxial core stock strengths, P_{mx} and P_{my}, along with the dimensions of the core, Equations (77) and (78) can be used to estimate core torque strength.

A different estimate of core strength results if Assumption (2) is utilized instead of Assumption (1). In this case it is necessary to know the cross-direction normal stress component, σ_y, of the applied shear stress, τ_{ac} (Fig. 29). Referring to Equation (94), Appendix VI, we have

$$\sigma_y = \tau_{ac} \sin 2\alpha \tag{79}$$

By definitions we know that

$$P_{my} = h_c \sigma_y \tag{80}$$

Substituting Equations (79) and (80) into (77) leads to:

$$T = \frac{\pi}{16} \frac{(D_o^4 - D_i^4)}{D_o h_c} \frac{P_{my}}{\sin 2\alpha} \tag{81}$$

Both Equations (77) and (81) have limitations. Equation (78) predicts that core torque strength is independent of angle of wind, since the core stock shear strength was assumed to be independent of angle [Equation (98), Appendix VI]. Since the data from the present tests all apply to cores of the same wind angle, this assumption cannot be tested. Limited data do exist, however, to suggest that core torque strength is dependent on the angle of wind.

Equation (81) is based on an assumption (no. 2) which is known to be grossly inaccurate for small angles of wind. Assumption two states that the cross-direction normal stress component governs core failure. This situation will only exist for angles of wind within certain bounds. As the angle of wind decreases, the cross-direction normal stress component decreases while the normal stress components in other directions increase. Eventually, one of the other normal stress components will govern failure and Equation (81) will not apply.

Discussion of the other assumptions pertaining to these equations may be found elsewhere in this report.

SYMBOLS

α = angle of wind; angle between core axial direction and core stock machine-direction, degree

D_i = inside core diameter, in.

D_o = outside core diameter, in.

h_c = core stock thickness, in.

K = 1 when interaction theory of anisotropic failure is used

= 2 when distortional energy theory of anisotropic failure is used

P_{mx} = core stock tensile strength in the machine-direction, lb./in.

P_{my} = core stock modified ring strength in the cross-machine direction, lb./in.

τ_{ac} = shear stress acting on elements with faces in the "a" and "c" directions, p.s.i.

τ_{xy} = shear stress acting on elements with faces in the "x" and "y" directions, p.s.i.

T = maximum applied torque, in.-lb.

APPENDIX VI

THE PREDICTION OF NORMAL AND SHEAR STRENGTHS FOR VARIOUS ORIENTATIONS

The coordinate systems to be used in the derivation are illustrated in Fig. 26-28. The a-c directions correspond to the tube geometry, referring to the axial and circumferential directions, respectively. The x-y directions correspond to the natural axes of the core stock, referring to the machine-direction and cross-direction, respectively. Figure 28 illustrates the stress field existing during a uniaxial modified ring test together with an equivalent stress field aligned with the natural axes of the core stock. The stresses induced on an element face orientated at an angle γ to the axial direction (Fig. 27) can be expressed in terms of the known normal and shearing stresses in the a-c directions as follows (29):

$$\sigma_\gamma = \sigma_a \cos^2\gamma + \sigma_c \sin^2\gamma + \tau_{ac} \sin 2\gamma \tag{82}$$

$$\tau_{\gamma\beta} = -\sigma_a \frac{\sin 2\gamma}{2} + \sigma_c \frac{\sin 2\gamma}{2} + \tau_{ac} \cos 2\gamma \tag{83}$$

Referring to Fig. 27 and 28, it may be seen that by choosing $\gamma = 90-\Theta$, σ_γ becomes σ_x, the stress in the machine direction so that

$$\sigma_x = \sigma_a \sin^2\Theta + \sigma_c \cos^2\Theta + \tau_{ac} \sin 2\Theta \tag{84}$$

By choosing $\gamma = -\Theta$, σ_γ becomes σ_y, the stress in the cross-direction, and substitution of these values into Equation (82) gives

$$\sigma_y = \sigma_a \cos^2\Theta + \sigma_c \sin^2\Theta - \tau_{ac} \sin 2\Theta \tag{85}$$

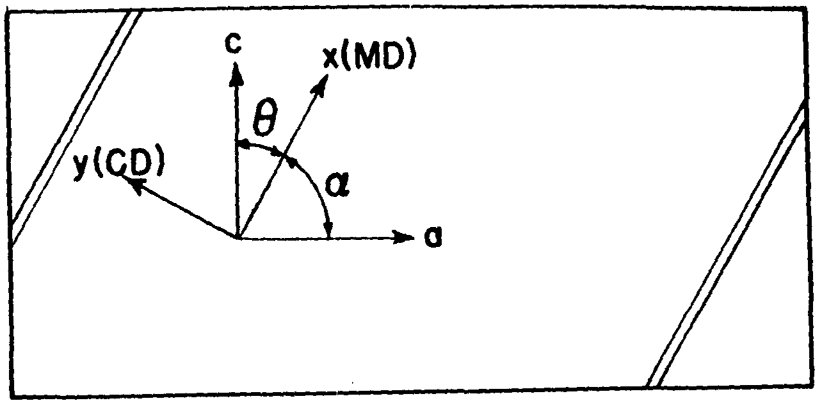

Figure 26. Coordinate Systems: Core (a-c), and Orthotropic (x-y)

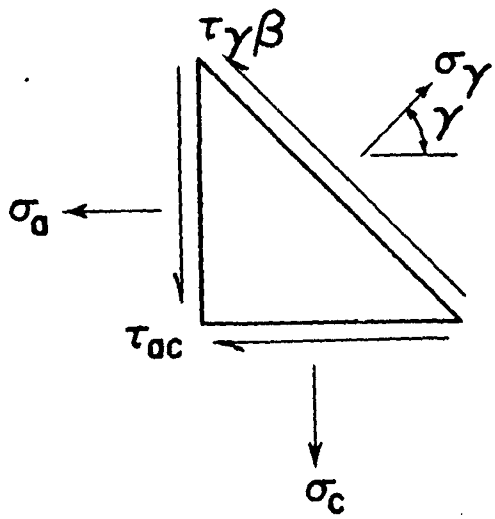

Figure 27. Stresses on an Element Face Whose Normal Makes an Angle γ with the Axial Direction

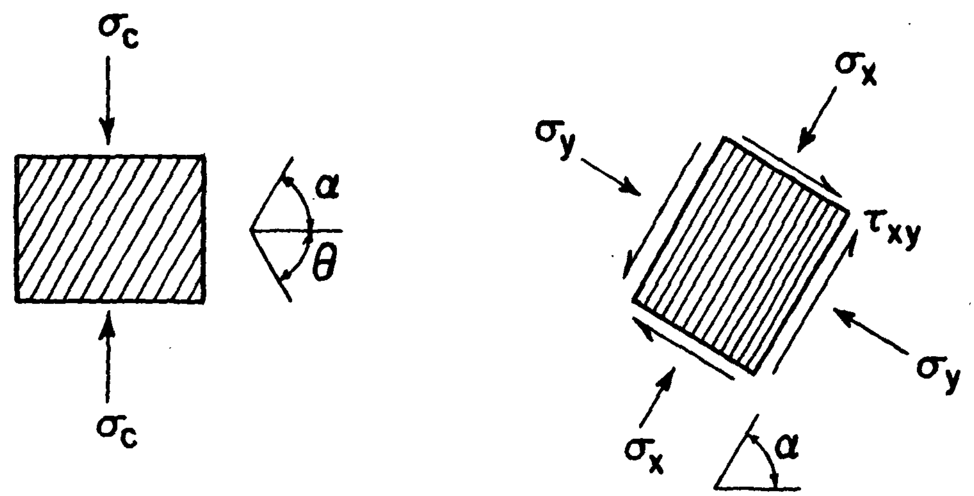

Figure 28. Stresses on Elements Aligned with the Stress Applied during Modified Ring Test, σ_c, and Aligned with Orthotropic Axes

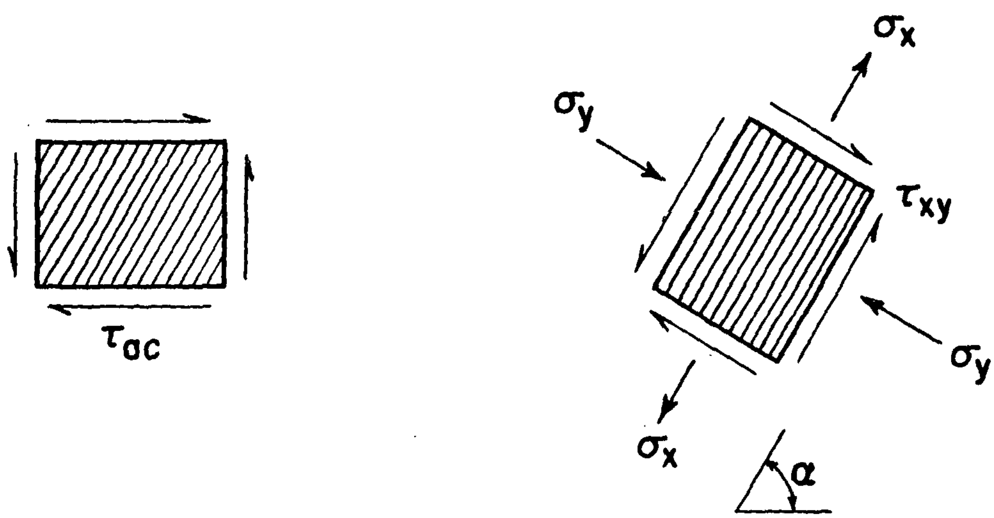

Figure 29. Stresses on Elements Aligned with Applied Shear Stress during Torsion, τ_{ac}, and Aligned with Orthotropic Axes

By choosing $\gamma = 90-\Theta$, the shearing stress $\tau_{\gamma\beta}$ becomes equal to the shearing stress acting in the x-y directions:

$$\tau_{xy} = -\sigma_a \frac{\sin 2\Theta}{2} + \sigma_c \frac{\sin 2\Theta}{2} - \tau_{ac} \cos 2\Theta \qquad (86)$$

Referring to the case of uniaxial strength tests such as illustrated in Fig. 28, we note that the only nonzero stress in the unaligned direction is σ_c, so that Equations (82)-(84) become:

$$\sigma_x = \sigma_c \cos^2\Theta \qquad (87)$$

$$\sigma_y = \sigma_c \sin^2\Theta \qquad (88)$$

$$\tau_{xy} = \sigma_c \frac{\sin 2\Theta}{2} \qquad (89)$$

To account for the effect of combined stresses acting simultaneously on an element, where the uniaxial strengths are known, two prominent anisotropic strength theories were used (28), and may be expressed as follows:

$$\left(\frac{\sigma_x}{X}\right)^2 - \left(\frac{Y}{X}\right)^{K-1} \frac{\sigma_x\sigma_y}{XY} + \left(\frac{\sigma_y}{Y}\right)^2 + \left(\frac{\tau_{xy}}{S_{xy}}\right)^2 = 1 \qquad (90)$$

where

K = 1 for interaction formula (FPL)

K = 2 for distortional energy formula (Hill)

For the case of a uniaxial strength test (Fig. 28), the stresses in the x-y plane are related to the stress σ_c applied at an angle Θ from the machine-direction by Equations (87)-(89). Substituting Equations (87)-(89) into (90) and noting that for the uniaxial test at failure $\sigma_c = \Theta$, we get the following equation:

$$\left(\frac{1}{S_{xy}}\right)^2 = -\left(\frac{\cos}{\sin}\right)^2 \frac{1}{X^2} + \left[\left(\frac{Y}{X}\right)^K - \left(\frac{\sin}{\cos}\right)^2\right] \frac{1}{Y^2} + \left(\frac{2}{\sin 2\theta}\right)^2 \frac{1}{\Theta^2} \qquad (91)$$

Equation (91) provides an estimate of the material shearing strength in the x-y plane in terms of the known uniaxial strengths, x, y, Θ obtained by three separate tests. Thus, if the uniaxial strengths are known in any three directions the strength in any other direction (or shearing strength) can be estimated. If, for example, Equation (91) were used twice, once using the strength at θ and once at angle γ, and the constant shearing strength were eliminated the following equation results:

$$\left(\frac{1}{\Gamma}\right)^2 = \left(\frac{1}{\Theta}\right)^2 \left[\frac{\sin\gamma\ \cos\gamma}{\sin\theta\ \cos\theta}\right]^2 - (\sin\gamma\ \cos\gamma)^2 \left\{\left[\left(\frac{\cos\theta}{\sin\theta}\right)^2 - \left(\frac{\cos\gamma}{\sin\gamma}\right)^2\right]\left(\frac{1}{X}\right)^2 + \left[\left(\frac{\sin\theta}{\cos\theta}\right)^2 - \left(\frac{\sin\gamma}{\cos\gamma}\right)^2\right]\left(\frac{1}{Y}\right)^2\right\} \tag{92}$$

Equation (92) relates the uniaxial normal strength at an angle γ from the machine-direction, Γ, to three other known uniaxial normal strengths, X, Y, and Θ, the uniaxial normal strength at an angle Θ from the machine direction. For the case of torsion, it may be seen by Fig. 29 that different stress fields arise, both in the a-c plane and the x-y plane, as a result of applying a torque to the ends of a core. The only nonzero stress in the a-c plane is a shearing stress, τ_{ac}, so that Equations (84)-(86) become:

$$\sigma_x = \tau_{ac} \sin 2\Theta \tag{93}$$

$$\sigma_y = \tau_{ac} \sin 2\Theta \tag{94}$$

$$\tau_{xy} = -\tau_{ac} \cos 2\Theta \tag{95}$$

Substituting Equations (93)-(95) into Equation (90) leads to:

$$\left(\frac{1}{S_{ac}}\right)^2 = \left(\frac{1}{S_{xy}}\right)^2 + \sin^2 2\theta \left\{\left(\frac{1}{X}\right)^2 \left[1 + \left(\frac{X}{Y}\right)^K + \left(\frac{X}{Y}\right)^2\right] - \left(\frac{1}{S_{xy}}\right)^2\right\} \tag{96}$$

Equation (96) relates the shearing strength in the a-c plane (a-c axes make an angle Θ with x-y axes), S_{ac}, to the uniaxial normal strengths X and Y, and the shearing strength in the x-y plane (axes aligned with the core stock machine and cross-machine directions). Since the shearing strength, S_{xy}, is usually not known, an estimate of S_{xy} can be obtained from Equation (91) by using three known uniaxial strengths. The result can then be substituted into Equation (96) to obtain an estimate of the shearing strength in the a-c plane, S_{ac}.

Since Equations (91), (92), and (96) are complex, a simplifying approximation would be desirable. A suggestion for such a simplification is afforded by rewriting Equation (96) in the following form:

$$\left(\frac{S_{xy}}{S_{ac}}\right)^2 = 1 + \sin^2 2\theta \left\{\left(\frac{S_{xy}}{X}\right)^2 \left[1 + \left(\frac{X}{Y}\right)^K + \left(\frac{X}{Y}\right)^2\right] - 1\right\} \tag{97}$$

It may be seen that the ratio $(S_{xy}/S_{ac})^2$ is equal to a constant term and sinusoidal component which varies with Θ, the angle between the a-c and x-y axes. For the 21 samples used in this study, the average value for the bracketed quantity in Equation (97) was -0.015. Thus, a maximum error of only 1.5% would occur if one were to introduce the following approximation:

$$S_{xy} = S_{ac} \tag{98}$$

Substituting Equation (98) into Equation (97) results in the following simplified expression for the shearing strength, in terms of the known uniaxial strengths, X, Y:

$$\left(\frac{1}{S_{xy}}\right)^2 = \left(\frac{1}{x}\right)^2 \left[1 + \left(\frac{X}{Y}\right)^K\right] + \left(\frac{1}{Y}\right)^2 \tag{99}$$

Substituting Equation (99) into Equation (91) leads to the following simplified expression for the uniaxial normal strength, Θ, in terms of the machine- and cross-machine strengths, X, Y:

$$\frac{1}{\Theta^2} = \frac{\cos^2\theta}{X^2} + \frac{\sin^2\theta}{Y^2} \tag{100}$$

Table XXVI lists the results when Θ was computed from Equation (100) for 30° and 60° and compared to observed values. The comparisons were made with modified ring data (stress x sheet thickness) and are expressed in lb./in. It may be seen that the estimates were quite good, being 3.03 and 5.02% in error on the average for the 30° and 60° estimates, respectively.

TABLE XXVI

ESTIMATES OF CORE STOCK STRENGTHS AT 30° AND 60° FROM M.D. AND C.D. DATA
[Equation (100)]

No.	P_{m30}, lb./in. Theoretical	P_{m30}, lb./in. Observed	Error, %[a]	P_{m60}, lb./in. Theoretical	P_{m60}, lb./in. Observed	Error, %[a]
1	37.6	38.5	-2.27	27.5	29.1	-5.39
2	58.2	60.5	-3.78	46.4	47.5	-2.26
3	48.9	48.4	1.23	37.4	39.1	-4.16
4	38.5	39.0	-1.19	29.3	30.8	-4.65
5	30.7	30.4	1.20	22.1	23.8	-6.87
6	44.8	45.7	-1.75	34.8	36.0	-3.26
7	42.8	42.4	1.06	32.8	33.2	-1.08
8	58.9	61.9	-4.83	46.0	46.9	-1.87
9	55.8	56.0	-0.30	43.4	44.6	-2.60
10	45.3	43.4	4.52	35.5	36.5	-2.47
11	38.0	34.6	9.85	32.5	31.5	3.39
12	38.3	40.4	-4.99	29.0	31.6	-7.98
13	39.3	39.5	-0.50	29.3	33.2	-11.48
14	54.3	50.3	8.13	42.7	43.6	-1.89
15	43.5	43.4	0.30	32.2	35.6	-9.48
16	48.3	49.0	-1.25	37.1	41.8	-11.20
17	48.3	45.4	6.57	39.2	40.3	-2.54
18	45.8	44.8	2.29	35.6	38.4	-7.11
19	45.4	44.6	1.97	35.8	36.2	-0.90
20	34.3	34.8	-1.17	25.5	27.0	-5.35
21	35.3	37.0	-4.49	28.0	31.0	-9.42
	Average absolute error		3.03			5.02

[a]Based on observed results as reference.

SYMBOLS

γ = angle between element face normal and the axial direction, deg.

Γ = uniaxial core stock strength at an angle γ from the machine direction, p.s.i.

$\underline{K}$ = 1 or 2; see Appendix V.

$\sigma_{\underline{a}}$ = normal stress in the axial direction, p.s.i.

$\sigma_{\underline{c}}$ = normal stress in the circumferential direction, p.s.i.

σ_{γ} = normal stress in the direction γ degrees from the axial direction, p.s.i.

$\sigma_{\underline{x}}$ = normal stress in the machine direction, p.s.i.

$\sigma_{\underline{y}}$ = normal stress in the cross-machine direction, p.s.i.

$\underline{S}_{\underline{ac}}$ = core stock shear strength in a plane whose axes make an angle Θ with the $\underline{x}$-$\underline{y}$ orthotropic axes, p.s.i.

$\underline{S}_{\underline{xy}}$ = core stock shear strength in the orthotropic $\underline{x}$-$\underline{y}$ plane, p.s.i.

$\tau_{\underline{xy}}$, $\tau_{\underline{ac}}$ = shear stresses; see Appendix V.

$\tau_{\gamma\beta}$ = shear stress acting on elements with faces in the γ and β directions, p.s.i.

θ = angle between uniaxial modified ring test direction and machine direction, deg.

Θ = uniaxial core stock strength at an angle θ from the machine direction, p.s.i.

$\underline{X}$ = uniaxial core stock strength in the machine direction, p.s.i.

$\underline{Y}$ = uniaxial core stock strength in the cross-machine direction, p.s.i.